ELECTRON SPIN RESONANCE IN SOLID STATE SYSTEMS.

by

S. P. Burley B.Sc.

A Thesis
presented for the Degree of
Doctor of Philosophy
in the
Physics Department
University of Adelaide.

May 1964.

FRONTISPIECE

THE SUPERHETERODYNE SPECTROMETER

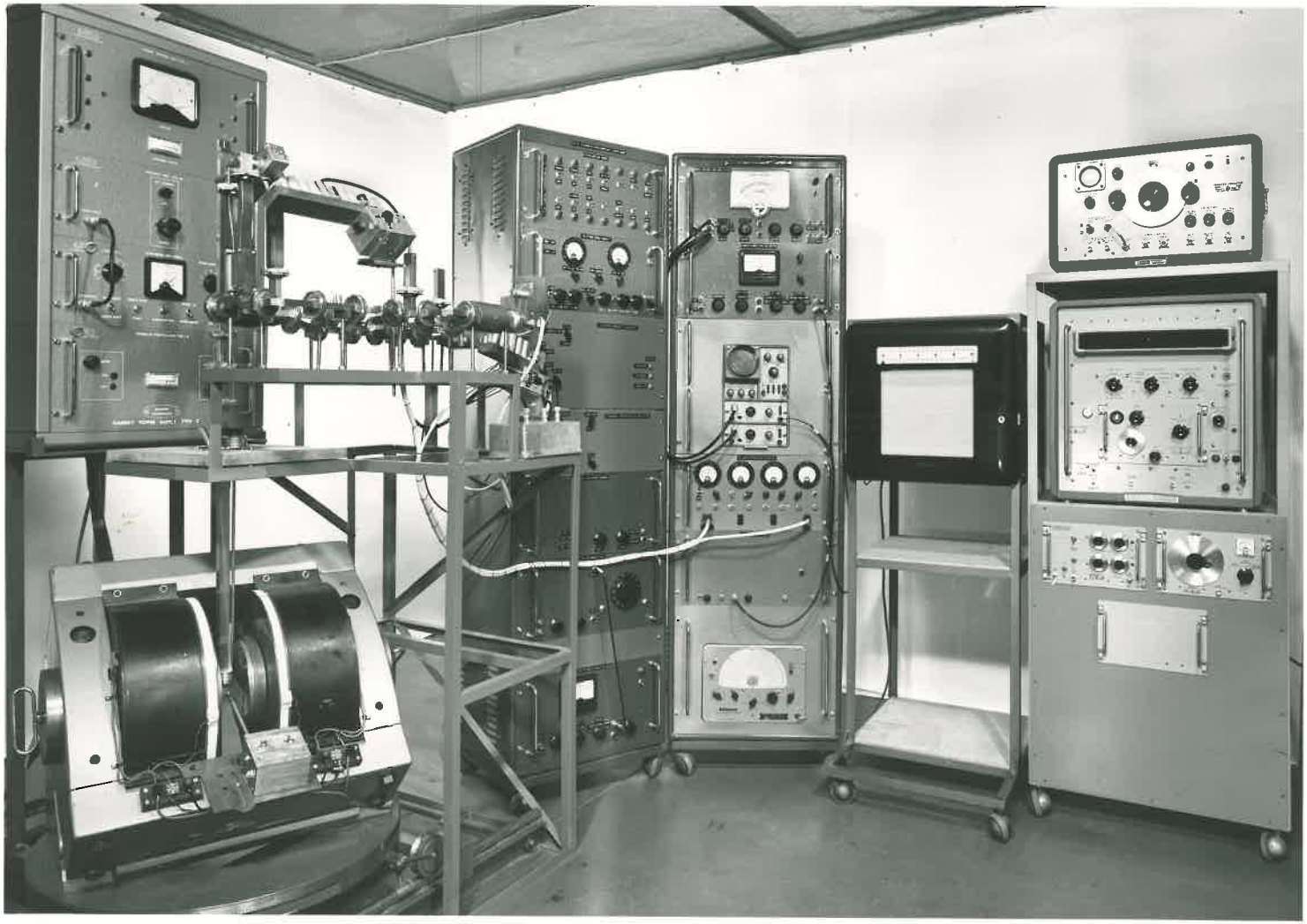

CONTENTS

Page.

SUMMARY

An experimental investigation of the paramagnetism due to transition metals in some solid state systems was made by the method of electron spin resonance (e.s.r.).

For this purpose, a superheterodyne electron spin resonance spectrometer was developed to operate at X band frequencies. It is evident that a comparison between such a spectrometer and the more conventional high frequency field modulation models involves a consideration of a large number of factors including the nature of the materials being investigated. Some of these factors were investigated in detail, particular attention being paid to the role of microphonics and klystron frequency fluctuations.

In the absence of facilities for cooling the samples to liquid Helium temperatures, it seemed to the author that one useful way of extending existing knowledge of paramagnetic effects would be by a study of the high spin S-state ions occurring as impurities in crystal lattices which had not yet been studied by e.s.r.. These ions, e.g. Mn^{++}, Fe^{+++} and Gd^{+++} are known to give strong spectra at room temperatures and so could easily be investigated with the apparatus available. The search for new materials was made by a survey of natural minerals since these have the advantage of posessing well known physical properties and crystal structures.

A large number of mineral samples were examined for e.s.r. effects, and hitherto unreported lines were observed in the following sixteen minerals : Feldspar, Neptunite, Apatite, Tourmaline, Danburite, Sphene, Kunzite, Scheelite, Smithsonite, Benitoite, Apophyllite, Chili Nitre, Jade, Turquoise, Australite and Opal. All these minerals, except the last two (which were glassy)

and the previous two (which were polycrystalline) gave several distinct lines.

The spectra examined in detail were those due to Fe^{+++} in Benitoite, and Mn^{++} in Smithsonite. The Spin Hamiltonian constants were determined in both these cases. In addition, an analysis was made of some hitherto unrecorded forbidden lines due to Mn^{++} in Apatite and Scheelite. Natural Apatites and Apophyllites were often observed to have characteristic defect centre resonances and these were also analysed.

Observations of broad resonance lines in glassy Australites and Opals prompted an investigation of the better known Borax glasses, doped with transition metals. Here evidence for the existence of complex ions with strong axial Jahn-Teller deformations was found. Defect centres were also induced in Borax glasses and studied by the method of e.s.r..

PREFACE

This thesis contains no material which has been accepted for the award of any other degree or diploma in any University, and to the best of the candidate's knowledge and belief, the thesis contains no material previously published or written by another person except where due reference is made in the text of the thesis.

The research described in the thesis was carried out in the Physics Department of the University of Adelaide during the period from March 1961 to February 1964. The work was supervised by Dr. S. G. Tomlin.

The author wishes to thank Dr. S.G. Tomlin for many stimulating discussions and suggestions and also for his unfailing and understanding encouragement throughout the progress of the work. In addition he acknowledges with sincere gratitude discussions with Mr. G.J. Troup and other members of the staff of the Physics Department at Monash University. Special thanks are due for the access allowed to their Q band spectrometer and for assistance with the Q band measurements.

No work undertaken in this field in Australia could fail to show the inspiration and leadership of the late Dr. G.S. Bogle of the National Standards Laboratories, Chippendale, New South Wales. His guidance, and also the assistance of his colleague, Mr. H.F. Symmons, in taking the zero field measurements on Benitoite is gratefully acknowledged.

The author, in collaboration with Mr. B. C. Cavenett of the Physics Department at the University of Adelaide, was responsible for the design and construction of the superheterodyne spectrometer. The

cavities and several other microwave components were built in the Physics Workshop by Mr. W. Jamieson.

All programming of the data and its execution on the Adelaide University I.B.M. 1620 Computor was done by the author, as was also the programming for the Weapons Research Establishment 7090 Computor.

The drawing of the diagrams was the work of Miss Heather Barrow and the photography was done by Mr. G. Tomlinson and Miss Anne Millbank.

The candidate wishes to record his thanks for the "Philips Scholarship" (1961) and for a "Commonwealth Postgraduate Award" (1962-4). He is also grateful to the Radio Research Board of Australia for equipment grants.

CHAPTER I

Introduction.

1.1 Historical.

The development of centimetre radar sources and detectors during the second world war provided a background of experience and technique for the post-war development of microwave spectroscopy.

One important branch of this field is concerned with the study of magnetic energy level separations in systems showing electronic paramagnetism. This had its origin in experiments by Zavoisky (1945), Cummerow and Halliday (1946) and Bleaney and Penrose (1946) which showed the possibility of observing resonances between a microwave magnetic field and a system of electronic dipoles perturbed by Zeeman interactions with magnetic fields originating from both a variable external source and the parent atomic system. Usually the bulk of the electronic magnetic dipole moment has its origin in the electron spins and so this phenomenon is often referred to as electron spin resonance or e.s.r..

These resonances have been very extensively studied in recent years and have yielded a considerable amount of information on a wide variety of paramagnetic atomic systems. Several review articles have appeared :- Bleaney and Stevens (1953), Bowers and Owen (1955) and Low (1960). Also several introductory books to the subject have been published by Ingram (1955), Ingram (1958), Pake (1962) and Slichter (1963).

1.2 The Present Project

In 1961 it was decided to develop an electron spin resonance spectrometer at the University of Adelaide. The aim was to assist with the biophysics and solid state physics research conducted in the Physics Department there. This decision resulted in the following

investigation by the author of the electron spin resonance spectra of transition-metal ions dispersed in solid state systems.

CHAPTER II

The Spectrometer.

2.1 The Spectrometer Used in the Present Project.

Commercial spectrometers are of the "high frequency field modulation type" (Tinkham (1956)). However, superheterodyne spectrometers have been described by Schneider and England (1951), Hirshon and Fraenkel (1955), Misra (1958) and Shamfarov (1960). At the time this project was initiated, superheterodyne spectrometers were commonly held to be inherently more sensitive than those of the high frequency field modulation type (Feher (1957)), and so it was decided to build such a model.

The overall design of the superheterodyne spectrometer which was developed is indicated by the block diagram in Fig.2.1. Here, the signal power from a stabilised klyston was fed through a variable attenuator and then coupled into the sample cavity via a slide-screw tuner. The paramagnetic resonance signal appeared as part of the out-of-balance power from the bridge (T1) and fed a balanced mixer having two matched crystal detectors. In addition, this mixer received power from a stabilised local oscillator klyston, separated in frequency from the signal klystron by 45Mc./s.. The output of the mixer was fed to a low noise i.f. amplifier and audio detector. The audio frequency detector output was fed to an audio amplifier and low pass filter and then either to a video display or to a chart recorder via a narrow band amplifier and phase-sensitive detector.

The microwave frequency was measured by a Hewlett Packhard transfer oscillator and high speed counter. The magnetic field was measured by a nuclear magnetic

SUPERHETERODYNE SPECTROMETER

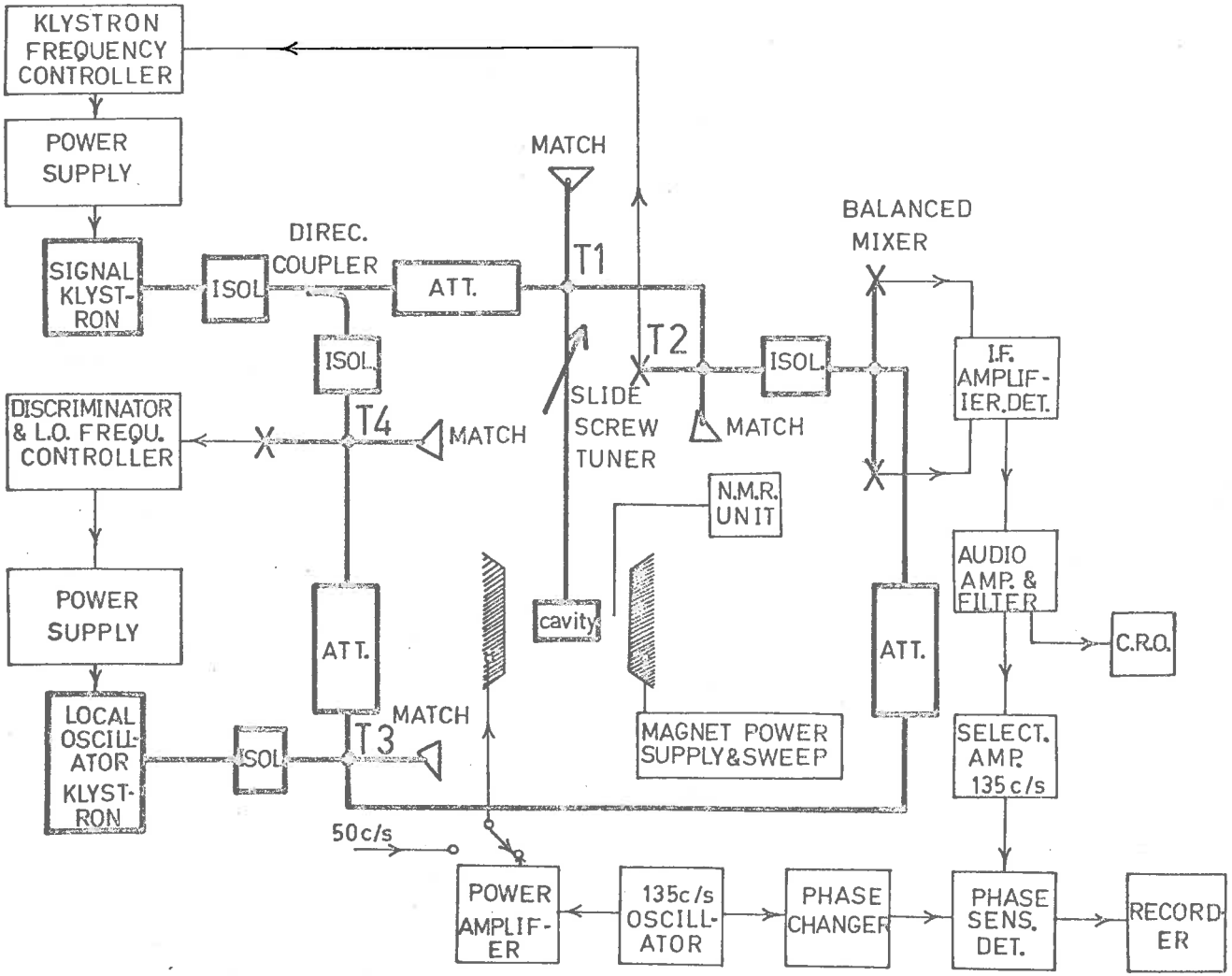

Fig. 2·1

resonance probe whose frequency was measured on the same counter. The H_{012} mode cavity could be cooled to liquid air temperatures and had provision for rotating the sample about an axis in the horizontal plane while the magnet could be rotated about a vertical axis.

2.2 Design Factors Bearing on Spectrometer Sensitivity.

Most of the electronic units built for this spectrometer are of conventional design. Their circuit diagrams are shown in Appendix A (A1-19). Consequently the following sections deal only with those design features which are relevant to a discussion of spectrometer sensitivity.

2.2.1 Signal Klystron Frequency Controller.

The signal klystron frequency (ϖ) was locked to the frequency corresponding to the minimum value of the cavity reflection coefficient (Γ) by a simple controller developed in the National Standards Laboratory, Chippendale, N.S.W., (see A6 and 7). In this circuit, a small voltage, amplitude modulated at 455Kc./s., was applied to the klystron reflector, putting a small frequency modulation on the power fed to the cavity. Any consequent sign-sensitive amplitude modulation produced by a movement of the klystron frequency from the top of the cavity Q curve (where $\frac{d\Gamma}{d\varpi}=0$) was amplified and phase detected to control the D.C. reflector voltage. This servo loop tended to neutralise any reactive shifts from the cavity resonance and hence ensured that $\frac{d\Gamma}{d\varpi}=0$ (with a response time of the order of 2μ sec.).

2.2.2 Local Oscillator Klystron Frequency Controller.

The local oscillator was frequency stabilised with the aid of a radar A.F.C. discriminator unit (Frequency Control Unit Type 100), whose circuit (modified) is shown in A 16. This unit gave a D.C.

error signal when the signal klystron frequency minus the local oscillator frequency differed from 45Mc./s.. This error signal was then used to retune the local oscillator klystron by altering the reflector potential by means of the control circuit shown in A 17. This circuit is, effectively, a D.C. amplifier whose correct operating range was obtained by adjusting the potentiometers R 13 and R 14.

2.23 The Microwave System.

A photograph of the actual waveguide system used is shown in Fig. 2.2, and a simplified version without stabilisation circuits is given in the diagram in Fig. 2.3 (A).

Here, the transmission line leading from the cavity coupling system is terminated in its characteristic impedance; and so, near resonance, the cavity coupling system can be represented by the simple equivalent circuit in Fig. 2.3 (B), (Montgomery et al. (1948)).

The iris and slide-screw tuner, which couple the cavity to the imput guide, reflect a series impedance (R_o) into this tuned circuit. For the following analysis, R_o can be taken as purely resistive and any (very small) reactive component will be incorporated in L. Hence we define the "coupling coefficient":

$$\beta = \begin{cases} R_o/R , & R \geq R_o, \\ R/R_o , & R_o \geq R. \end{cases} \qquad (1)$$

It is common in the study of low frequency resonant circuits and cavity coupling systems to specify losses in the circuit by means of a Q-factor which is

Fig. 2.2 : Photograph of the Waveguide System.

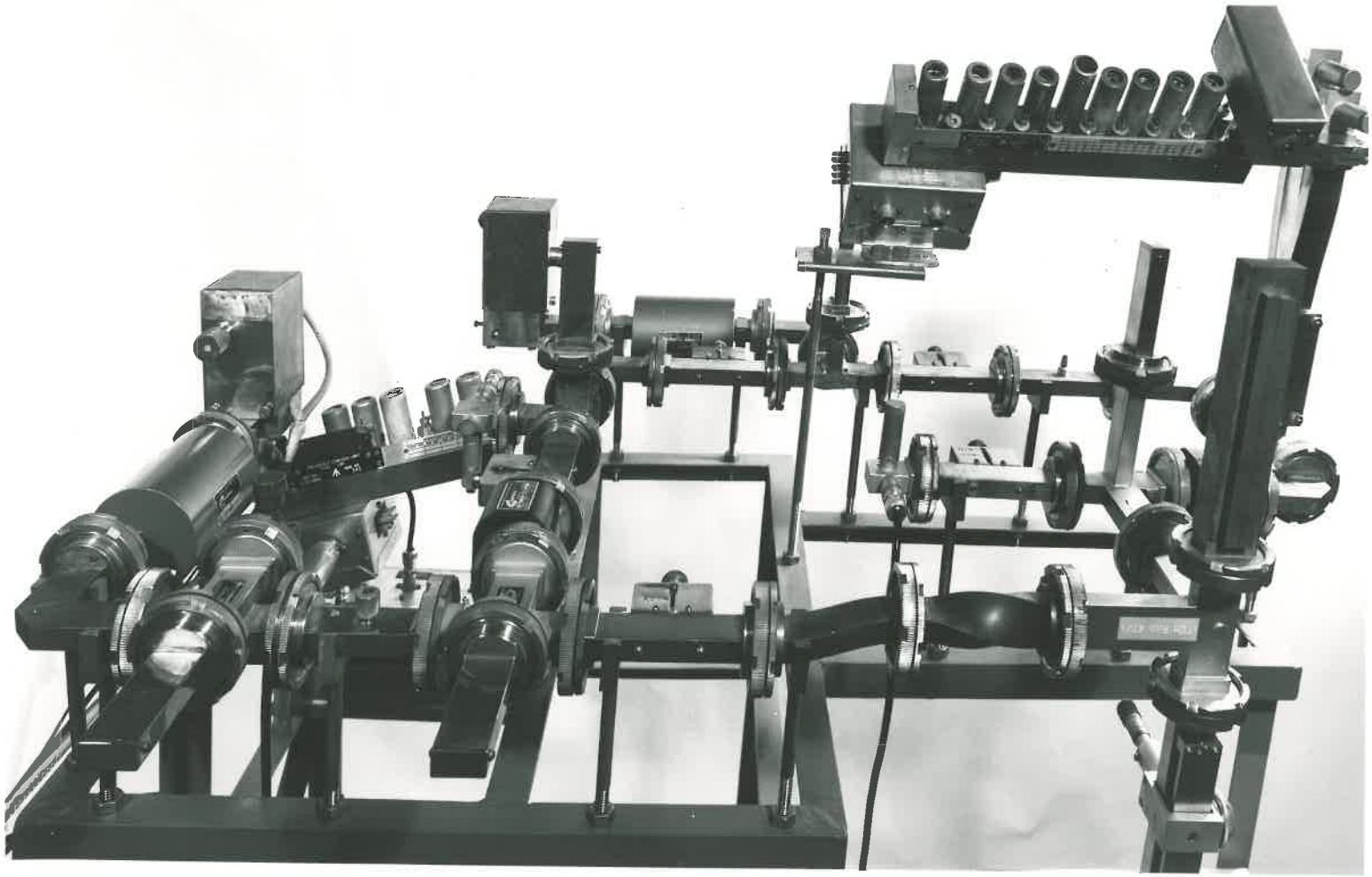

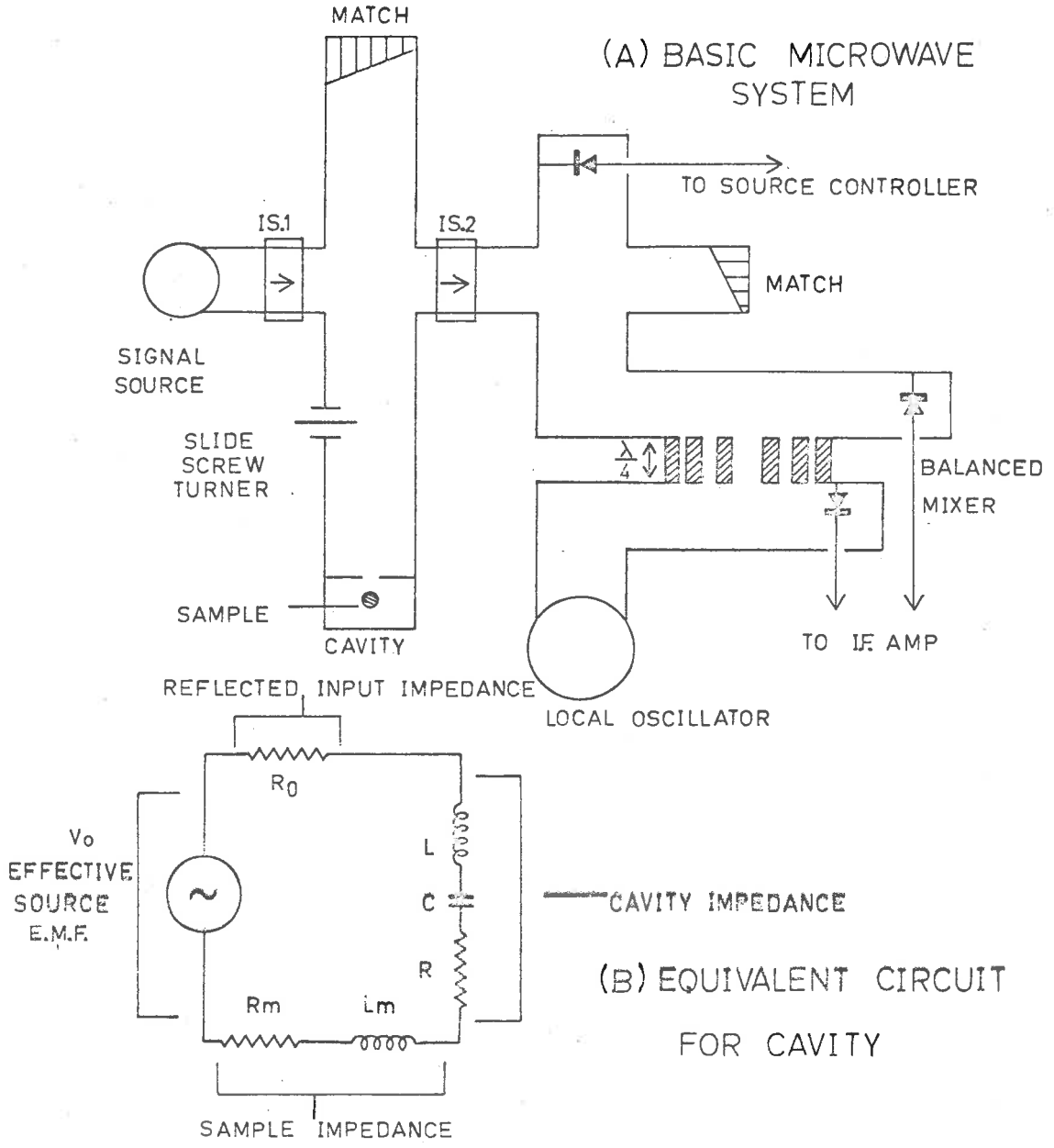
MATCH
(A) BASIC MICROWAVE SYSTEM
TO SOURCE CONTROLLER
IS.1
IS.2
MATCH
SIGNAL SOURCE
SLIDE SCREW TURNER
λ/4
BALANCED MIXER
SAMPLE
CAVITY
TO I.F. AMP
REFLECTED INPUT IMPEDANCE
LOCAL OSCILLATOR
R0
Vo
EFFECTIVE SOURCE E.M.F.
L
C
R
CAVITY IMPEDANCE
Rm
Lm
(B) EQUIVALENT CIRCUIT FOR CAVITY
SAMPLE IMPEDANCE

Fig. 2-3

defined as:

$$Q = \frac{2\pi \times \text{energy stored}}{\text{energy lost per cycle}} .$$

There are a number of Q-factors in common use which, for a cavity coupling system, differ only in the sources of dissipation included in the denominator of the equation. These are illustrated by a consideration of the circuit in Fig. 2.3 (b). In the absence of magnetic resonance and external loading, we can take R_m, L_m and R_o as short circuited, and then the Q of the system is the so-called "unloaded Q":

$$Q_u = \frac{\omega_o L I^2/2}{RI^2/2} , \qquad (2)$$

$$= \frac{\omega_o L}{R} ,$$

where $\omega_o = \frac{1}{\sqrt{LC}}$ is the angular resonant frequency of the cavity. If we now include losses in the external load, we have the "loaded Q":

$$Q_L = \frac{\omega_o L}{R + R_o} .$$

In the general case of magnetic resonance, the sample introduces an additional resistive and reactive component. But when the cavity is held to resonance by a frequency controller as in our case, the reactive component vanishes and the resistive component is given by :

$$R_m = \eta R \omega \chi''(H) Q_u , \qquad (3)$$

(Bleaney and Stevens (1953)), where η is the "cavity filling factor", and $x''(H)$ is the imaginary component of the susceptibility. Hence we can define the "magnetic Q":

$$Q_m = \frac{\omega_o L}{R + R_o + R_m} .$$

To complete the analysis, we must now introduce the "complex reflection coefficient" of the cavity for arbitrary microwave frequency and magnetic resonance absorption :

$$\Gamma = \frac{\left[R + R_m + i(L\omega - \frac{1}{C\omega}) \right] - R_o}{\left[R + R_m + i(L\omega - \frac{1}{C\omega}) \right] + R_o}$$

Remembering that $\omega_o = \frac{1}{\sqrt{LC}}$, and using equation (3) above this may be written :

$$\Gamma = \frac{R\left[1 + \eta 4\pi x''(H) Q_u \right] + i\frac{L}{\omega}(\omega^2 - \omega_o^2) - R_o}{R\left[1 + \eta 4\pi x''(H) Q_u \right] + i\frac{L}{\omega}(\omega^2 - \omega_o^2) + R_o} .$$

For small excursions of ω about ω_o, we have $\Delta\omega = 2(\omega - \omega_o)$ is small, and hence we can write :

$$\Gamma = R\left[1 + \eta 4\pi x''(H) Q_u \right] + iL\omega\frac{\Delta\omega}{\omega} - R_o$$
$$\left[1 + \eta 4\pi x''(H) Q_u \right] + iL\omega\frac{\Delta\omega}{\omega} + R_o$$

Then substituting from equation (1) we have :

$$\Gamma = \frac{1 + \eta 4\pi x''(H) Q_u + i \frac{L\varpi}{R} \frac{\Delta\varpi}{\varpi} - \beta}{1 + \eta 4\pi x''(H) Q_u + i \frac{L\varpi}{R} \frac{\Delta\varpi}{\varpi} + \beta} .$$

Equation (2) implies that this can be written:

$$\Gamma = \frac{1 - \beta + \eta 4\pi x''(H) Q_u + i Q_u \frac{\Delta\varpi}{\varpi}}{1 + \beta + \eta 4\pi x''(H) Q_u + i Q_u \frac{\Delta\varpi}{\varpi}} ,$$

which can also be put in the form :

$$\Gamma = \frac{\frac{1-\beta}{1+\beta} + \frac{1}{1+\beta}\left[\eta 4\pi x''(H) Q_u + i Q_u \frac{\Delta\varpi}{\varpi}\right]}{1 + \frac{1}{1+\beta}\left[\eta 4\pi x''(H) Q_u + i Q_u \frac{\Delta\varpi}{\varpi}\right]} .$$

When the term in the square brackets is small, this becomes:

$$\Gamma = \frac{1-\beta}{1+\beta} + \frac{1}{1+\beta}\left[\eta 4\pi x''(H) Q_u + i Q_u \frac{\Delta\varpi}{\varpi}\right] - \frac{1-\beta}{(1+\beta)^2}\left[\eta 4\pi x''(H) Q_u + i Q_u \frac{\Delta\varpi}{\varpi}\right] .$$

Finally on simplying this expression, we obtain:

$$\Gamma = \frac{1-\beta}{1+\beta} + \frac{2\beta}{(1+\beta)^2}\left[\eta 4\pi x''(H) Q_u + i Q_u \frac{\Delta\varpi}{\varpi}\right] . \quad (4)$$

Hence paramagnetic effects, and the noise associated with klystron frequency variations, cause the effective Γ of the cavity to vary and thus modify the power reflected from the cavity.

One half of the power reaching the cavity magic tee is absorbed in the matched load and the other half goes to the cavity. Then, one half of the power reflected from the cavity is absorbed in the isolator (I S. 1 of Fig. 2.3 A) and the other half is again halved by the second magic tee before it reaches the balanced mixer. So for a matched generator, the incident voltage at the cavity is $V_0(\sin \omega t)/2\sqrt{2}$ (Wilmshurst et al. (1962)). Consequently the voltage due to the signal klystron at the balanced mixer is:

$$V_s \sin \omega t = \frac{1}{4\sqrt{2}} V_0 \Gamma \sin \omega t \quad . \qquad (5)$$

Following a useful analysis of spectrometer operation communicated to the author by Dr. Faulkner of the University of Reading we note that the local oscillator klystron superimposes an additional voltage

$V_h \sin (\omega_h t + \alpha)$ on the $V_s \sin \omega t$ (where $\omega - \omega_h$ is 45Mc./s.).

Hence the total power in a matched detector of resistance R_1 is :

$$P_c = \frac{| V_s \sin \omega t + V_h \sin (\omega_h t + \alpha)|^2}{R_1} \quad .$$

When V_h is large enough, the output voltage (V_D) of the detector is given by the simple square law relation :

$$V_D \propto P_c$$

Hence we have for the I.F. signal voltage :

$$V_D = C\left\{ V_h^2 + V_s^2 + 2 V_s V_h \cos\left[(\omega - \omega_h)\, t - \alpha \right] \right\}$$

(on averaging over a period greater than $\left(\frac{1}{\omega}\right)$ but much shorter than $1/(\omega - \omega_2)$), where C depends on the detection conditions. This gives :

$$V_D \propto V_h^2 + \frac{1}{32}\left(\frac{1-\beta}{1+\beta}\right)^2 V_o^2 + \frac{1}{32}\left[\frac{2\beta Q_u}{(1+\beta)^2}\right]^2 \left(\frac{\Delta\omega}{\omega}\right)^2 V_o^2$$

$$+ \frac{V_h V_o}{\sqrt{2}} \frac{\beta}{(1+\beta)^2}\, \eta k \omega r''(H) Q_u \quad , \qquad (6)$$

on substituting (4) and (5) above, and with $V_h >> V_s$.

Similarly we can obtain the total power in the klystron frequency controller detector (again assuming perfect match to the waveguide resistance R_1) :

$$P_s = \frac{\left| V_s \sin \omega t \right|^2}{R_1}$$

This can also be written :

$$P_s = C'\left\{ \left(\frac{1-\beta}{1+\beta}\right)^2 V_o^2 + \left[\frac{2\beta Q_u}{(1+\beta)^2}\right]^2 \left(\frac{\Delta\omega}{\omega}\right)^2 V_o^2 \right\}. \qquad (7)$$

An inspection of the last term in equation (6) above shows that the maximum signal voltage occurs when $\beta = 1$. However, this makes the frequency noise term (second last term) large in two ways :-

1) the $\frac{\beta}{(1+\beta)^2}$ component of the term is at a maximum for $\beta = 1$,

2) the $\Delta\omega/\omega$ component becomes large when $\beta = 1$. This is due to the fact that putting $\beta = 1$ makes the first term in equation (7) equal to zero and so turns off the bias applied to the detector crystal in the klystron frequency control loop (since the second term is negligible). Hence the stabiliser becomes inoperative.

In practice the iris was cut so that $\beta \doteq 1$ and small adjustments were made by means of the slide-screw tuner till an optimum signal to noise ratio was obtained on the video display. (This was found to correspond to a current of 15μ amps. at the controller crystal).

Although the frequency noise term shown above is a second order effect, it was found to be very important, (Feaney et al. (1961) have argued that a term of this form limited the sensitivity of their spectrometer for klystron powers above about 10mw).

It should be noted that the above calculation of the effect of frequency noise assumed that small frequency excursions were made about the cavity resonance frequency. Any overall reactive drift in the cavity parameters would introduce an imaginary component of the reflection coefficient ($i\Delta\Gamma$), which would form a cross term with the imaginary $\Delta\omega/\omega$ term and so introduce frequency noise as a first order effect in the power into the detector. This fact places stringent requirements on the mechanical stability of the cavity coupling system and indicates the significance of microphonics.

Another important source of microwave noise might originate in the noise sidebands of the local oscillator signal. Two portions of these sidebands, equal in width to the i.f. bandwidth of the receiver and located symmetrically with respect to the local oscillator frequency at a distance equal to the i.f., might contribute noise to the receiver output. In our case, where the signal voltage was a small fraction of the detected r.f., this source of noise might become the limiting factor in the overall spectrometer noise figure - especially as the local oscillator was a conventional 723A/B klystron which is known to have strong noise sidebands (Hamilton et al. (1948)).

This limitation was eliminated by use of a balanced mixer (Fig.2.3A and A 8). Here the $\lambda/4$ phase change between the two arms ensured that the mixer crystals (of opposite polarity) were driven in shunt by the local oscillator and in push-pull by the received signal. Hence in their summed i.f. output, the signal voltages reinforced one another, while the local oscillator frequency noise components cancelled, (provided the mixer crystals were carefully matched).

2.2.4 The I.F. Amplifier and Detector.

The output of the balanced mixer was fed to the cascode input and thence into the two following pentode stages of a radar i.f. unit (Receiver Unit I.F. Type 219), whose circuit (modified) is shown in A 9. The germanium diode detector was placed in the plate circuit of the second 6AM6 tube, since later stages were found to saturate.

2.2.5 The Audio Amplifier and Filter.

The detected signal was amplified by the low noise transistorised video amplifier shown in A 10, and then filtered in the following 10 Kc./s. low pass filter (to reduce the contribution from noise components). This filter passed enough of the Fourier components of the line shape function to prevent significant distortion in its video display.

2.2.6 The Phase-Sensitive Detection System.

One common way of further reducing the bandwidth without distorting the line shape is to use some form of phase-sensitive detection (Ingram (1958)).

For the spectrometer being described, this meant that the D.C. magnetic field (H_o), applied to the specimen, had superimposed on it an A.C. component modulated sinusoidally at 135c/s. with an amplitude (H_m) which was less than the half width of the resonance line being studied. This modulation was supplied by the

oscillator (A 14) and power amplifier (A 15).

Hence from equation (4) of section 2.2.3, it can be seen that if the microwave frequency is held constant, then the reflection coefficient of the cavity becomes modulated with a frequency of 135c/s. (and an amplitude proportional to $H_m \left[\frac{dx''(H)}{dH}\right]_{H_o}$ as Andrew (1958) showed by a simple Taylor series expansion). So, by comparison with equation (6) of section 2.2.3 the A.C. output of the audio detector is seen to be of the form :

$$V^1 = \left[K V_h V_o \frac{\beta}{(1+\beta)^2} \eta Q_u \right] \left[\frac{dx''(H)}{dH}\right]_{H_o} H_m \sin 2\pi f t, \quad (7)$$

where K is a function of the detectors and amplifiers and f is the frequency of the phase sensitive detection system, (135c./s. in this case).

This output was fed through a 135c./s. selective amplifier (A 11, 12) to a phase-sensitive detector (A 13). This phase-sensitive detector included a centre-tapped secondary winding on a signal transformer. Alternate ends of this winding were grounded on successive half cycles of the 135c./s. reference voltage, and the output was taken from the centre tap of the winding. The effect of this action was to reverse the polarity of the signal every half cycle of the reference voltage. A mathematical analysis (Lawson and Uhlenbeck (1948)) shows that this would produce an output of the form :

$$V = A \left[\frac{dx''(H)}{dH}\right]_{H_o} \left[\cos\phi + \cos(4\pi f t + \phi)\right],$$

where ϕ (which was set equal to zero for maximum output) is the phase difference between the signal and reference voltages.

This output was then fed into a long time constant (~ 1 sec.) filter which eliminated the second term in the second set of square brackets and reduced the noise bandwidth (Bw) to ~ 1c./s. centred on 135c./s.. So the signal which went to the chart recorder via a D.C. amplifier was a measure of $\left[\frac{dx''(H)}{dH}\right]_{H_o}$.

In order to observe resonance lines, it was necessary to sweep H_o linearly so that $\left[\frac{dx''(H)}{dH}\right]_{H_o}$ might be graphed as a function of H_o on a chart recorder.

2.3 Comparison with High Frequency Field Modulation Spectrometers.

A comprehensive treatment of spectrometer sensitivity considerations was given by Feher (1957) who analysed a wide variety of cavity arrangements and detection systems. He showed that the limit of spectrometer sensitivity is set by the over-all noise figure:

$$F = (G N_k + F_d + F_a)/G$$

where, G is the conversion gain of the mixer,

N_k is the noise figure at the mixer input due to random amplitude or frequency fluctuations originating in the microwave sources or components.

F_a is the noise figure of the amplifier,

F_d is the noise figure of the mixer.

The sensitivity discussion then centres around an analysis of G, N_k, F_a and F_d. As Feher (1957) shows,

the sum of F_a and F_d can be minimised by using a superheterodyne spectrometer with an i.f. in the region of 20-60Mc./s., and G can then be maximised by adjustment of the local oscillator power.

Feher indicates that the calculated sensitivity of a superheterodyne detection scheme is ten times that of the best possible straight detector using high frequency field modulation. The calculation anticipates that the crystal detector noise is the limiting factor. However, during the course of this project, evidence has appeared that the superheterodyne may be less effective than Feher calculates at higher klystron powers (above about 10mw), because klystron frequency noise, not detector noise, becomes dominant (Feaney et al. (1961)). Since klystron noise (and also that due to microphonics in the cavity coupling system) is like crystal flicker noise in having a power spectrum inversely proportional to the frequency, high frequency field modulation is helpful whether microwave or crystal noise is dominant.

In the above spectrometer, where low frequency field modulation was used, instabilities in the cavity coupling system, due to mechanical vibrations, were found to contribute strongly to noise. This is probably due to the fact that(in order to eliminate pickup from near-by radar transmitters) the spectrometer was built inside a Faraday cage which turned out to have a microphonic floor. Accordingly, it is now proposed to prepare a concrete base for the spectrometer and to shock mount the microwave components more carefully.

However there seem to be certain advantages in this low frequency field modulation superheterodyne spectrometer which are not available in high frequency field modulation systems:

1) Large field modulation amplitudes are easily achieved at low frequencies (up to 35 oersteds in this case instead of the 5 oersteds or so which is convenient in a high frequency device). This gives extra sensitivity on the wide lines (up to 50 oersteds wide) commonly found in this project, (as equation (7) of Section 2.2.6 shows).

2) Low frequency field modulation facilities can be external to an ordinary metal cavity. These are easy to construct and permit a wide diversity of design convenient for irradiation and low temperature work.

3) With extremely stable klystrons operating at low powers, the reduction in crystal flicker noise achieved by detecting at 45Mc./s. instead of 100Kc./s. is probably significant.

4) Modulation of the resonant frequency of the cavity by mechanical distortions due to field modulation (the so-called "cavity effect") introduces frequency noise to first order (see Section 2.2.3). This is more readily removed by the signal klystron frequency controller when the field modulation frequency is low, as it is in this spectrometer.

Also, unless special bucking arrangements are made, as in the homodyne system of Gordon (1961), the high frequency field modulation spectrometer may saturate the sample in the cavity before enough power is available at the crystal detector for efficient operation. Whereas in the superheterodyne, the crystal may be biassed by the local oscillator, and so the cavity power can be reduced until it does not saturate the sample. This is useful in measuring the absorption of centres with long spin-lattice relaxation times such as

the free radicals, damage centres and some S-state ions which are all to be studied at Adelaide University.

The sensitivity of the spectrometer was measured using a sample of $CuSO_4 \cdot 5H_2O$ containing 2×10^{16} spins. A signal to noise ratio of at least 100 : 1 was obtained with a 0.1c./s. bandwidth and a field modulation width of 17 gauss peak to peak. The signal klystron (a Varian V-A201B) was then operating with a power output of about 40mW, and the local oscillator at about 10mW. Hence, allowing for a reduction in the line width to 2.7 gauss and reducing the field modulation amplitude to less than this, we can estimate that the minimum number of DPPH spins observable would be about 12×10^{12}, which is the same as that observed by Llewellyn (1957) for a high frequency field modulation system, and by Hirshon and Fraenkel (1955) for a superheterodyne system. This corresponds to a x''_{min} of 10^{-11}, (all measurements being taken at 300°K).

Lower signal to noise ratios were obtained with larger bandwidths (Bw), (see Fig. 2.4). This figure shows traces from a sample of 2×10^{16} spins of $CuSO_4 \cdot 5H_2O$ taken with different bandwidths. Conversely, the signal to noise ratio could in principle be increased indefinitely by reducing the bandwidth below 0.1c/s.. In practice, this would give rise to distortion of the line shape and also to problems arising from instabilities in the D.C. amplifiers.

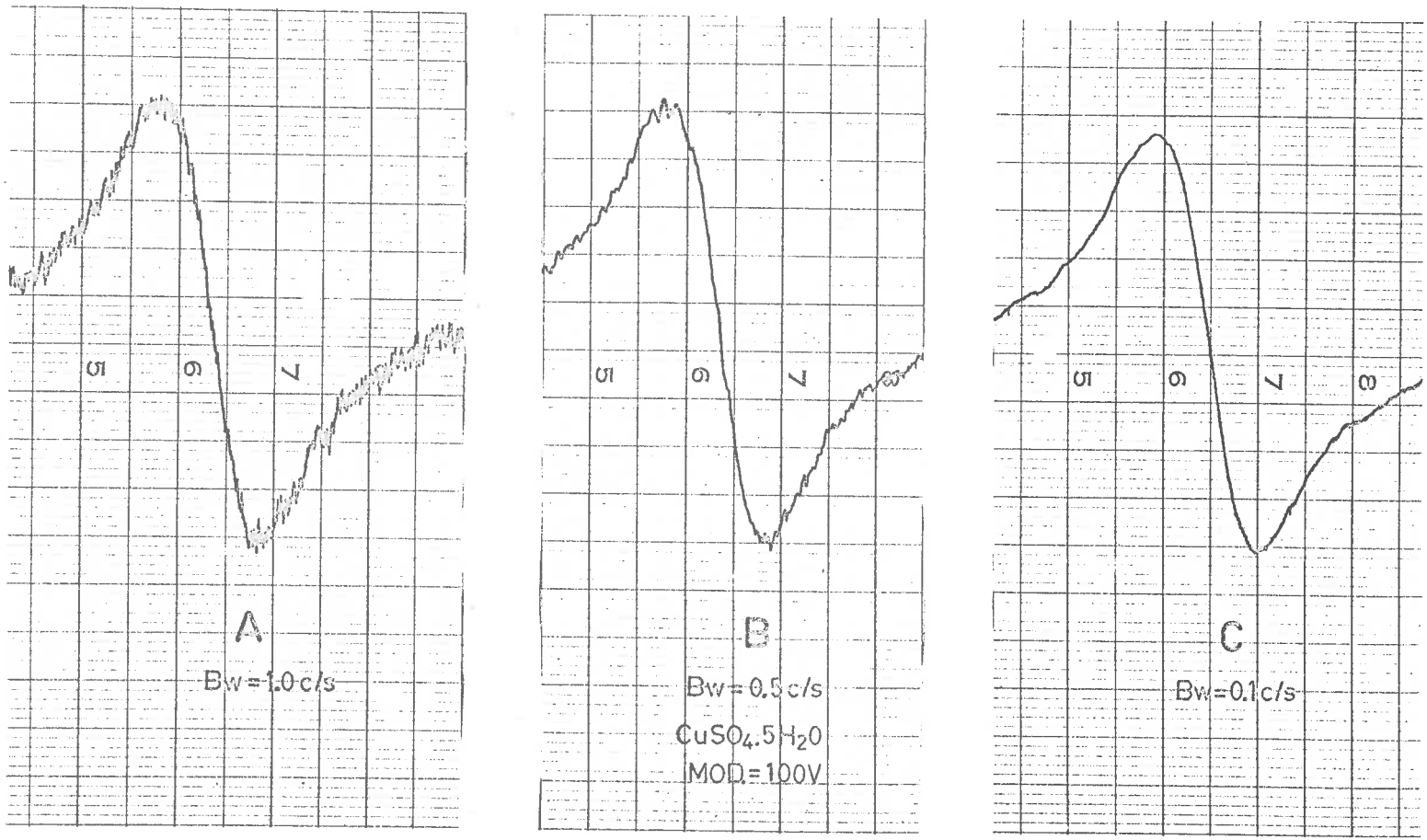

Fig. 2·4

CHAPTER III

Electron Spin Resonance in Minerals.

3.1 The Orientation of this Project.

It seemed to the author that one useful way of extending existing knowledge of the paramagnetism due to transition metals in solid state systems would be by a study of the high spin S-state ions occurring as impurities in hitherto unexamined host lattices. These ions, especially Mn^{++}, Fe^{+++}, and Gd^{+++}, are known to give strong spectra at room temperatures (Bleaney and Stevens (1953)) and so can conveniently be studied with the aid of the apparatus described in Chapter II.

In addition to the quest for measurements to aid in the theoretical analysis of the ground state splitting of S-state ions (see Chapter IV), the aim of this project was to seek further experimental data on some other aspects of electron spin resonance phenomena that await detailed explanation. In particular measurements were sought on :

1) The adequacy of the Spin Hamiltonian description of e.s.r. phenomena.
2) The effects of covalency and other departures from the crystal field model.
3) The existence of interactions between the nuclear quadrupole moment and the gradient of the electric field acting on it.
4) The accurate fitting of the position and intensity of the forbidden $\Delta M=2$ lines found near $g=4$.
5) The existence of Jahn-Teller effects and other modifications of the site by the paramagnetic impurity.

3.2 The Source of Specimens.

At the present time it is useful for purposes of analysis to study paramagnetic resonance in substances with fully established physical and chemical properties.

Accordingly it seemed that the search for new materials could profitably be undertaken by a survey of natural minerals, as these have their physical properties conveniently tabulated by Dana (1932), and their structures are usually described by Wyckoff (1960). Another useful source of mineralogical information which appeared recently is Deer et al. (1962).

The author is grateful to the directors of the South Australian Museum, to Dr. Jones of the Geology Department at the University of Adelaide and to Mr. Troup of Monash University for the loan of most of the samples studied in this investigation. Several other samples were purchased from dealers in ornamental stones.

3.3 The Experimental Results.

More than one hundred mineral samples were examined for e.s.r. effects and thirty one gave positive results. Of these, fifteen were sets of lines which had been previously discussed in literature. This resulted in the observation of previously unreported lines in the following sixteen minerals :- Feldspar, Neptunite, Apatite, Tourmaline, Danburite, Sphene, Kunzite, Smithsonite, Scheelite, Benitoite, Apophyllite, Chili Nitre, Jade, Turquoise, Australite and Opal. All these, except the last two (which were glassy) and the previous two (which were polycrystalline), gave distinct structural spectra.

The spectra examined in detail were those due to Fe^{+++} in Benitoite and Mn^{++} in Smithsonite. In addition, an analysis was made of some hitherto unrecorded forbidden lines due to Mn^{++} in Apatite and Scheelite. Observations of broad resonance lines in glassy Australites and Opals prompted an investigation of synthesised Borax glasses doped with transition metals. Defect centres were studied by means of e.s.r. in these Borax glasses as well as in natural Apophyllites and Apatites.

3.4 The Accuracy of Measurement.

The resolution of the fine structure and hyperfine structure of the spectra was found to be limited by the width of the absorption lines. The most important sources of broadening encountered in this survey and the means adopted for offsetting them were as follows :

1) Spin-spin broadening :

This is due to coupling between paramagnetic centres (Van Vleck (1948)). It could be reduced by selecting magnetically dilute crystals — containing about 10 parts per million, by weight, of paramagnetic material.

2) Inhomogeneities of the crystal field :

These give rise to different zero-field splittings of the energy levels and an anisotropic variation in the e.s.r. line width, which was at a maximum for lines furthest from g=2. This was important in all samples studied and could only be reduced by selecting crystals relatively free from twinning or mosaic structure.

3) Saturation by the radiation field :

Broadening due to saturation occurred in materials having long spin lattice relaxation times (e.g. Mn^{++} in Smithsonite and damage centres in most materials). This effect was worse at low temperatures where the spin-lattice relaxation times were longer. Such broadening could be offset by attenuating the power from the signal klystron, but this of course entailed a loss of sensitivity (as is indicated by equation (6) of Section 2.2.3).

With practice it was found possible to measure line centres to within about one tenth of the line width, either by setting the n.m.r. line to coincidence with the e.s.r. line on the oscilloscope display, or (if the lines were very narrow) by graphical interpolation on the charts from the pen recorder.

In some cases, such as Benitoite, where the lines were highly anisotropic, an important source of error might originate from uncertainty in orientation of the sample. However this was overcome by use of a H_{012} mode cavity where the sample platform could be rotated about an axis in the horizontal plane while the magnet was rotated about a vertical axis. Here it was possible to align the crystals very accurately (to within $\frac{1}{2}°$) by observing the effect of small angular corrections on the position of the lines on the oscillograph display.

CHAPTER IV

Fe^{+++} in Trigonal Sites in Benitoite.

4.1 Properties of Benitoite.

Benitoite ($BaTi(SiO_3)_3$) has been found only near the headwaters of the San Benito River in Southern California. It is quite hard (H=6.2-6.5), is usually bluish in colour and fuses near 1200°C. The strong dichroism (O = colourless, E = deep blue) enables the c axis to be found by using polarised light. The author's comparisons of the e.s.r. spectra with the flame spectroscopy analyses done at the Australian Mineral Development Laboratories, Parkside, South Australia, indicate that the sapphire-bluish colouring is due to traces of Fe^{+++} present as an impurity in the Barium and Titanium sites. All samples studied were found embedded in a hard matrix along with crystals of Naptunite. The matrix could be removed by dilute HCℓ.

The symmetry class of Benitoite was established by Palache (1909) following a preliminary observation of forms by Rogers (1908). Figure 4.1 shows a typical combination of forms. These make it the only known crystal representing class 22 of Groth ($\bar{6}m2$). All crystals observed by the author were devoid of twinning and showed the $(10\bar{1}1)$ faces prominent. These aided in mounting the crystals by eye with the c axis orientated in a desired direction.

A complete determination of the crystal structure was given by Zachariasen (1930). Fig. 4.2 shows the projection of the structure on the 0001 plane. From the point of view of the impurity centres to be discussed, the following structural details only are important.

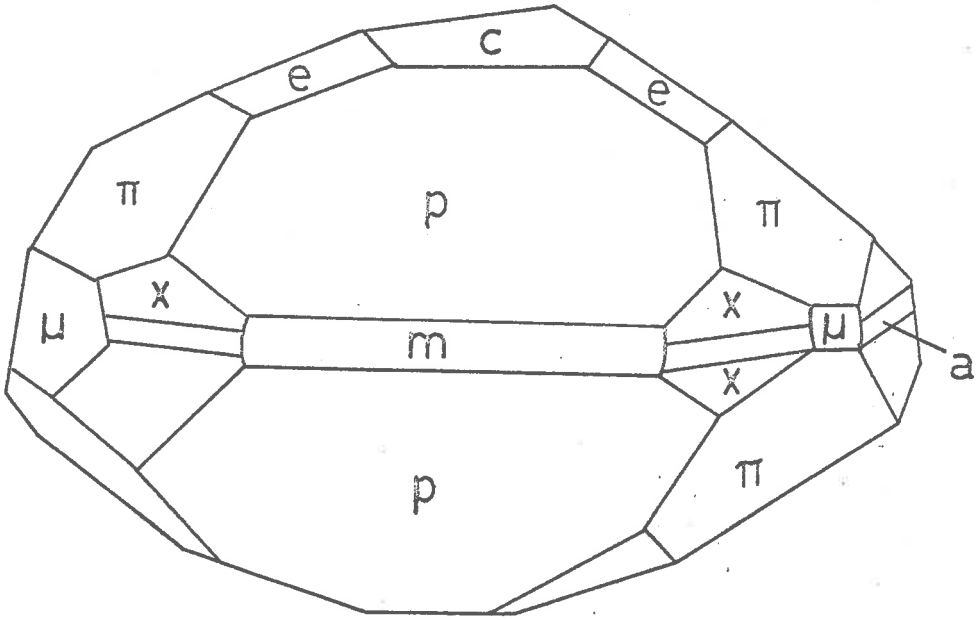

Prisms : m(10$\bar{1}$0), μ (01$\bar{1}$0), a(11$\bar{2}$0).

Pinacoid : c(0001).

Trigonal pyramids : p(10$\bar{1}$1), π (01$\bar{1}$1), e(01$\bar{1}$2).

Second order Pyramid : x(22$\bar{4}$1).

Fig. 4-1 The forms of Benitoite.
(After Palache (1909)).

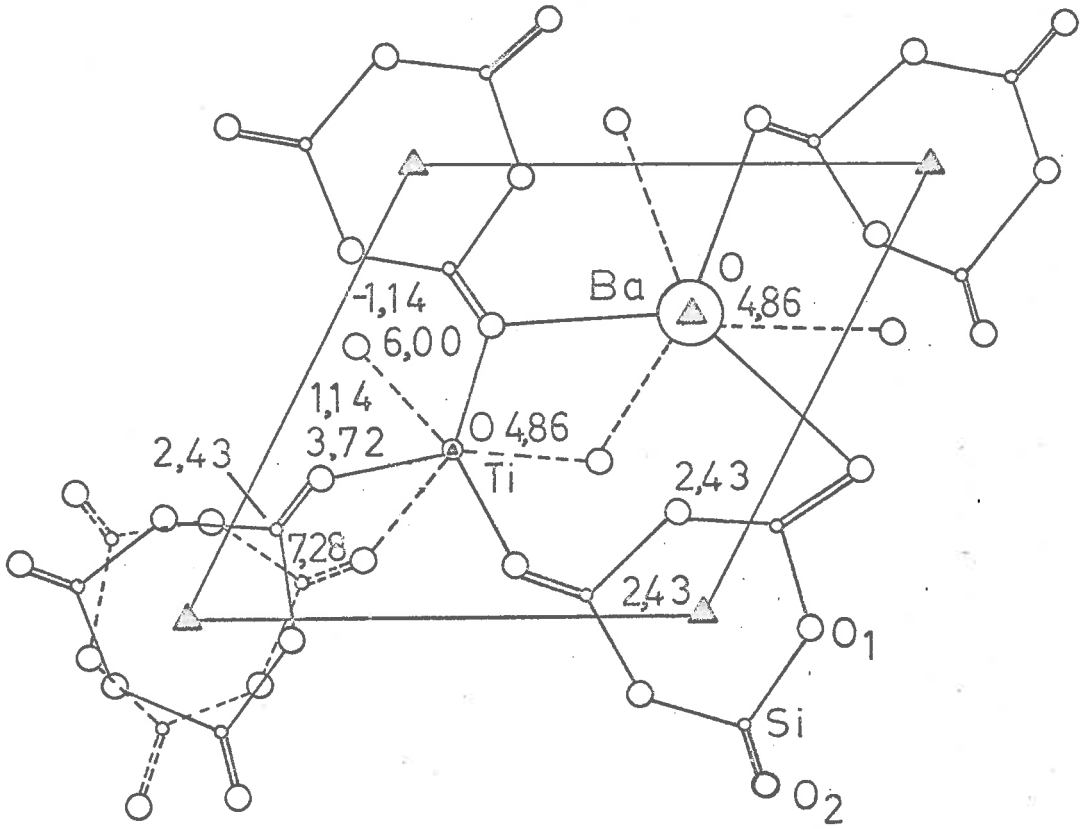

Fig. 4·2 Projection of Benitoite cell on the plane 0001.

(After Zachariasen (1930)).

The two Ba and the two Ti atoms lie on trigonal axes parallel to the c axis in twofold positions on either side of a mirror plane. The Ba atoms are surrounded by six oxygen atoms at a distance 2.74 A.U. forming a distorted octahedron. Six other oxygen atoms have a distance of about 3.4 A.U. from the Ba, but we cannot consider them as belonging to the first sphere of co-ordination around the Ba. Ti atoms are surrounded by six oxygen atoms in an almost regular octahedron, the distance Ti - O being 1.96 A.U..

4.2 General Characteristics of the Spectrum.

The room temperature e.s.r. spectrum of Fe^{+++} introduced isomorphically into Benitoite lattices to an ion concentration of 10^{-5}-10^{-4} (as shown by flame spectroscopy) was investigated at X band and Q band frequencies for magnetic fields up to 15,000 oersteds. In addition X band measurements were made at liquid air temperatures, where the zero field splittings were also measured.

Very many lines were observed in the X band measurements taken at full spectrometer sensitivity; but it was found that there were ten main lines in two similar systems each of five lines. When the external magnetic field was applied parallel or perpendicular to the c axis, both the 5 line spectra overlapped each other exactly. Also the combined spectrum was isotropic in the equatorial plane.

With the aid of a stereogram (Barrett (1943)), it was seen that if θ, ϕ are the angular polar coordinates of the D.C. magnetic field measured relative to the c axis and an arbitrarily chosen x axis in the equatorial plane, then the two sets of five lines coincided for all θ at values of ϕ 60° apart. Between these values of ϕ the two sets of lines moved apart. Both spectra were observed to collapse to a minimum

spread for θ near 55° no matter what the value of ϕ.

A much weaker set of ten lines which appeared to have similar angular properties to the main set, was observed to be spread over a narrower range of magnetic fields.

The ten main lines have tentatively been assigned to Fe^{+++} substituted into the two different Barium sites of trigonal symmetry. This is because the large size of the Barium sites could be expected to facilitate prolific substitution and so give rise to strong lines. Also the wide splitting of the lines was seen to indicate a strong axial component of the crystal field which is in accordance with the X-ray data quoted above for the Barium sites. Conversely, the ten weak lines, whose splitting was less than that of the main set, were assigned to the much smaller and more nearly octahedral pairs of Titanium sites. However it should be borne in mind that these sites may be distorted on substitution of the Fe^{+++} ions.

Some very weak lines at low fields, close to $g = 4$, were attributed to forbidden $\Delta M = 2$ lines of the main spectrum. Also four weak lines near $g = 2$ were thought to be due to the Cu^{++} ions whose presence was indicated by flame spectroscopy.

Other very weak lines were observed but have not yet been assigned to any centre. They may result from many possibilities, e.g. :

1) Iron ions located at the Silicon sites.
2) Spectra caused by neighbouring ion pairs.
3) Other unknown paramagnetic impurities.

4.3 The Zeeman Effect in ^6S-State ions in Trigonal Electric Fields.

At ordinary temperatures, free Fe^{+++} ions are

in the ground configuration $3d^5$ and ground term ^6S. In octahedrally coordinated Fe^{+++} ions, this ground term becomes $^6A_1$ and is typically at least 10,000 cm.$^{-1}$ below the nearest excited term $^4T_1$ (Griffith (1961)). Consequently, in estimating the very much smaller splittings of the ground term studied in e.s.r. (of the order of 0.3 cm.$^{-1}$), we can ignore any additional mixing with the distant excited terms caused by an operator (H') which corresponds to the small magnetic perturbations. The resulting error, as estimated by second order perturbation theory, is then only :

$$\Delta E = \sum_j \frac{|(0|H'|j)|^2}{E_0 - E_j} \quad , \text{(where } j = \text{excited states).}$$

For fine structure splittings of the order of an X band quantum this becomes :

$$\Delta E \sim \sum_j \frac{|\pm 0.3|^2}{10^4} \text{ cm.}^{-1}.$$

As we sum over the higher multiplets the terms in this series tend to cancel and so we obtain finally :

$$\Delta E \sim 10^{-5} \text{ cm.}^{-1} ,$$

which is negligible.

We know that the wave functions of the ground multiplet are of the general form :

$$|M_s') = \Sigma C_0 |M_s) + \Sigma C_j |x_j) ,$$

where

$$|M_s) = |3d^5, {}^6S, M_s) ,$$

and the $|x_j)$ are the excited states coupled in by spin-orbit or spin-spin operators, or else states mixed in by interaction with the nearest neighbours.

We expect $\Sigma C_0 \doteq 1$ and the $C_j \ll 1$ since the observed ground state splittings, resulting from the

interaction of the admixed orbital moments with the crystal field, are very small. (Also the only excited terms within the $3d^5$ configuration which can be mixed in by spin-orbit coupling are the $|3d^5, {}^4P, M_s)$, and in this case the $C_j = 0.003$, as may be seen by substituting appropriate values of the spin orbit and Racah parameters into the treatment given by Griffith (1961)).

The exact admixing is not yet known although various order of magnitude arguments have been developed to explain the observed interaction with the various symmetry components of the crystal field. Thus recently, Pryce (1950) proposed a spin-spin interaction to account for the splitting by the axial components of the crystal field. Van Vleck and Penney (1934), Watanabe (1957) and Powell et al. (1960) have considered the effect of higher order processes involving spin-orbit coupling and the components of the crystal field, and Kondo (1960) has analysed the effects of overlap and covalency. Further e.s.r. and optical studies should add to our knowledge of these effects. Meanwhile we can proceed as follows.

In the absence of an applied magnetic field, a Heitler-London treatment of the interaction of all other ions in the lattice with the Fe^{+++} ion would consider their combined effect as being that of a system of external point charges collectively giving a potential V which acts as a perturbation on the d electrons of the Fe^{+++} ion. Hence we consider matrix elements of an electrostatic operator of the form :

$$\left(M_s'' = k \left| \sum_i V_i e \right| M_s'' = \ell \right) , \qquad (1)$$

(where e is the electronic charge, i runs over the perturbed d electron wave functions of the ion, and suitable linear combinations of the M_s'' approximate the M_s').

In this case, where the other ions are assumed to be external to the perturbed wave functions, V_i would be a solution of Laplace's equation for the space in the region of the wave functions, and so could be expressed as a power series in the homogeneous polynomials :

$$V_i = \sum_{\ell=0}^{\infty} \sum_{m=-\ell}^{\ell} A_\ell^m \; r^\ell \; Y_\ell^m \; (\theta_i, \phi_i) \quad , \qquad (2)$$

where $r^\ell \; Y_\ell^m$ are the spherical harmonic polynomial functions which form the basic vectors of the irreducible representations $D_\ell(R)$ of the full rotation group, (see Appendix C5).

If now we choose the C_3 axis as the polar axis for expressing the field of V, then V will have 3-fold axial symmetry i.e. :

$$V\ (\phi + 2n\pi/3\ ) = V(\phi)$$

Hence in (2), $m = 0, \pm 3, \pm 6, \pm 9, \ldots$ (since the ϕ dependence of $r^\ell \; Y_\ell^m$ is indicated by noting that $Y_\ell^m = P_\ell^m (\cos\theta) \exp(im\phi)$ where the $P_\ell^m (\cos\theta)$ are the generalised Legendre polynomials).

We can further reduce the number of effective terms in (2) by restricting the $|x_j\ )$ to configurations involving s,p and d electron functions (which can be expressed in terms of linear combinations of spherical harmonics with $\ell < 2$). In this case, the triangle rule of spherical harmonic integration eliminates any effect on(1) by terms in (2) with $\ell > 4$, and so these may be ignored.

Still, the matrix elements of the few remaining terms of the form $A_\ell^m \; r^\ell \; Y_\ell^m$ cannot be evaluated since we do not know either the A_ℓ^m or the detailed nature of the set of states $|M_s'\ )$. However two procedures have been suggested for using what information we do have to get the general form of these matrix elements, and those

including Zeeman interactions, in terms of arbitary constants which may then be determined by experiment. These procedures are outlined in the following two sections.

4.3.1 Calculation Using Zero Magnetic Field States as Basic Vectors.

This very general approach was developed by Koster and Statz (1959) and Statz and Koster (1959) and applied to Fe^{+++} in cubic sites by Aisenberg, Statz and Koster (1959). We shall carry through a calculation of this type for Fe^{+++} in a trigonal field, and hence show that the usual analysis of this case in terms of a "Spin Hamiltonian" involves a number of physical assumptions in addition to those already made, and so may not accurately describe the results of experiment.

We assume as above, that L,S, and J are good quantum numbers (but M_L, M_S and M_J are mixed states), and we apply perturbations to the isolated ground term ^6S. We have already shown that these assumptions would only give rise to errors of the order of $10^{-5}cm.^{-1}$.

We do not know the exact effect of the small magnetic/pertubations within the atomic system which, together with the crystal field, give rise to a splitting of the ^6S ground state, even in the absence of an applied magnetic field. However we do know that in zero magnetic field, the ground state eigenfunctions must transform as basic vectors of the irreducible representations of the C_3 double group for this case of trigonal symmetry. If we consider only the lowest antisymmetrised state of the free ion, i.e.that with angular momentum 5/2, then we have to find out what linear combinations we can make of the 6 substates such that these combinations form bases for irreducible

representations of C_3. These new states can be taken as having the general (geometrical) form of the exact low-lying eigenstates of the ion in the crystal (including all interactions with higher orbits and neighbouring ions).

In our case it is easy to see, from the characters of the irredusible representations of the C_3 double group and the representation whose basic vectors are the six $S = 5/2$ sublevels, that, as the crystal field operator (H_o) is applied to the free ion, the sixfold degeneracy will split into three doubly degenerate energy levels whose states form the bases for the irreducible representations $2\Gamma_4$, $2\Gamma_5$ and $2\Gamma_6$. (see Appendix C 1).

We assume as before that these levels lie so far from the higher levels that we need not consider the latter when we apply the magnetic field, i.e. the magnetic splitting is very much less than the distance to the higher levels.

On applying the magnetic field, the new Hamiltonian is :

$$H_1 = H_o + \beta \ \underline{H}.\underline{J} \ ,$$

where the $\beta \ \underline{H}.\underline{J}$ is considered as a perturbation acting on the eigenstates of H_o found above. We make use of the symmetry of the case to reduce the number of independent matrix elements in the perturbation calculation. We note that J_z forms a basis for one irreducible representation of C_3, and J_+ and J_- are bases for a pair of representations that are complex conjugates of one another. We can therefore write our Hamiltonian in the form :

$$H_1 = H_o + \beta \left[\tfrac{1}{2} H_+ J_- + \tfrac{1}{2} H_- J_+ + H_z J_z \right] \ ,$$

where $H_\pm = H_x \pm i H_y$ and $J_\pm = J_x \pm i J_y$.

Hence using the orthogonality relations described in Appendix C 2, the perturbation matrix may now be written down with the number of independent constants that symmetry permits, plus the two energy separations ΔE_1, ΔE_2 between the doublets at zero magnetic field. This gives the secular matrix :

$$\begin{vmatrix} a_1 H_z, & a_7 H_z, & -a_{12} H_-, -a_8^* H_-, & -a_{18} H_+, & a_{14}^* H_+ \\ & a_2 H_z + \Delta E_1, & -a_8 H_-, -a_{13} H_-, & -a_{13}^* H_+, & a_{10}^* H_+ \\ & & -a_1 H_z, -a_7^* H_z, & -a_{14} H_-, & -a_{18} H_- \\ & & & -a_2 H_z + \Delta E_1, & -a_{10} H_-, -a_{15} H_z \\ & & & a_5 H_z + \Delta E_2, & a_{11} H_z \\ & & & & -a_5 H_z + \Delta E_2 \end{vmatrix}$$

where only the upper triangle is shown and a_1^* is the complex conjugate of a_1.

This matrix takes into account the geometry of the wave functions and the lattice and so the constants are nongeometrical. The matrix is Hermitian, therefore the diagonal elements are real. Hence ΔE_1, ΔE_2 and a_{1-6} are real, and all other a_1 are in general complex and so represent two physical constants each. The inclusion of time inversion symmetries (Appendix C 3) and the choice of suitable phase factors in the wave functions make it possible to reduce the total number of physical constants to a minimum of 20. This result may be compared with that of the more usual approach outlined in the next section.

4.3.2 Calculation Using Strong Magnetic Field States as Basic Vectors.

Here we note that, since we are working within a multiplet with a fixed, (but unknown) total angular momentum, and since the $r^{\ell}Y_{\ell}^{m}$ transform like the basic vectors of D_{ℓ} (see Appendix C5), their matrix elements have the same dependence on the magnetic quantum number as the Wigner coefficients S_{JMM_L} (Wigner (1959)).

To carry out the formal calculation of these coefficients for an S-state ion, it is convenient to use the classical Spin Hamiltonian method of Pryce (1950). Here a symmetrised polynomial in the components of $\underline{S}$ which displays the symmetry of the effective terms in the $\Sigma\ \Sigma\ A_{\ell}^{m} r^{\ell} Y_{\ell}^{m}$ series, is constructed. Then the matrix elements of this new operator (which is equivalent to the operator representing the effect of the crystal field) are taken between the various strong magnetic field substates $|M_s)$. These new matrix elements correspond (to within a constant factor) with those sought. We are assuming that the admixed higher levels act only via their angular momentum and the effect of this admixed angular momentum is allowed for by adjustable constants which will be determined experimentally. Further it is assumed that these constants are the same for all three Kramers doublets and that they are independent of the strength of the magnetic field.

Before substituting equivalent spin operators for the spherical harmonics, we note, that in the absence of a magnetic field, the Hamiltonian operator shows time reversal symmetry; and hence Kramers' theorem excludes any contribution from odd order polynomials in the components of $\underline{S}$ (i.e. odd ℓ in Y_{ℓ}^{m}) since these would remove the even degeneracies of the doublets found in 4.3.1 (Wigner (1932)).

Thus from equations (1) and (2) of section 4.3, we are seeking spin operator equivalents for the effective electrostatic operator :

$$H_o = \sum_i e(A_2^0 r^2 Y_2^0 + A_4^0 r^4 Y_4^0 + A_4^3 r^4 Y_4^3 + A^{-3}_4 r^4 Y^{-3}_4)_i \ ,$$

where i runs over the coordinate of the d electrons, as before. Using the usual formulae for spherical harmonics, this may be written :

$$H_o = \sum_i e \left[A_2^0 \sqrt{\frac{5}{16\pi}} \frac{3z_i^2 - r_i^2}{r_i^2} + A_4^0 \sqrt{\frac{9}{246\pi}} \frac{35z_i^4 - 30z_i^2 r_i^2 + 30r_i^4}{r_i^4} \right.$$

$$+ A_4^3 \sqrt{\frac{315}{64\pi}} \frac{z_i (x_i + iy_i)^3}{r_i^4} \exp(-3i\phi)$$

$$\left. + A^{-3}_4 \sqrt{\frac{315}{64\pi}} \frac{z_i (x_i - iy_i)^3}{r_i^4} \exp(3i\phi) \right] \ .$$

For a real operator we require $A_4^3 = A^{-3}_4$ for the particular choice of the phase of the angles θ, ϕ we have made (c.f. Jackson (1962)).

Using the spin operator equivalents for these functions as given by Stevens (1952) and Judd (1955), we arrive at an operator whose matrix elements within the ground term may be made equal to those of the crystal field by suitable choice of the constants :

$$H_o = B_2^0\left\{3S_z^2 - S(S+1)\right\} + B_4^0\left\{35S_z^4 - 30S(S+1)S_z^2\right.$$

$$\left. + 25S_z^2 - 6S(S+1) + 3S^2(S+1)^2\right\} + B_4^3\left\{S_z\left[S_+^3\exp(-3i\phi)\right.\right.$$

$$\left.\left. + S_-^3\exp(3i\phi)\right] + \left[S_+^3\exp(-3i\phi) + S_-^3\exp(3i\phi)\right]S_z\right\} \quad ,$$

where $S_\pm = S_x \pm iS_y$.

Other spin operator equivalents have been given by Ambler et al. (1962); we use the above, however, since they have become conventional. The phase of B_4^3 depends on the choice of the phase angles in the spherical harmonics. We have chosen ours so as to make B_4^3 positive real for the ions with S_z parallel to an arbitrarily chosen sense of the c axis, (for ions in the mirror symmetry sites there will be a phase difference of $\pi/3$ in ϕ and so in that case, B_4^3 is negative real).

If now we apply a magnetic field, we have to consider a tensor interaction netween $\underline{H}$ and $\underline{J}$ viz. $\beta\underline{H}.\underline{J}$ which for our case of C_3 symmetry may be written as :

$$g_{\parallel}\beta H_z\, S_z + g_{\perp}\beta(H_x S_x + H_y S_y) \quad ,$$

or :

$$g_{\parallel}\beta H\cos\theta\, S_z + g_{\perp}\beta H\sin\theta\left[S_+\exp(-i\phi) + S_-\exp(i\phi)\right] \quad ,$$

where the deviation of the $g_{\parallel}$ and $g_{\perp}$ from 2 represents the effect of any orbital angular momentum introduced into the ground state by higher state mixing or covalency.

Thus we have derived a Spin Hamiltonian for the two sets of Fe^{+++} ions in trigonal sites in Benitoite perturbed by a magnetic field, of the form :

$$H_s = g_\perp \beta H \cos\theta S_z + \tfrac{1}{2} g_\perp \beta H \sin\theta \left\{ S_+ \exp(-i\phi) + S_- \exp(i\phi) \right\}$$

$$+ B_2^0 \left\{ 3S_z^2 - S(S+1) \right\} + B_4^0 \left\{ 35S_z^4 + 30S(S+1)S_z^2 + 25S_z^2 \right.$$

$$\left. - 6S(S+1) + 35^2 (S+1)^2 \right\}$$

$$\pm B_4^3 \left\{ S_z \left[S_+^3 \exp(-3i\phi) + S_-^3 (\exp(3i\phi) \right] \right\}$$

$$\pm B_4^3 \left\{ \left[S_+^3 \exp(-3i\phi) + S_-^3 \exp(3i\phi) \right] S_z \right\} \quad .$$

Using the usual formulae for the matrix elements of S_z, S_+ and S_- between the $|M_s)$ states, (Bowers and Owen (1955)), and ignoring arbitrary constant terms, this operator can be represented within the ground term by a 6x6 Hermitian matrix. The eigenvalues of this matrix are the energy levels which are to be investigated. In the next section various methods of estimating these will be given.

Meanwhile we note that if we put :

$$w = \exp(i\phi) \quad ,$$
$$h_+ = g_\perp \beta (H_x + iH_y) \quad ,$$
$$h_- = g_\perp \beta (H_x - iH_y) \quad ,$$
$$h_z = g_{\parallel} \beta H_z \quad ,$$

then the matrix may be put in the form given on the next page :

M_s	$-\frac{5}{2}$	$-\frac{3}{2}$	$-\frac{1}{2}$	$\frac{1}{2}$	$\frac{3}{2}$	$\frac{5}{2}$
$-\frac{5}{2}$	$-5h_z/2$ $+10B_2^0$ $+60B_4^0$	$\sqrt{5}h_+/2$	0	$\pm 12\sqrt{10}$ $\times B_4^3 \varpi^3$	0	0
$-\frac{3}{2}$	$\sqrt{5}h_-/2$	$-3h_z/2$ $-2B_2^0$ $-180B_4^0$	$\sqrt{8}h_+/2$	0	0	0
$-\frac{1}{2}$	0	$\sqrt{8}h_-/2$	$-h_z/2$ $-8B_2^0$ $+120B_4^0$	$3h_+/2$	0	$\pm 12\sqrt{10}$ $\times B_4^3 \varpi^3$
$\frac{1}{2}$	$\pm 12\sqrt{10}$ $\times B_4^3 \varpi^{-3}$	0	$3h_-/2$	$h_z/2$ $-8B_2^0$ $+120B_4^0$	$\sqrt{8}h_+/2$	0
$\frac{3}{2}$	0	0	0	$\sqrt{8}h_-/2$	$3h_z/2$ $-2B_2^0$ $-180B_4^0$	$\sqrt{5}h_+/2$
$\frac{5}{2}$	0	0	$\pm 12\sqrt{10}$ $\times B_4^3 \varpi^{-3}$	0	$\sqrt{5}h_-/2$	$5h_z/2$ $+10B_2^0$ $+60B_4^0$

This is similar (apart from a phase factor and the labelling of the constants) to the matrix obtained by Kornienko and Prokhorov (1961), using the Spin Hamiltonian obtained by Bleaney and Trenam (1954), for the Spin Hamiltonian of Fe^{+++} in a cubic site with an axial distortion across the body diagonal.

We notice that this operator gives matrix elements containing only five empirical constants, which is less than the number allowed by the group theory treatment in 4.3.1 . So we can see that the Spin Hamiltonian involves physical assumptions in addition to symmetry arguments.

These are associated with the fact that we have used the same constants to incorporate the effect of higher state mixing in all the Kramers doublets. But, as the group theory analysis shows, we might in practice expect to find different values of these constants for each doublet, corresponding to a variation of the values of the Spin Hamiltonian parameters with the magnetic field. Accordingly, exact solutions of the Spin Hamiltonian secular equation were sought (as well as the customary perturbation theory approximations which were not expected to be very accurate in this case) and compared with the experimentally determined energy level differences, for magnetic fields ranging from 0 to 15,000 oersteds in an effort to find such variations.

4.4 The Energy Levels of the Spin Hamiltonian of Fe^{+++} in Benitoite.

Using the form of the constants given by Bleaney and Trenam (1954), the secular determinant corresponding to the matrix of 4.3.2 can be rewritten with :

$$B_2^0 = D/3, \quad B_4^0 = -(a-F)/180, \quad B_4^3 = \sqrt{2}\, a/36 \ .$$

In the Benitoite Hamiltonian, the off-diagonal elements were found to be quite large, and so, in addition to the perturbation theory energy levels, we have derived exact algebraic solutions for the cases of $\underline{H}$ parallel and perpendicular to the c axis. These were useful in fitting the spectrum accurately and in checking the numerical solutions to the general case (in which $\underline{H}$ may have any direction) which were found by computor diagonalisation of the above matrix.

4.4.1 Energy Levels With H Parallel to the c Axis.

For $\underline{H}$ parallel to the c axis, putting $\phi = 0$ and using the traditional form of the constants, the secular determinant can be factorised, by row and column operations, to give :

$$\begin{vmatrix} -\frac{5}{2}g_{\parallel}\beta H + \frac{10}{3}D - \frac{a-F}{3} - E \ , & \pm\frac{\sqrt{20}}{3}a \\ \pm\frac{\sqrt{20}}{3}a & , \ \frac{1}{2}g_{\parallel}\beta H - \frac{8}{3}D - \frac{2}{3}(a-F) - E \end{vmatrix} = 0 \ ,$$

$$\begin{vmatrix} -\frac{1}{2}g_{\parallel}\beta H - \frac{8}{3}D - \frac{2}{3}(a-F) - E \ , & \pm\frac{\sqrt{20}}{3}a \\ \pm\frac{\sqrt{20}}{3}a & , \ \frac{5}{2}g_{\parallel}\beta H + \frac{10}{3}D - \frac{1}{3}(a-F) - E \end{vmatrix} = 0 \ ,$$

$$\left| -\tfrac{3}{2}g_{\parallel}\beta H - \tfrac{2}{3}D + (a-F) - E \right| = 0 ,$$

$$\left| \tfrac{3}{2}g_{\parallel}\beta H - \tfrac{2}{3}D + (a-F) - E \right| = 0 ,$$

whence we get the eigenvalues :

$$E = \mp g_{\parallel}\beta H + \tfrac{1}{3}D - \tfrac{1}{2}(a-F) \mp \sqrt{\left[3D+\tfrac{1}{6}(a-F) \mp \tfrac{3}{2}g_{\parallel}\beta H\right]^2+\tfrac{20}{9}a^2} ,$$

$$E = \pm g_{\parallel}\beta H + \tfrac{1}{3}D - \tfrac{1}{2}(a-F) \mp \sqrt{\left[3D+\tfrac{1}{6}(a-F) \pm \tfrac{3}{2}g_{\parallel}\beta H\right]^2+\tfrac{20}{9}a^2} ,$$

$$E = \mp \tfrac{3}{2}g_{\parallel}\beta H - \tfrac{2}{3}D + (a-F) ,$$

(c.f. Kornienko and Prokhorov (1961)).

For small values of $\dfrac{20a^2/9}{3D + (a-F)/6 \pm 3g_{\parallel}\beta H/2}$, the first two terms of a binomial expansion of the terms under the square root sign give the following energy levels :

$$E_{-5/2} = -\tfrac{5}{2}g_{\parallel}\beta H + \tfrac{10}{3}D - \tfrac{1}{3}(a-F) + \frac{20a^2}{27\left[-g_{\parallel}\beta H+2D+\frac{1}{9}(a-F)\right]} ,$$

$$E_{-3/2} = -\tfrac{3}{2}g_{\parallel}\beta H - \tfrac{2}{3}D + (a-F) ,$$

$$E_{-1/2} = -\tfrac{1}{2}g_{\parallel}\beta H - \tfrac{8}{3}D - \tfrac{2}{3}(a-F) + \frac{20a^2}{27\left[-g_{\parallel}\beta H-2D-\tfrac{1}{9}(a-F)\right]} ,$$

$$E_{1/2} = \tfrac{1}{2}g_{\parallel}\beta H - \tfrac{8}{3}D - \tfrac{2}{3}(a-F) + \frac{20a^2}{27\left[g_{\parallel}\beta H-2D-\tfrac{1}{9}(a-F)\right]} ,$$

$$E_{3/2} = \tfrac{3}{2}g_{\parallel}\beta H - \tfrac{2}{3}D + (a-F) ,$$

$$E_{5/2} = \tfrac{5}{2}g_{\parallel}\beta H + \tfrac{10}{3}D - \tfrac{1}{3}(a-F) + \frac{20a^2}{27\left[g_{\parallel}\beta H+2D+\tfrac{1}{9}(a-F)\right]} .$$

These are easily seen to be equivalent to the results given by second order perturbation theory in which we consider as the zeroth order Hamiltonian :

$$H_o = g_{\parallel}\beta H S_z + D\left[S_z^2 - \tfrac{1}{3}S(S+1)\right] - \frac{1}{180}(a-F)\left[35S_z^4+30S(S+1)S_z^2 + 25S_z^2 + 6S(S+1) + 3S^2(S+1)^2\right] .$$

The terms in $20a^2/9$ are then the squared off-diagonal elements in the matrix above (in the same row as the corresponding first order term). These results differ

slightly from the values given by Kornienko and Prokhorov (1957) since these authors use a zero order operator which does not include the (a-F) term.

Note that, apart from mixing by the terms of the form $aS_z S_+^3$ (which is small in all materials studied in this project), the eigenstates are the pure $|M_s\rangle$ states.

4.4.2 Energy Levels With H Perpendicular to the c Axis.

For H perpendicular to the c axis and putting $\phi = 0$, the determinant can easily be factorised to :

$$\begin{vmatrix} \frac{10}{3}D - \frac{1}{3}(a-F) - E, & \frac{\sqrt{5}}{2}g_\perp\beta H & , \frac{\sqrt{20}}{3}a \\ \frac{\sqrt{5}}{2}g_\perp\beta H & , -\frac{8}{3}D+(a-F) - E & , \sqrt{2}g_\perp\beta H \\ \frac{\sqrt{20}}{3}a & , \sqrt{2}g_\perp\beta H & , -\frac{8}{3}D - \frac{2}{3}(a-F) \pm \frac{3}{2}g_\perp\beta H - E \end{vmatrix} = 0 ,$$

which on multiplying out and solving, by the usual method used for solving third order polynomials of this kind (Turnbull (1952)), gives the eigenvalues :

$$E = c + 2\sqrt{d/3}\cos\left[\frac{1}{3}\cos^{-1}\left(-\frac{b}{2}\sqrt{d^3/27}\right) + 2n\pi/3\right] ,$$

where $n = 0, 1, 2$,

$$c = \mp \frac{3}{2}g_\perp\beta H ,$$

$$d = -4(g_\perp\beta H)^2 \pm (4D+3(a-F))g_\perp\beta H - \frac{28}{3}D^2 - \frac{7}{9}(a-F)^2 - \frac{20}{9}a^2 ,$$

$$b = \left[-\frac{160}{27}D^3 - \frac{40}{27}D^2(a-F) + \frac{168(a-F)^2D}{27} + \frac{6}{27}(a-F)^3 \right]$$

$$\pm g_\perp \beta H \left[\frac{10}{3}D^2 - \frac{16}{3}D(a-F) + \tfrac{1}{2}(a-F)^2 \right]$$

$$+ (g_\perp \beta H)^2 \left[\frac{10}{3}D - \frac{3}{2}(a-F) \right]$$

$$- \left(\frac{2 \mp 15}{2} \right)(g_\perp \beta H)^3 + \frac{a^2}{3} \left[\frac{20}{3}(a-F) - \frac{20}{9}D \right]$$

$$- \frac{2\sqrt{10}}{3} a(g_\perp \beta H)^2 \pm \tfrac{1}{2} g_\perp \beta H \left[d + \frac{3}{4}(g_\perp \beta H)^2 \right] .$$

(This checks with the answers in the parallel case for the zero field and strong field limits).

However this form of the eigenvalues, although useful in checking the final solutions, especially those describing the low field lines, is rather cumbersome. For more convenient but approximate solutions, the following perturbation theory estimates were derived. These were especially useful in describing the Manganese spectra discussed in the next chapter and are derived here for the sake of convenience.

The off-diagonal Zeeman terms of the matrix in 4.3.2 were larger than the diagonal terms for $\underline{H}$ perpendicular to the c axis, and so a perturbation series in this representation would not converge. Hence a new polar axis for the crystal field terms was chosen

parallel to the magnetic field. In this new system, the (large) Zeeman terms are diagonal. Rotating the z axis of H_s in 4.3.2 above into the x direction corresponds to applying the transformations given in Appendix C 6 to the components of $\underline{S}$. Thus we substitute into H_s new components given by the equations :

$$S_z = -\tfrac{1}{2}(S'_+ + S'_-)$$

$$S_+ = \tfrac{1}{2}(S'_+ - S'_-) + S'_z$$

$$S_- = \tfrac{1}{2}(-S'_+ + S'_-) + S'_z \quad ,$$

(where the primed operators are in the new coordinate system). Then on cancelling (but bearing in mind the non-commutative character of these operators) we obtain in the new coordinate system on ignoring the primes :

$$H_s = g\beta\underline{H}.\underline{S} + \tfrac{1}{4}D\left[S_+^2 + S_-^2 + S_-S_+ + S_+S_-\right]$$

$$- \frac{(a-F)}{2880}\Big[35(S_+^4+S_+^2S_-S_+ + S_+^3S_- + S_+^2S_-^2 + S_-S_+^3 + S_-S_+S_-S_+$$

$$+ S_-S_+^2S_- + S_-S_+S_-^2 + S_+S_-S_+^2 + S_+S_-^2S_+ + S_+S_-S_+S_- + S_+S_-^3$$

$$+ S_-^2S_+^2 + S_-^3S_+ + S_-^2S_+S_- + S_-^4) - 950(S_+^2 + S_-^2 + S_+S_- + S_-S_+)\Big]$$

$$+ (* \text{ small off-diagonal term in "a"}) \quad .$$

(* This last term is evaluated in Appendix C7, and

although it gives corrections of the order of three oersteds in the Benitoite spectrum, it is negligible in the Manganese spectra discussed in the next section, and so we shall ignore it henceforth.)

Applying second order perturbation theory to the new Spin Hamiltonian we get, using $g\beta\underline{H}\cdot\underline{S} + \frac{1}{4}D(S_-S_+ + S_+S_-)$ as the zeroth order Hamiltonian, the approximate eigenvalues :

$$E_{-5/2} = -\frac{5}{2}g_\perp\beta H + D + \frac{10D^2}{4(2g_\perp\beta H+3D)} ,$$

$$E_{-3/2} = -\frac{3}{2}g_\perp\beta H + 3D + \frac{9D^2}{2(2g_\perp\beta H+D)} ,$$

$$E_{-1/2} = -\tfrac{1}{2}g_\perp\beta H + 4D + \frac{9D^2}{2(2g_\perp\beta H+D)} - \frac{10D^2}{4(2g_\perp\beta H+3D)} ,$$

$$E_{1/2} = \tfrac{1}{2}g_\perp\beta H + 4D - \frac{9D^2}{2(2g_\perp\beta H+D)} + \frac{10D^2}{4(2g_\perp\beta H+3D)} ,$$

$$E_{3/2} = \frac{3}{2}g_\perp\beta H+3D - \frac{9D^2}{2(2g_\perp\beta H+D)} ,$$

$$E_{5/2} = \frac{5}{2}g_\perp\beta H + D - \frac{10D^2}{4(2g_\perp\beta H+3D)} .$$

The corresponding estimates of the eigenvectors are :

$$|\underline{-\tfrac{5}{2}}) = \frac{1}{a}\left[|-\tfrac{5}{2}) + \frac{\sqrt{10}D}{2(2g_\perp\beta H+3D)}\,|-\tfrac{1}{2})\right] ,$$

$$|\underline{-\tfrac{3}{2}}) = \frac{1}{b}\left[|-\tfrac{3}{2}) + \frac{3D}{\sqrt{2}(2g_\perp\beta H+D)}\,|\tfrac{1}{2})\right] ,$$

$$|\underline{-\tfrac{1}{2}}) = \frac{1}{c}\left[|-\tfrac{1}{2}) + \frac{3D}{\sqrt{2}(2g_\perp\beta H+D)}\,|\tfrac{3}{2}) - \frac{\sqrt{10}D}{2(2g_\perp\beta H+3D)}|-\tfrac{5}{2})\right] ,$$

$$|\underline{\tfrac{1}{2}}) = \frac{1}{d}\left[|\tfrac{1}{2}) - \frac{3D}{\sqrt{2}(2g_\perp\beta H+D)}\,|-\tfrac{3}{2}) + \frac{\sqrt{10}D}{2(2g_\perp\beta H+3D)}|\tfrac{5}{2})\right] ,$$

$$|\underline{\tfrac{3}{2}}) = \frac{1}{e}\left[|\tfrac{3}{2}) - \frac{3D}{\sqrt{2}(2g_\perp\beta H+D)}\,|-\tfrac{1}{2})\right] ,$$

$$|\underline{\tfrac{5}{2}}) = \frac{1}{f}\left[|\tfrac{5}{2}) - \frac{\sqrt{10}D}{2(2g_\perp\beta H+3D)}\,|\tfrac{1}{2})\right] ,$$

where a, ... f are normalisation factors.

4.4.3 Numerical Values of the Energy Levels With H in Any Direction.

For real symmetric matrices, the Jacobi procedure of iterative reduction of the off-diagonal terms by a series of orthogonal binary transformations is readily simulated on a computor, giving highly accurate eigenvalues (Wilkinson (1961)). Further it is possible to convert our eigenproblem (of a complex Hermitian matrix) to an equivalent one of a real symmetric matrix of twice the order, as the following calculation shows.

We seek to solve the Schrödinger equation :

$$H_s|\underline{m}) = E_{\underline{m}}|\underline{m}) \quad , \tag{1}$$

where $|\underline{m})$ is a linear combination of the S_z states, (and is not to be confused with the nuclear spin quantum number m used in later chapters).

$$\text{Hence} \quad |\underline{m}) = \sum_M d(\underline{m}, M)\ |M) \quad , \tag{2}$$

where $d(\underline{m}, M)$ is a linear coefficient. Therefore :

$$\sum_M (M'|H_s|M)\ d(\underline{m}, M) = E_{\underline{m}}\, d(\underline{m}, M') \quad ,$$

which, for a given value of $\underline{m}$, can be written in the matrix form :

$$Ad = E_{\underline{m}} Id. \tag{3}$$

where $A = B+iC$ is a complex matrix,

and $d = u+iv$ is a complex vector. (4)

B, C, u and v are all real, and so (3) can be written as the pair of real matrix equations :

$$Bu - Cv = E_{\underline{m}} u \quad ,$$

$$Cu + Bv = E_{\underline{m}} v \quad ,$$

which are identical with :

$$\begin{bmatrix} B, & -C \\ C, & B \end{bmatrix} \begin{bmatrix} u \\ v \end{bmatrix} = E_{\underline{m}} \begin{bmatrix} u \\ v \end{bmatrix} \quad . \qquad (5)$$

This is symmetric if A is Hermitian (since C is then antisymmetric and B is of course symmetric).

One computor diagonalisation routine which proved satisfactory (SHARE 5.0.016) would only handle positive definite real symmetric matrices. Hence it was necessary to modify the matrix further by loading the diagonal elements with a large positive constant so that all the eigenvalues would turn out positive. This procedure merely shifted all the eigenvalues by a constant and so did not affect their spacing.

The matrix of 4.3.2 was modified according to these principles and its eigenvalues were evaluated for specified values of $g_{\parallel}$, $g_{\perp}$, D, a and F on the Adelaide University I.B.M. 1620 computor. The Fortran source programme developed to erect and diagonalise this matrix is listed in Appendix B1. Originally, the output was printed, but this wasted a lot of time so the output statements were altered to ensure that the eigenvalues were punched out on cards and then listed on an I.B.M. 704 printing machine. The eigenvalues were evaluated in units of kilomegacycles per second (Gc./s.) for direct

comparison with experiment. It was decided to run the programme until the maximum value of the off-diagonal terms was 10^{-4}Gc./s.. This, according to second order perturbation theory, would result in the eigenvalues being accurate to :

$$O\left[\frac{(10^{-4})^2}{10}\right] \sim O\,(10^{-7})\text{Gc./s.} \quad ,$$

(where "O" stands for "order of magnitude"), for energy levels approximately 10Gc./s. apart, (as they are for X band measurements). For this accuracy, each set of eigenvalues took about 7 minutes to compute. For H parallel and perpendicular to the c axis, the computor programme was checked against the algebraic solutions found in sections 4.4.1 - 2 and found to be accurate to within at least 10^{-3}Gc./s.. For the general direction of H, the algebraic checks in Appendix C 9 were employed and found to be satisfied to at least the same accuracy.

4.5 Fitting the Strong Lines to the Spin Hamiltonian.

It was found convenient to take accurate measurements of the strong transitions with the magnetic field parallel and perpendicular to the c axis (where the two sets of 5 lines paired up). In the "parallel" case, five distinct (paired) lines were observed at X band (Fig. 4.3), while for the "perpendicular" spectrum (Fig. 4.4) the two lower (paired) lines ran into each other making accurate measurement difficult due to the "line interaction" effect (Aisenberg et al. (1959)).

Similar results were obtained by the author with the aid of Mr.R.D. Hutton on the Monash University Q band spectrometer (Figs. 4.5 and 4.6).

Several samples were examined in this way and all gave consistent results. One typical set of measurements obtained at room temperature (296°K) is given in the following tables :

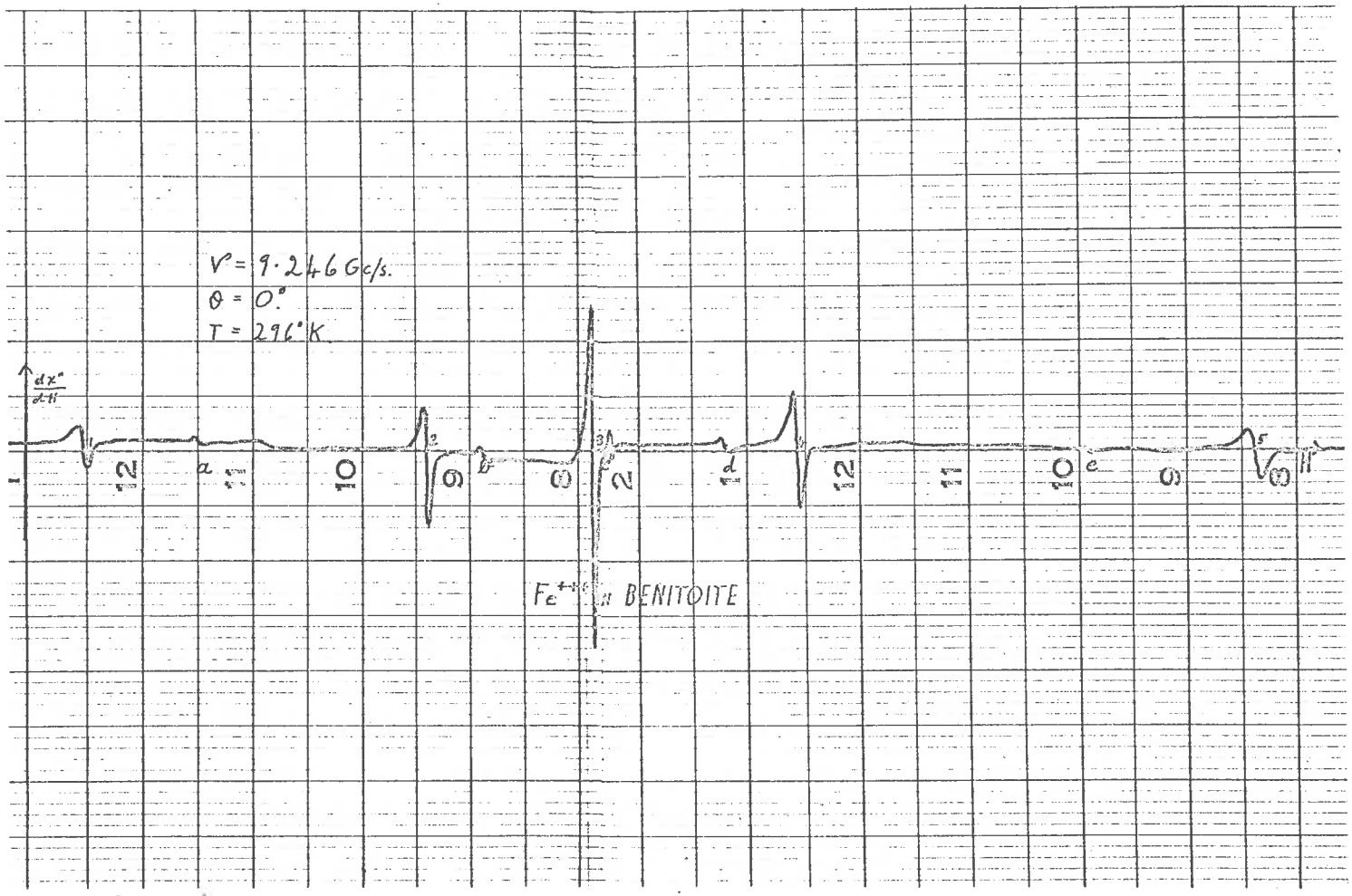

Fig. 4·3

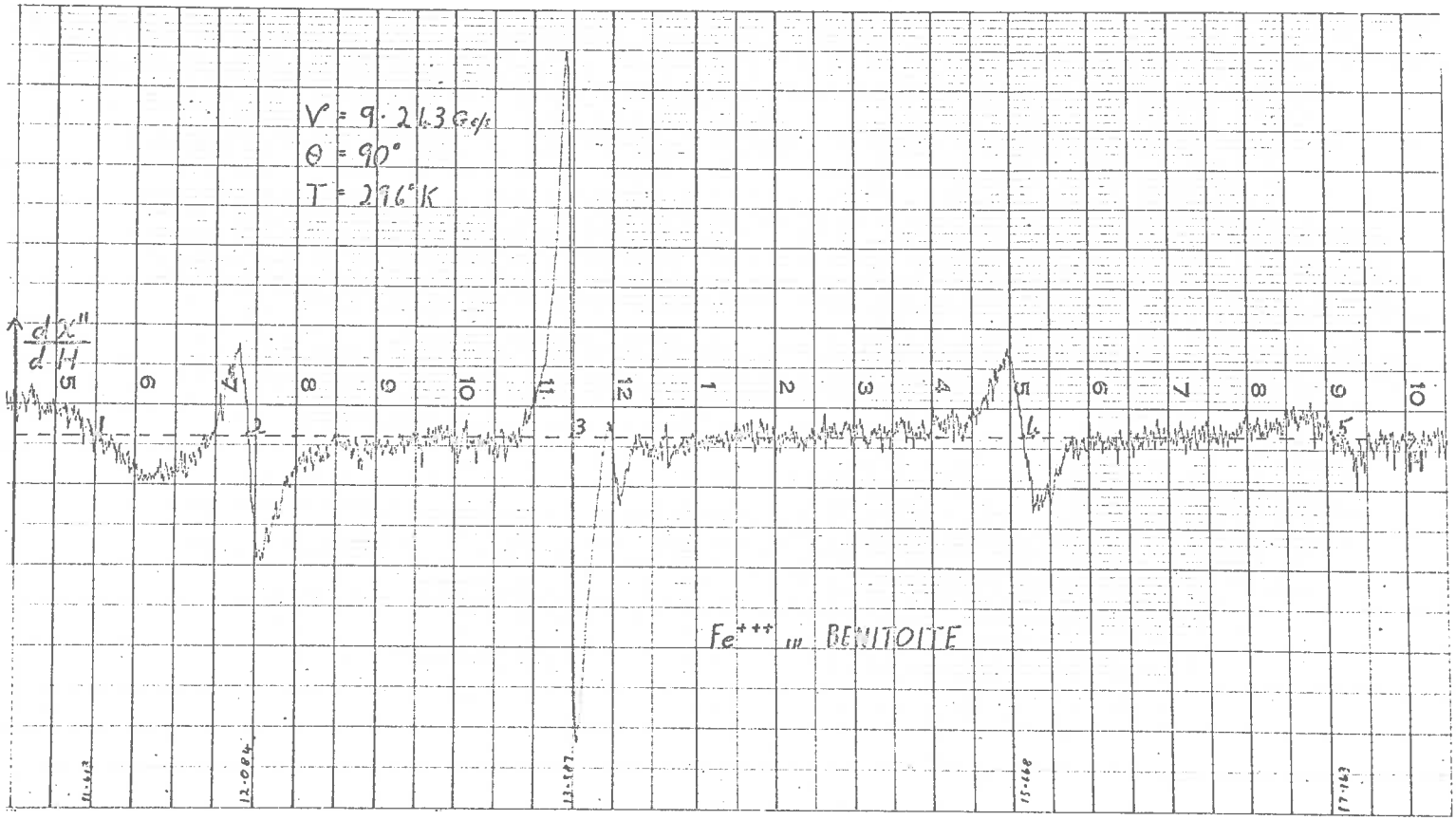

Fig. 4·4

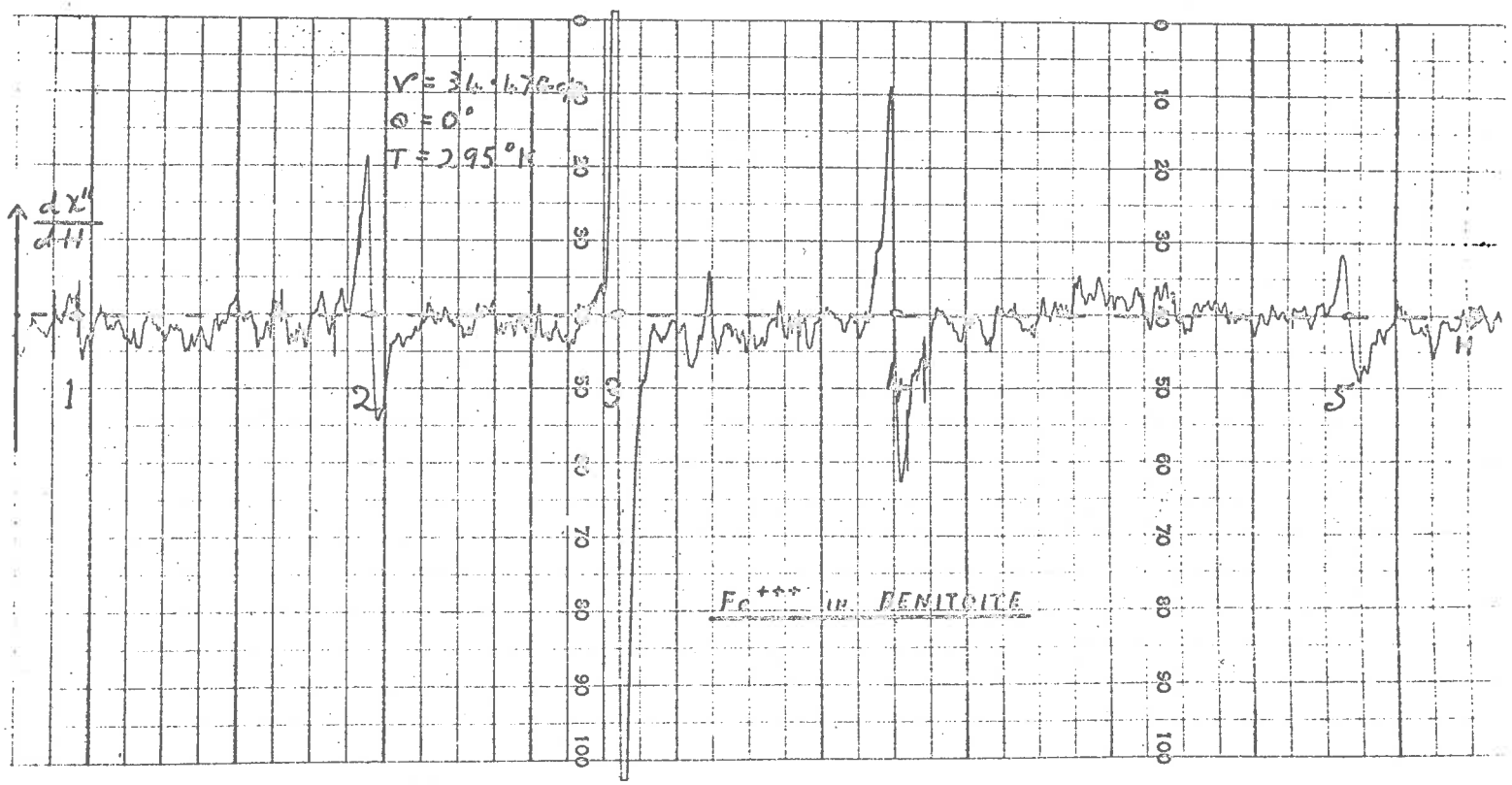

Fig. 4·5

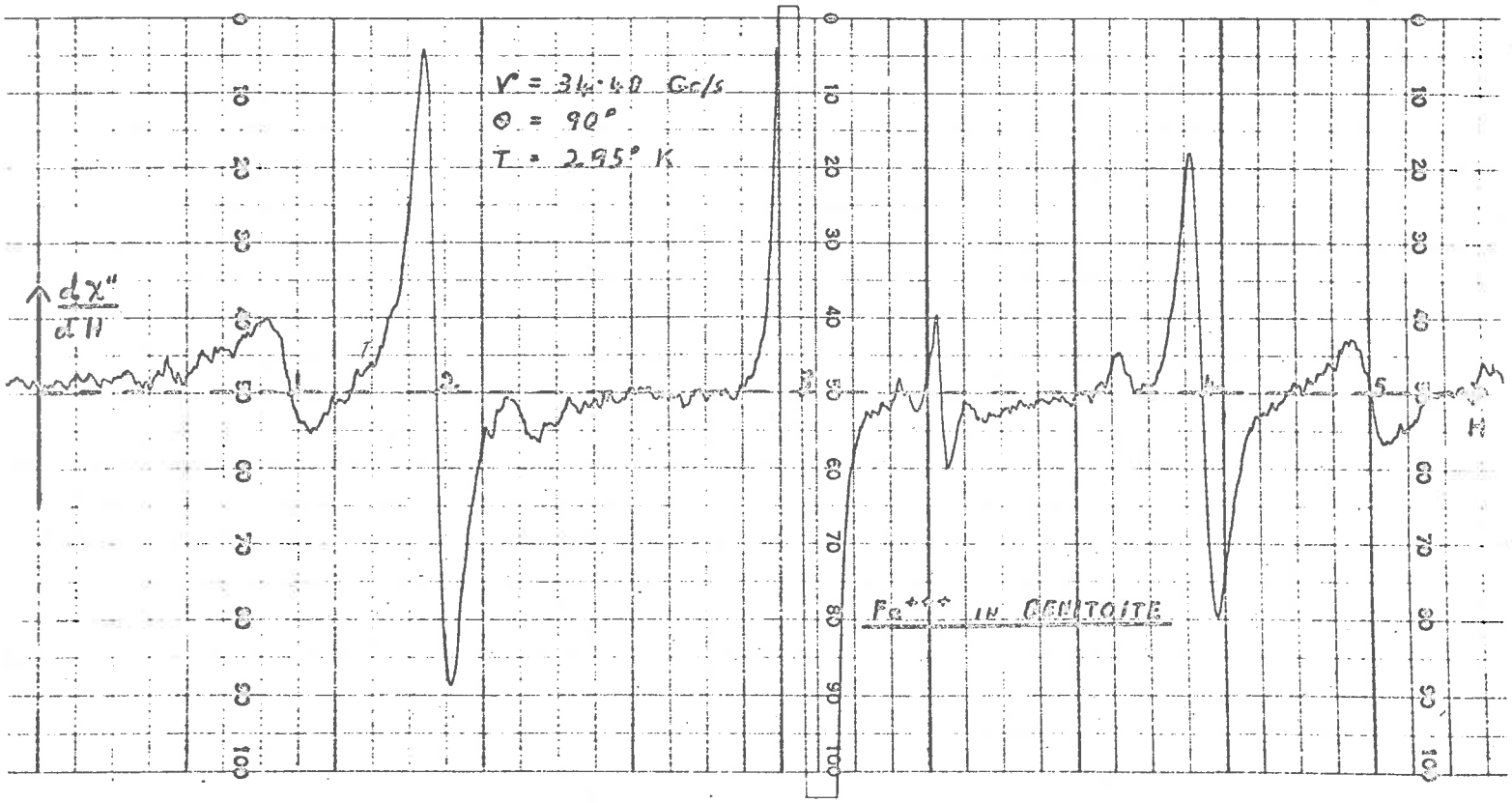

Fig. 4-6

Resonance conditions with the magnetic field parallel to the c axis.

Line No.	Magnetic Field* (oersteds)	Microwave Frequency (Gc./s.).
1	1,676.2 ± 3.0	9.243
2	2,789.2 ± 1.5	9.243
3	3,289.7 ± 0.5	9.243
4	3,815.1 ± 1.5	9.243
5	4,908.5 ± 3.0	9.243
2	11,799 ± 2.0	34.504
3	12,309 ± 1.0	34.504
4	12,728 ± 2.0	34.504

Resonance conditions with the magnetic field perpendicular to the axis.

Line No.	Magnetic Field(oersteds)	Microwave Frequency (Gc./s.).
1	2,706.5 ± 10.0	9.235
2	2,829.1 ± 1.5	9.235
3	3,185.5 ± 0.5	9.235
4	3,672.5 ± 1.5	9.235
5	3,996.5 ± 3.0	9.235
2	11,853 ± 2.0	34.489
3	12.275 ± 1.0	34.489
4	12,728 ± 2.0	34.489

(* Throughout this text, the magnetic field ($\underline{H}$)is quoted (expressed in oersteds): under the experimental conditions prevailing, this procedure gives the same numerical results as would be obtained if, instead, the magnetic induction ($\underline{B}$) were given in gauss; but the use of H seems to the author to make calculations clearer dimensionally.)

The constants in the approximate perturbation solutions to the energy levels in "parallel" and "perpendicular" cases were adjusted to give an approximate fit to these results. Then final corrections were

made using the computor programme, ultimately fitting the spectrum to within the nearest ± 10Mc./s. on the outermost lines (which corresponds to an uncertainty in their position of ± 3 oersteds). The appropriate values of the constants were then :

$$\begin{aligned} g_{\parallel} &= g_{\perp} = 2.0026 \ (\pm\ 0.0005)\ , \\ D &= \mp\ 1.014\ (\pm\ 0.001)\ \text{Gc./s.}, \\ (a-F) &= \pm\ 0.356\ (\pm\ 0.003)\ \text{Gc./s.}, \\ |a| &= 0.370\ \ (\pm\ 0.010)\ \text{Gc./s.}). \end{aligned}$$

The central line was comparatively narrow (5 oersteds), and by use of a DPPH marker it was measured to within 0.5 oersteds, giving an accurate value of g. The outer lines were much wider (10 and 25 oersteds in the best sample), making the limit of experimental accuracy of the fine structure measurements approximately 3 oersteds, which was the error noted above.

Measurements were also made at liquid air temperatures (77°K) at X band, and in this case, the approximate values of the constants were:

$$\begin{aligned} g_{\parallel} &= g_{\perp} = 2.0026 \ (\pm\ 0.0005)\ , \\ D &= \mp\ 1,074\ (\pm\ 0.001)\ \text{Gc./s.}\ , \\ (a-F) &= \pm\ 0.363\ (\pm\ 0.003)\ \text{Gc./s.}\ , \\ |a| &= \pm\ 0.375\ (\pm\ 0.010)\ \text{Gc./s.}\ . \end{aligned}$$

The significant change in the value of D apparently results from a change in the unit cell dimensions as the temperature is lowered.

4.6 Zero Field Measurements.

As a further check on the accuracy of the Spin Hamiltonian description of the spectrum, it was decided to measure the energy level separations at zero magnetic field. These measurements were kindly

taken by Mr. H.F. Symmons of the National Standards Laboratory, Chippendale, N.S.W. during a visit there by the author in December 1963.

This zero field spectrometer has been described by Bogle et al. (1961). At 77°K, with a four gm. polycrystaline sample of Benitoite, it showed one line at 4.84 Gc./s. and a weaker one in the range 1.56-1.65Gc./s. (the uncertainty in this latter case being due to an instrumental effect).

From the energy levels of Section 4.4.1, we see, that in zero magnetic fields, these transitions are approximately given by :

$$\nu = \pm \left[4D - \tfrac{4}{3}(a - F) + \frac{20\,a^2}{54D + 3(a - F)} \right],$$

$$\nu = \pm \left[2D + \tfrac{5}{3}(a - F) + \frac{20\,a^2}{54D - 3(a - F)} \right],$$

(to within $\pm$ 0.001 Gc./s.; for the parameters found above). On substituting the values of the constants obtained above from the X band measurements at liquid air temperatures, into these approximate equations, we obtain the values 4.830Gc./s. and 1.593Gc./s. for ν (the exact computed values are 4.829Gc./s. and 1.593Gc./s.). Hence these results check, (to within experimental error), with the e.s.r. results of section 4.5.

4.7. The Energy Level Schemes.

With the aid of the eigenvalue programme and experimentally determined constants, we can predict the energy levels of the Spin Hamiltonian of Fe^{+++} ions in the Barium sites in Benitoite for any direction and value of the applied magnetic field. The energy level schemes for values of the applied field, ranging from 0 to 5,000 oersteds both parallel and perpendicular to the c axis, are shown in Figs. 4.7 and 4.8, (where the

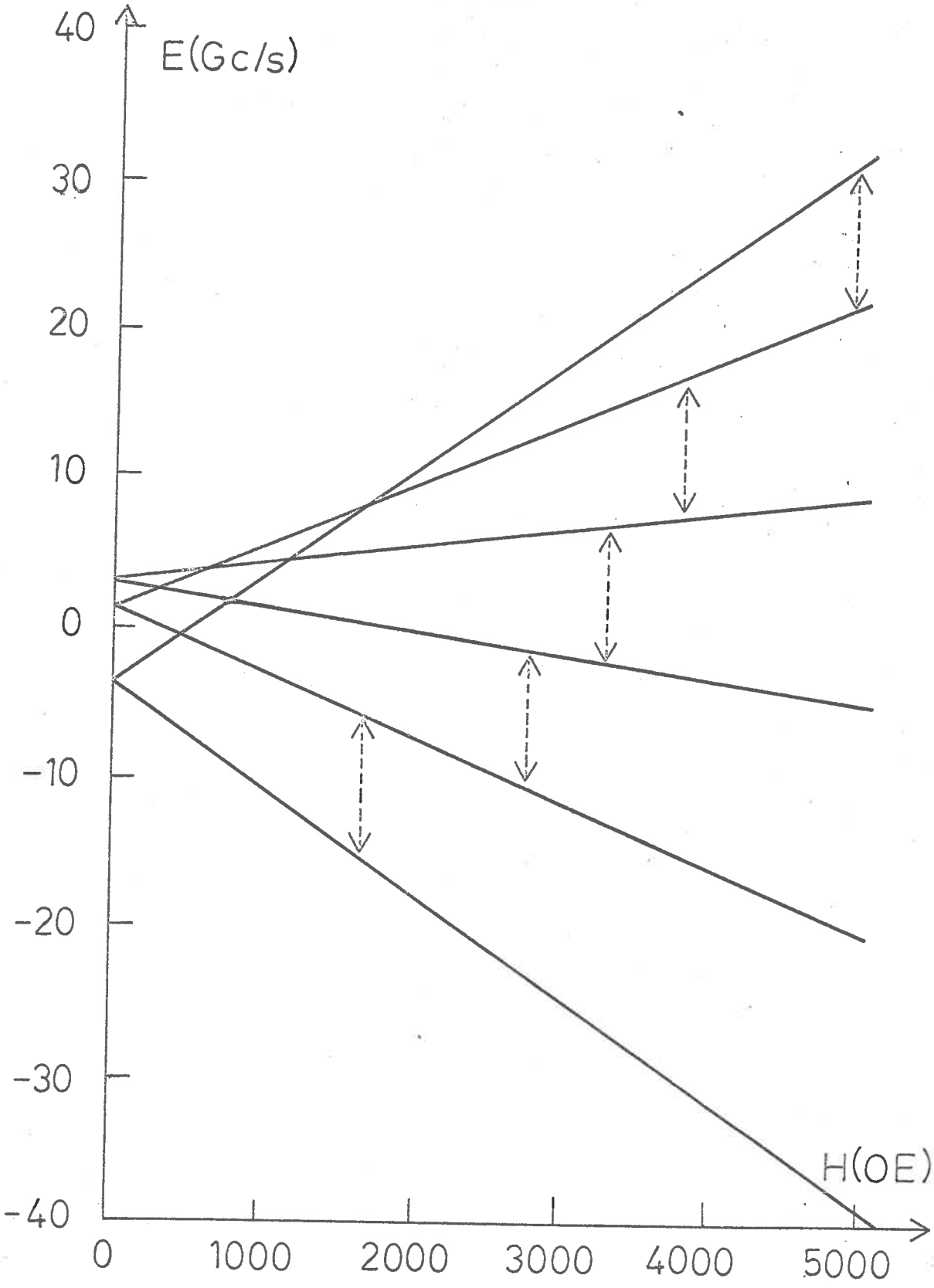

Fig. 4·7 The energy level scheme for the "parallel" spectrum of Fe^{+++} in Benitoite.

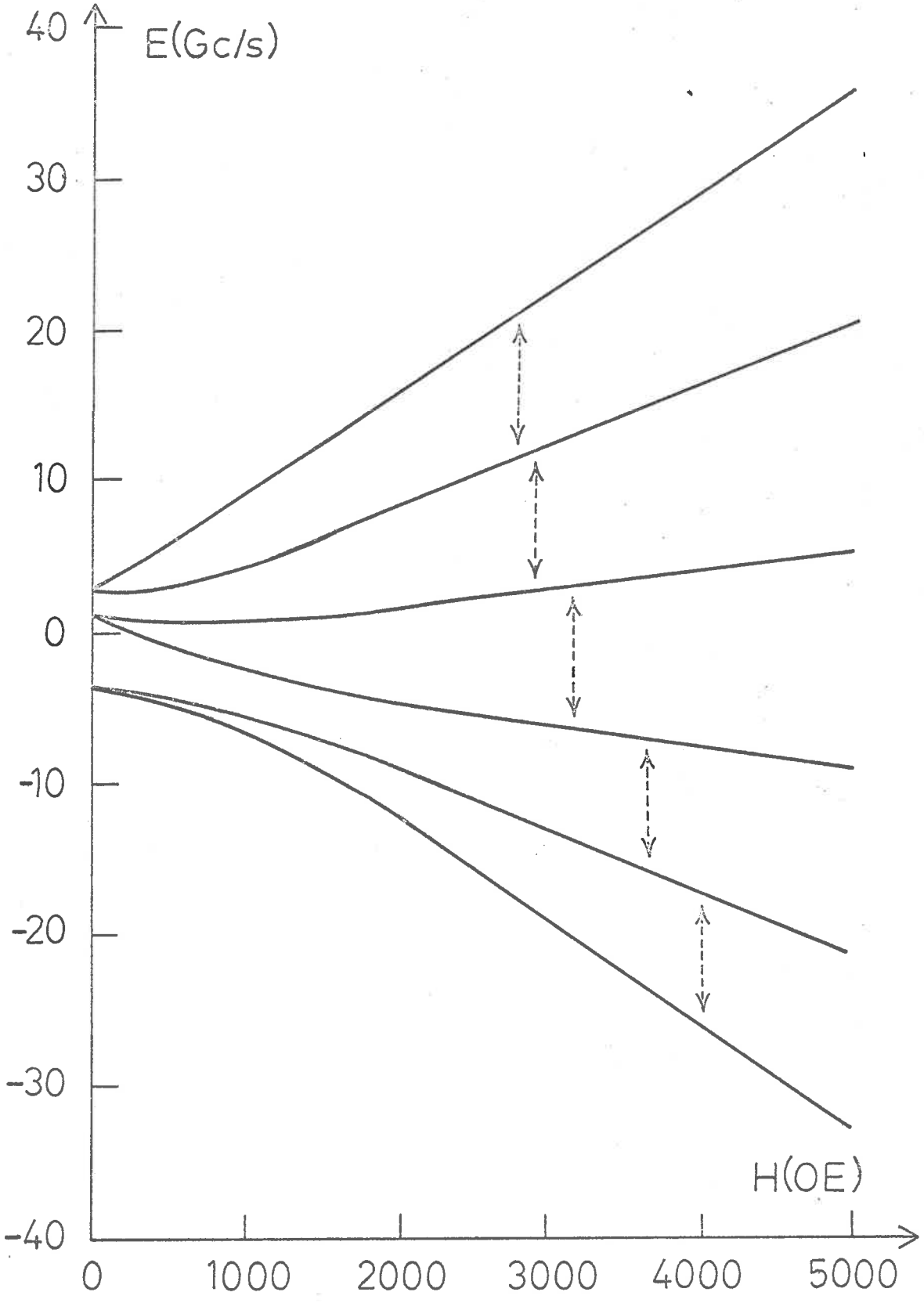

Fig. 4·8 The energy level scheme for the "perpendicular" spectrum of Fe^{+++} in Benitoite.

upper signs of the parameters given in Section 4.5 are used).

4.8 Transition Probabilities.

We have solved the time independent Schrödinger equation :

$$H_s|\underline{m}) = E_{\underline{m}} | \underline{m})$$

for the characteristic values of $E_{\underline{m}}$, and so we can find the corresponding characteristic vectors $|\underline{m})$ by solving the appropriate sets of simultaneous linear equations, and hence calculate transition probabilities. We begin this calculation by noting that the interaction energy of the microwave field with the sample can be represented by the time dependent operator :

$$H_1 = \tfrac{1}{2} g\beta \; \underline{H}_o \cdot \underline{S} \left[\exp(i\omega_o t) + \exp(-i\omega_o t) \right]. \quad (1)$$

So the total system including interactions with the static and microwave magnetic fields, can be described by the time dependent Schrodinger equation :

$$i\hbar \frac{\partial |\underline{M})}{\partial t} = (H_s + H_1) |\underline{M}) \; .$$

Following the usual procedure (Schiff (1955) for determining transition probabilities, we expand the $|\underline{M})$ in terms of the set of time dependent orthonormal state functions $|\underline{m})\exp(-iE_{\underline{m}}t/\hbar)$, thus :

$$|\underline{M}) = \sum_{\underline{m}} a_{\underline{m}} |\underline{m}) \exp(-iE_{\underline{m}}t/\hbar) \; .$$

Hence, substituting into (1) and cancelling, we get :

$$i\hbar \Sigma \frac{d}{dt}(a_{\underline{m}}) |\underline{m}) \exp(-iE_{\underline{m}}t/\hbar) = \Sigma a_{\underline{m}} H_1 |\underline{m}) \exp(-iE_{\underline{m}}t/\hbar) \; ,$$

whence on multiphying by $(\underline{n}|$ we obtain :

$$i\hbar \frac{d}{dt}(a_{\underline{n}}) = \Sigma a_{\underline{m}} (\underline{n}\,|H_1|\,\underline{m}) \exp\left[\, i(E_{\underline{n}} - E_{\underline{m}})\, t/\hbar \,\right].$$

Now assume that at time t = o, the system is in the stationary state $|\underline{m}\rangle$, hence on putting $\omega_{nm} = (E_{\underline{n}} - E_{\underline{m}})/\hbar$ we have :

$$i\hbar \frac{d}{dt}(a_{\underline{n}})_o = (\underline{n}\,|H_1|\,\underline{m})\exp(i\omega_{nm}t),$$

$$\therefore a_{\underline{n}} = \frac{-1}{i\hbar}\int_o^t (\underline{n}\,|H_1|\,\underline{m})\exp(i\omega_{nm}t)\,dt, \qquad (2)$$

for times (t) for which $a_{\underline{m}}$ is not appreciably different from unity. This will hold for all t in the absence of saturation effects. Hence on substituting (1) into (2) we get :

$$a_{\underline{n}} = \frac{-i}{\hbar}(\underline{n}|H_o \cdot S|\,\underline{m})\left\{ \frac{\exp\left[i(\omega_{nm}+\omega_o)t\right]-1}{\omega_{nm}+\omega_o} + \frac{\exp\left[i(\omega_{nm}-\omega_o)t\right]-1}{\omega_{nm}-\omega_o} \right\}$$

Hence for $E_{\underline{n}} > E_{\underline{m}}$ we have :

$$|a_{\underline{n}}|^2 = 4\,|(\underline{n}\,|H_o \cdot S|\,\underline{m})|^2 \frac{\sin^2\frac{1}{2}(\omega_{nm}-\omega_o)t}{\hbar^2(\omega_{nm}-\omega_o)^2}. \qquad (3)$$

In order to get a transition probability proportional to time for the resonance lines, we now take into account the distribution of the closely spaced group of energy differences $E_{\underline{n}} - E_{\underline{m}}$ provided by the various line broadening mechanisms. We assume that ω_{nm} has a normalised density function $\rho(\omega_{nm})$. Then the overall transition probability between the sets of states labeled by $\underline{n}$ and $\underline{m}$ is :

$$P_{nm} = \frac{1}{t}\int_{-\infty}^{\infty} |a_{\underline{n}}|^2\, \rho(\omega_{nm})\, d\omega_{nm}.$$

Since $\rho(\omega_{nm})$ changes comparatively slowly with ω_{nm} compared with $|a_{\underline{n}}|^2$, we have from (3) above :

$$P_{nm} = \frac{(g\beta)^2}{\hbar^2} \; | \; (\underline{n} \; | \underline{H}_o \cdot \underline{S} \; | \underline{m})^2 \rho(\omega_{nm}) \; | \quad ,$$

or

$$P_{nm} = \frac{(g\beta)^2}{\hbar^2} \; | (\underline{n} \; | \underline{H}_o \cdot \underline{S} \; | \underline{m} \;) \; |^2 \; f(\nu) \quad .$$

on putting $f(\nu)$ equal to the normalised frequency response of the oscillator to incident monochromatic radiation. This can then be seen to be equivalent to the result obtained by Shulz-Du Bois (1959).

We can write the interaction term $\underline{H}_o \cdot \underline{S}$ in the form :

$$\underline{H}_o \cdot \underline{S} = \tfrac{1}{2} (H_- S_+ + H_+ S_-) + H_z S_z \quad .$$

Hence we can compare line intensities, if we know the direction of $\underline{H}$ with respect to the crystal field co-ordinate system and the matrix elements of the basic components of the transition amplitude operator :

$$T_+ = (\underline{n} \; | \; S_+ \; | \underline{m} \;)$$
$$T_o = (\underline{n} \; | \; S_z \; | \underline{m} \;)$$
$$T_- = (\underline{n} \; | \; S_- \; | \underline{m} \;)$$

These matrix elements can be calculated using equation (2) of Section 4.4.3, viz.:

$$| \; \underline{m} \;) = \sum_{M} \; d(\underline{m}, M) \; | \; \underline{M} \;) \quad .$$

and the standard forms for the matrix elements $(N \; | \; S_+ \; | M)$, $(N \; | S_z \; | M)$ and $(N | S_- | M)$.

As was shown in Section 4.4.3, for the given value of $\underline{m}$, $d(\underline{m}, M)$ is given by :

$$d(\underline{m}, M) = d = u + i \, v \quad ,$$

where u and v can be found by solving the set of simultaneous equations (5) of 4.4.3 for the given value of $E_{\underline{m}}$. This was done on the 1620 computor using the programme listed in Appendix B 3-6. The first programme calculates the matrix elements of the Spin Hamiltonian and punches them on cards as data for the second programme which solves the $E_{\underline{m}}$, u and v.

4.8.1 Transition Probabilities of the Parallel Spectrum.

For the simple case in which $\underline{H}$ is parallel to the c axis, the off-diagonal elements of the Spin Hamiltonian matrix are very small and so we have approximately :

$$| \underline{m}) = |M) \ ,$$

where the value of M corresponding to $\underline{m}$ depends on the way in which we choose the labels $\underline{m}$ for the perturbed states. We can see that the only allowed transitions between different states are those calculated from the values of T_+ and T_- corresponding to $(M|S_-|M+1)$ and $(M|S_+|M-1)$. Thus for the radiation field H_o parallel to the x direction, the relative amount of energy absorbed per unit time for the transition $\underline{m} \rightarrow \underline{n}$ is given by :

$$E_x = |(\underline{m}|S_x|\underline{n})|^2 .$$

This can also be written as :

$$E_x = \frac{1}{4} |(M|S_+ + S_-| N)|^2 \ ,$$

which can be seen to be non-zero for :

$$E_x = \frac{1}{4} |(M|S_+|M\pm1) + (M|S_-|M\pm1)|^2 \ .$$

These are shown in Fig. 4.9. Here the values of the label $\underline{m}$ are chosen so as to increase in integral steps from the value $\underline{-5/2}$ in order of increasing energy; in this way the $| \underline{m})$ become the $| M)$ in the strong magnetic field limit. Hence we see that the discontinuities in the figure result from crossovers of the

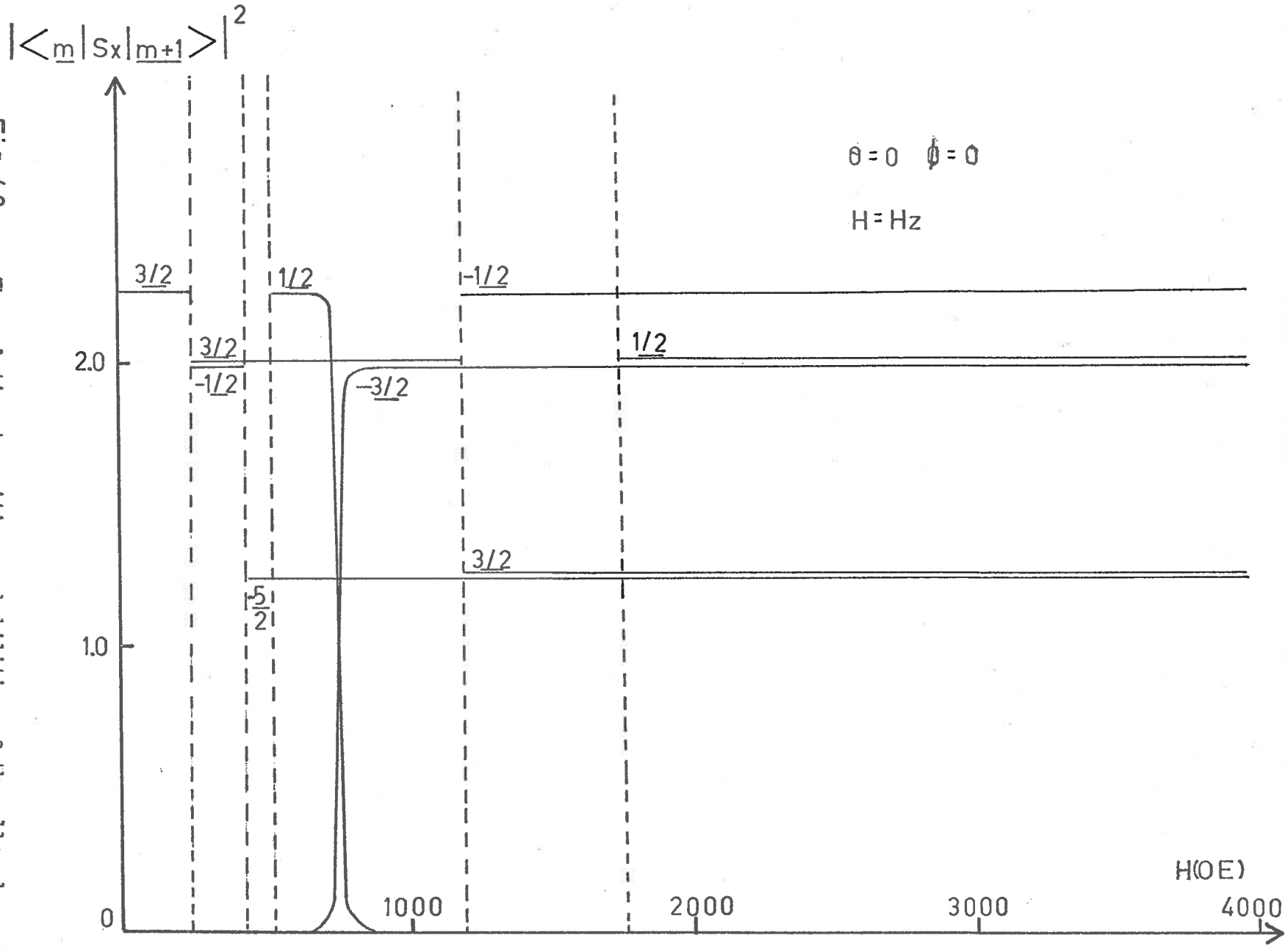

Fig. 4.9 The relative transition probabilities of the allowed "parallel" spectrum of Fe^{+++} in Benitoite.

energy levels (which cause a different value of M to correspond to a given m). The singularity in the 1/2 and -3/2 transitions in the neighbourhood of 700 oersteds is due to the repulsion of a pair of energy levels caused by the small non-zero off-diagonal matrix elements of the terms of the form "$aS_+ {}^3S_z$". The experimental values of the relative intensities of the lines obtained by a double numerical integration of the derivative lines of the "parallel" spectrum at X band were in the ratio 1.22 : 1.90 : 2.25 : 1.95 : 1.21, which is in agreement (to within experimental error) with the predicted ratio of 1.25 : 2.0 : 2.25 : 2.0 : 1.25.

4.8.2 Transition Probabilities of the Perpendicular Spectrum.

For H perpendicular to the c axis, the eigenvectors $|\ m\ )$ of the Spin Hamiltonian whose z axis is chosen parallel to the c axis are more complicated functions of the $|\ M\ )$. However, owing to the isotropy of the spectrum in the perpendicular plane, it suffices to consider the relatively simple case in which H is parallel to the x axis. Here the imaginary elements in the matrix (5) of Section 4.4.3 are zero, and so the d(m, M) vector corresponds to the u vector. This reduces the computing time required to calculate the values of d(m, M). These were calculated by the method shown in Section 4.4.3, then fed into the programme listed in Appendix B 7, to give the values of T_+, T_o, and T_-, and hence, the amount of energy absorbed per unit time from the radiation field H_o linearly polarised in the y direction, (E_y). A typical page of output is shown in Appendix B 8. Values of E_y for the allowed $\Delta m = 1$ transitions are shown in Fig. 4.10. No other transitions were large enough to be observed with the radiation field (H_o) in the y direction. Note that in the strong field approximation, the

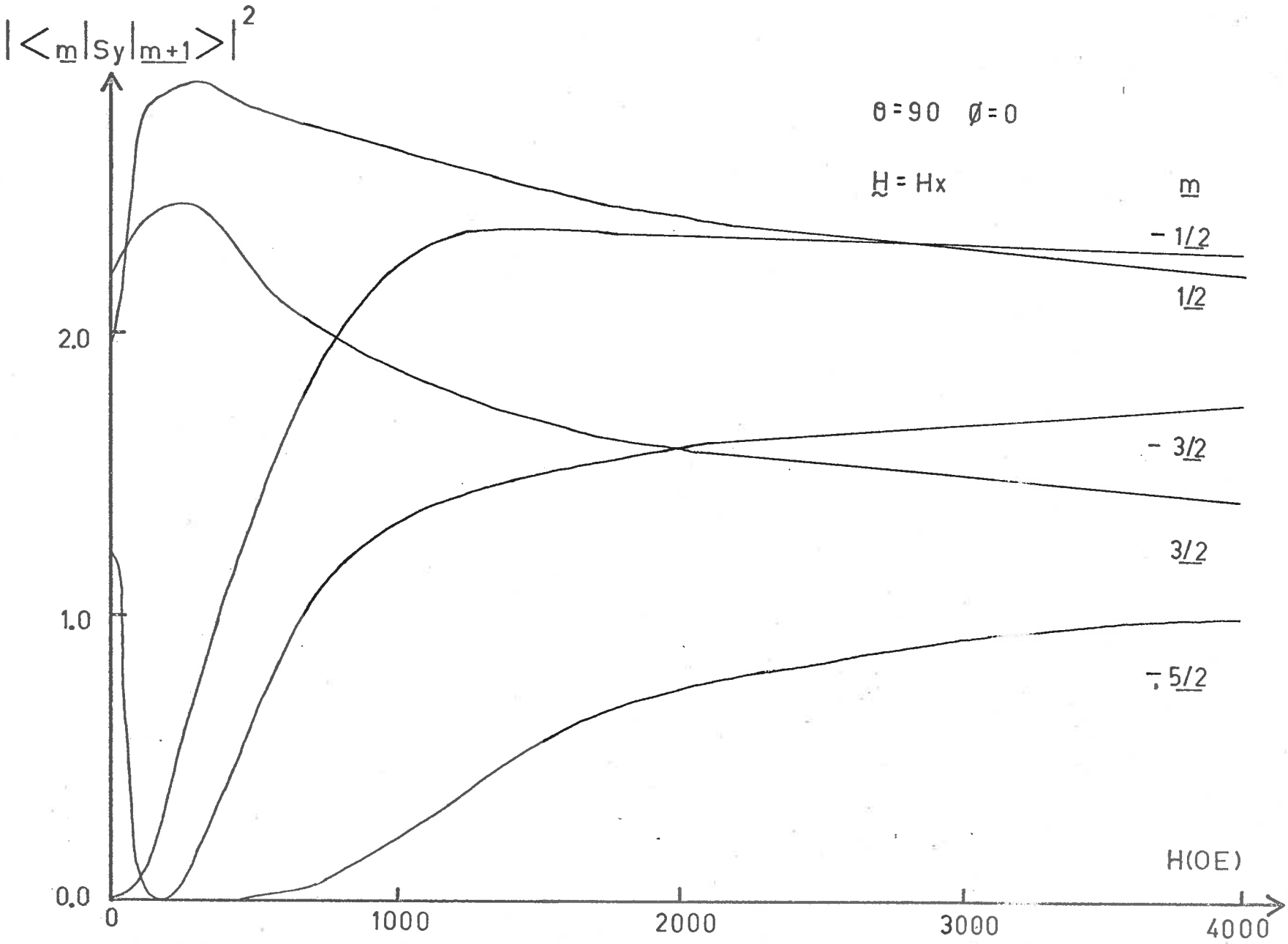

Fig. 4.10 The relative transition probabilities of the allowed "perpendicular" spectrum of Fe^{+++} in Benitoite.

transition probabilities tend to values corresponding to those of the pure | M) states which were seen in the case of the parallel spectrum.

We noticed in Section 4.4.2 that in the "perpendicular" case the D term mixes states | M) and |M ± 2) in a Spin Hamiltonian whose z direction corresponds to the present x direction. Hence the resulting values of $|(\underline{m} \mid S_z \mid \underline{m+2})|^2$ (which might become quite large for significant values of $D/g\beta H$) correspond to values of $|(\underline{m} \mid S_x \mid \underline{m+2})|^2$ in the present system. These matrix elements were computed exactly using the programmes discussed above and shown in Fig. 4.11. They were seen to correspond to the forbidden transitions(shown in Fig. 4.12, which were induced when the applied r.f. and D.C. magnetic fields were parallel to one another and perpendicular to the c axis.

The experimental ratios of the relative intensities at X band of the allowed lines labelled 3,4, and 5 in Fig. 4.4 were 2.28 : 1.72 : 0.83. These were in agreement with the predicted ratios of 2.28 : 1.75 : 0.99, (lines 1 and 2 overlapped and so were not analysed). The forbidden lines near g=4 shown in Fig. 4.12 were found experimentally to have about 10% of the intensity of the allowed lines — this again is in accordance with the calculated values shown in Fig. 4.11.

4.9 Fitting the Forbidden Lines.

Attempts to account for $\Delta M = 2$ transitions in other materials using perturbation theory usually involve considerable discrepancies, (e.g. Bleaney and Ingram (1951), Matarrese (1961)).

The four forbidden lines of the perpendicular spectrum studied in this project also could not be accounted for by using the second order perturbation

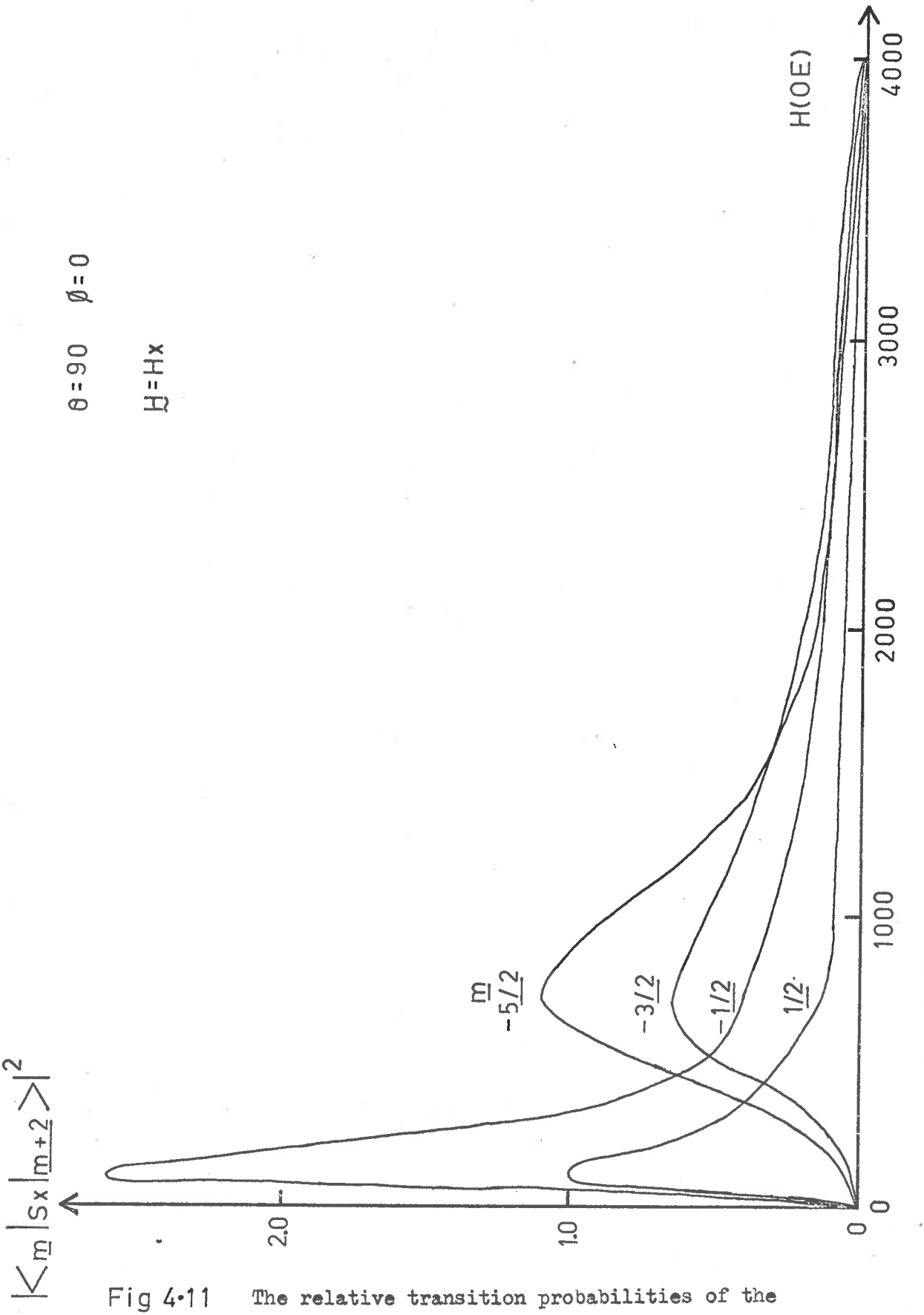

Fig 4·11 The relative transition probabilities of the forbidden "perpendicular" spectrum of Fe^{+++} in Benitoite.

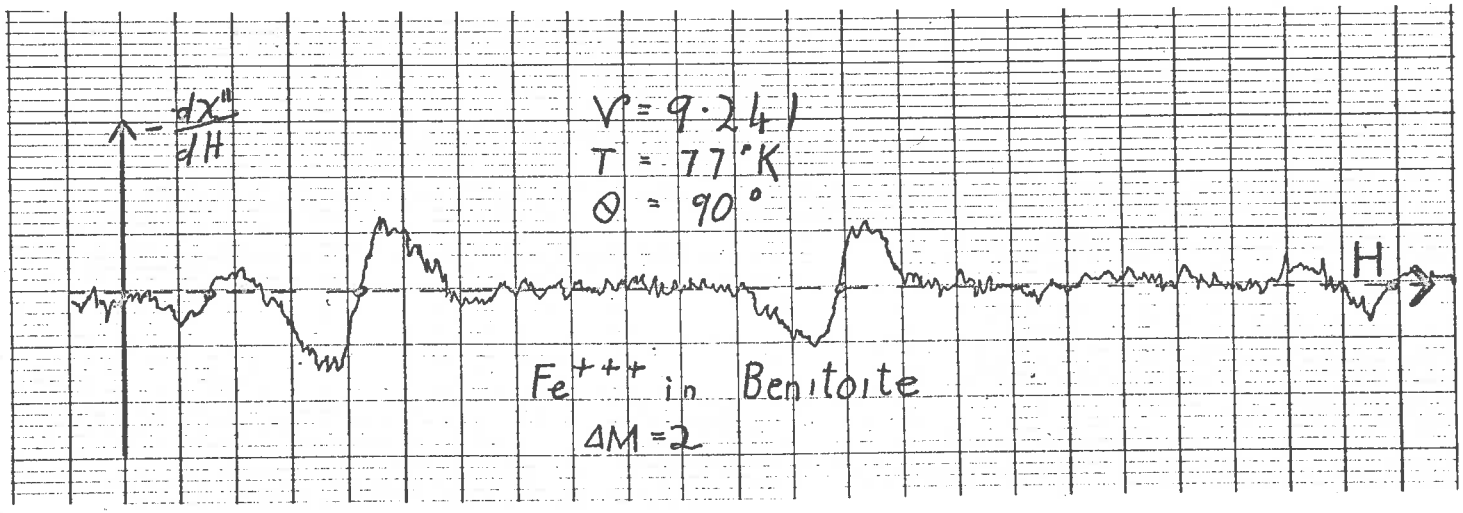

Fig. 4·12

theory of Section 4.4.2 ; (errors of up to 80 oersteds were found, while the experimental error was less than ±10 oersteds). However satisfactory agreement between the Spin Hamiltonian and the experimental results at 77°K could be obtained using the method of computor diagonalisation as the following table shows :

Magnetic Field(oersteds)	Computed Frequency (Gc./s.)	Observed Frequency (Gc./s.)
2,205 ± 10	9,264 ± 0.005	9.258
1,675 ± 6	9,254 ± 0.004	9.258
1,312 ± 6	9.265 ± 0.005	9.258
1,150 ± 10	9.244 ± 0.009	9.258

We may also note that second order perturbation theory incorrectly predicts that the relative transition probabilities shown in Fig. 4.12 have values tending asymptotically to infinity as $\underline{H}$ tends to zero.

4.10 Other Weak Lines.

Assuming they come from Fe^{+++} ions in a trigonal site (Ti^{+++} probably), the five lines labelled a,b,c,d and e in Fig 4.3 can be accounted for by a Spin Hamiltonian of the same form as that of the main spectrum, but whose parameters (at 300°K) are :

$$g = 1.998 \pm 0.001 ,$$
$$D = \pm 0.734 (\pm 3) \text{ Gc/s},$$
$$(a-F) = \pm 0.380(\pm 3) \text{ Gc/s}.$$

We note that the axial field term (D) is 30% smaller than it is in the main spectrum, indicating that the weak spectrum comes from a more nearly cubic site. This is consistent with the X-ray data which indicate that the Ti^{+++} site is more nearly cubic than the larger Ba^{+++} site, (we are assuming again that there

is no significant distortion of the site when the Fe^{+++} ion is substituted in).

4.11 Discussion of the Results.

The allowed and forbidden lines of the main spectrum, due to Fe^{+++} ions in trigonal sites in Benitoite, can be accounted for (within an experimental error determined by the line width) in terms of the Spin Hamiltonian, given in Section 4.3.2, for magnetic fields ranging from 0 to 13,000 oersteds. No experimental evidence was obtained for the variation in values of the parameters between the Kramers doublets, or the changes in values of the Spin Hamiltonian parameters with the magnetic field, which are implied by the more general group-theoretic treatment given in Section 4.3.2.

The ambiguity in sign of the Spin Hamiltonian parameters given in Section 4.5 could be resolved by measurements at liquid Helium temperature. However in the meantime we may observe that universal experience and the theoretical predictions of Powell et al. (1960) would lead us to expect that the sign of "a" is positive. Hence, if we assume that "F" is comparatively small (as its fourth order character would lead us to expect), we can see that it also must be positive, and that consequently "D" is negative. Making these assumptions, and converting the units to the conventional $cm.^{-1}$, the parameters (at room temperatures) are :

$$g = 2.0026(\pm 0.0005) \quad \text{(isotropic)} \ ,$$

$$D = -338.2\ (\pm 0.3) \times 10^{-4} cm.^{-1} \ ,$$

$$a = 123.4\ (\pm 1.0) \times 10^{-4} cm.^{-1} \ ,$$

$$F = 8.0\ (\pm 3.0) \times 10^{-4} cm.^{-1} \ .$$

We notice that the measured "g" value does not show any strong deviation from the free spin value of 2.0023 and so there is no evidence of covalency or other deviations from the crystal field model.

The possibility of distortion at the substitution sites makes it difficult to determine from the spectrum alone whether the main spectrum is due to Fe^{+++} ions in Ba or Ti sites. Assuming there is no such distortion, the Ba site seems the more likely.

CHAPTER V

Mn^{++} in Trigonal Sites in Smithsonite and Apatite.

5.1 Properties of Smithsonite.

Smithsonite ($ZnCO_3$) is an ore of zinc which has the Calcite structure. In mounting such crystals, it is necessary to allow for the fact that the tetramolecular cleavage rhombohedron differs from the true bimolecular unit, (Wyckoff, (1960)). The Zn^{++} ions are situated in two inequivalent sites on threefold axes (see Fig. 5.1). These are rather similar to the pairs of trigonal sites noted in Benitoite. Smithsonite rarely occurs in well crystallized forms, and even when it does, its fracture is uneven. It is brittle ; H = 5.5. In colour it is usually white, but impurities often give it a greyish, greenish or brownish tint.

One fairly well crystallized form from South-West Africa studied in this project was shown by flame spectroscopy to contain about 10 parts per million by weight of manganese; and it was also observed to have a structural e.s.r. spectrum with more than thirty lines, most of which were strongly angle-dependent.

5.2 General Characteristics of the Spectrum.

The spectrum was investigated at X band for magnetic fields up to 7,000 oersteds. At most angles many of the lines were poorly resolved; however, with the magnetic field along the c axis, the lines joined up in pairs and intensified, giving the spectrum shown in Fig. 5.2. This corresponds to two identical superimposed spectra, showing distinctly 22 of the 30 lines characteristic of the allowed manganese spectrum, together with

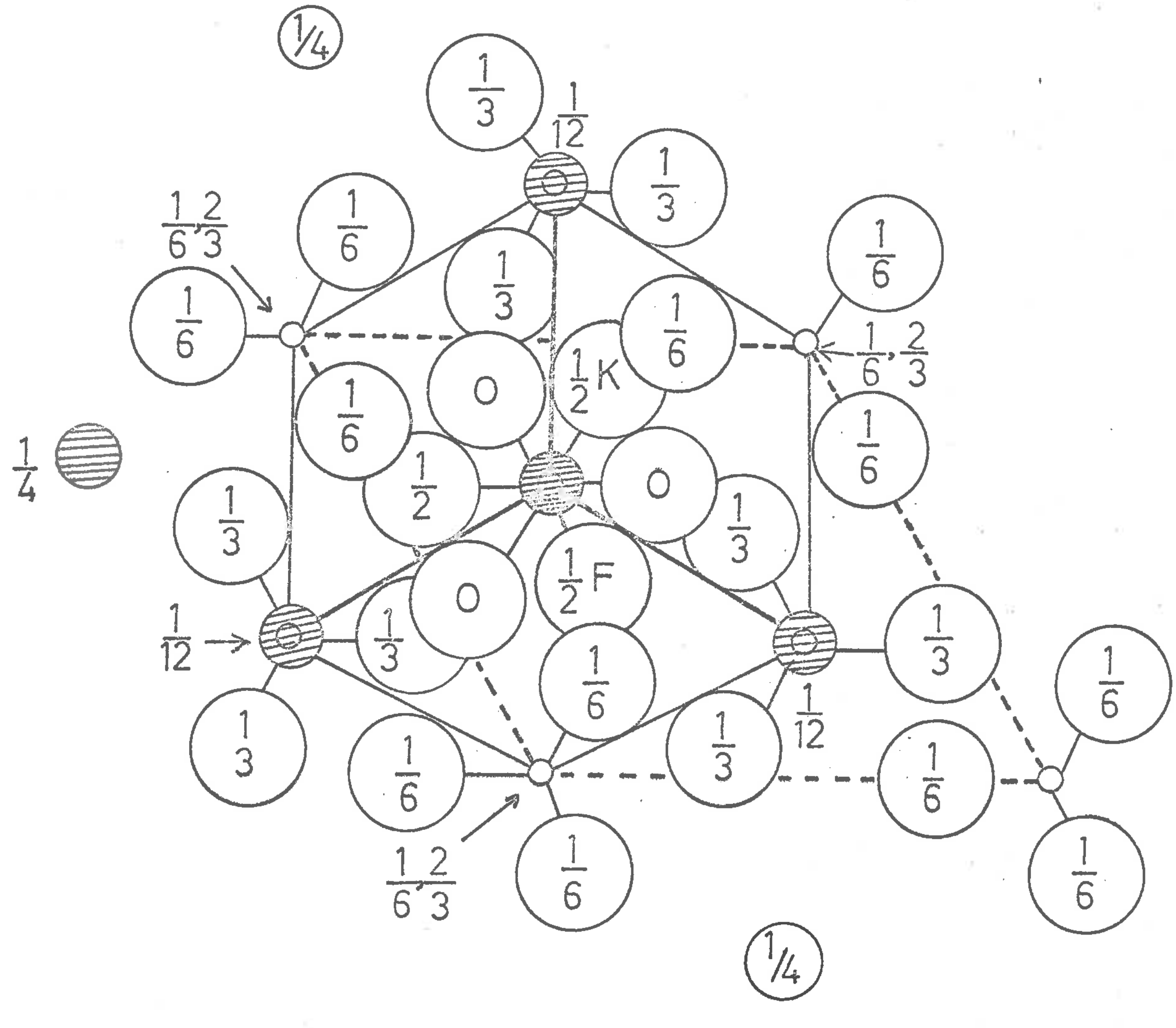

Fig. 5·1 Projection of the Smithsonite structure on the plane 001. (After Wyckoff (1960)).

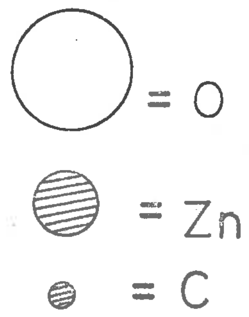

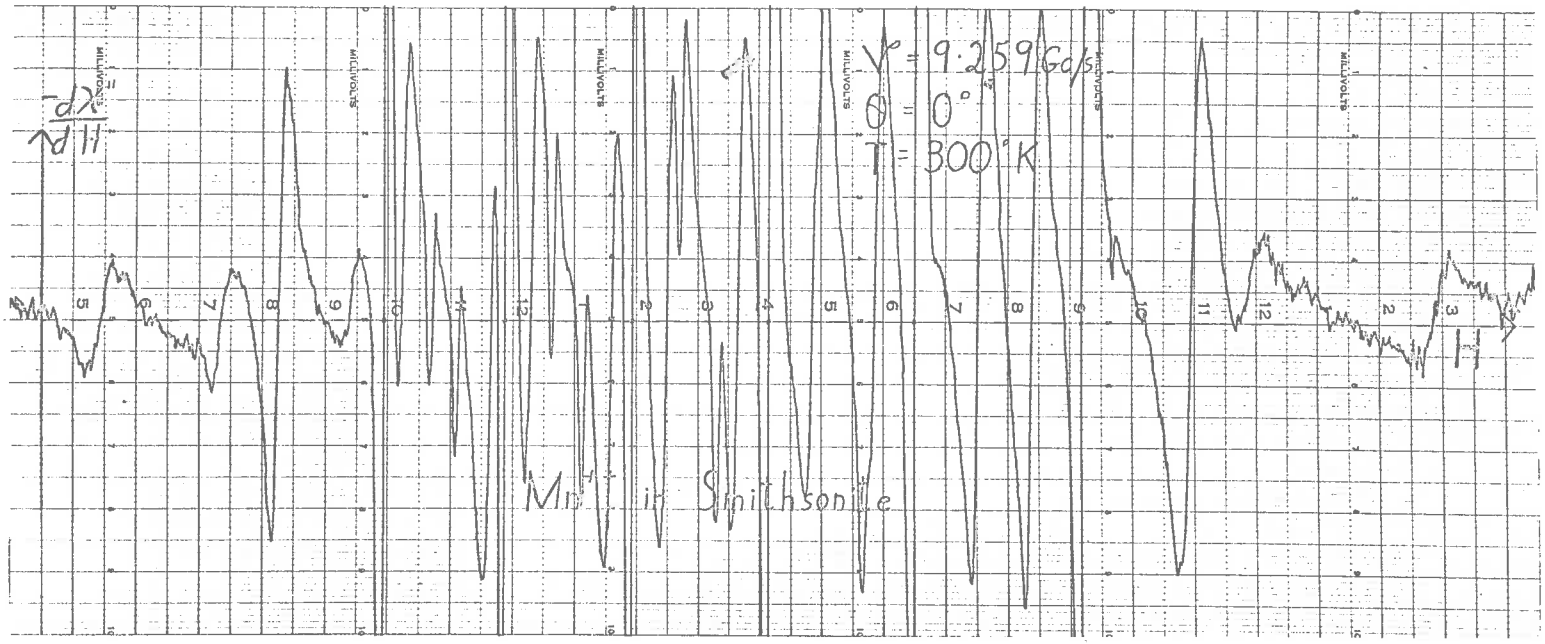

Fig. 5·2

the 10 forbidden $\Delta m = 1$ transitions associated with the central sextet, (Bleaney and Ingram (1951)). With the magnetic field in the plane perpendicular to the c axis, the spectrum was isotropic; but only the central sextet and associated forbidden lines were clearly resolved (see Fig. 5.3). This poor resolution of the fine structure of the allowed "perpendicular" spectrum turned out to be fortunate in that it did not obscure the forbidden $\Delta m = 1$ lines, as occurred in all other materials with Mn^{++} spectra studied in this project.

5.3 The Zeeman Effect in Mn^{++} Ions in a Trigonal Field.

Mn^{++} like Fe^{+++} has a ^6S ground state and so, when substituted into the two inequivalent trigonal sites in Smithsonite, could be expected to show crystal field splittings of the ground state of the same general form as in the case of Fe^{+++} in Benitoite (since in this case, as in the previous one, the two sites differ only in the direction of the axes of the cubic component of the crystal field). But in addition, in this case, the 100% abundant ^{55}Mn in natural Mn has a nuclear spin $I = 5/2$, which is known to have interactions which cause a further splitting of the energy levels studied by e.s.r.. In some substances, experimental evidence has also been obtained for the effect of nuclear quadrupolar interactions of this ion with the gradient of a trigonal electric field at the nucleus (Folen (1962)) and (Schneider and Sircar (1962)).

It has become customary to allow for all these nuclear interactions by adding to the fine structure Spin Hamiltonian (H_s of Section 4.3.2) nuclear hyperfine terms, which for a trigonal site are of the form :

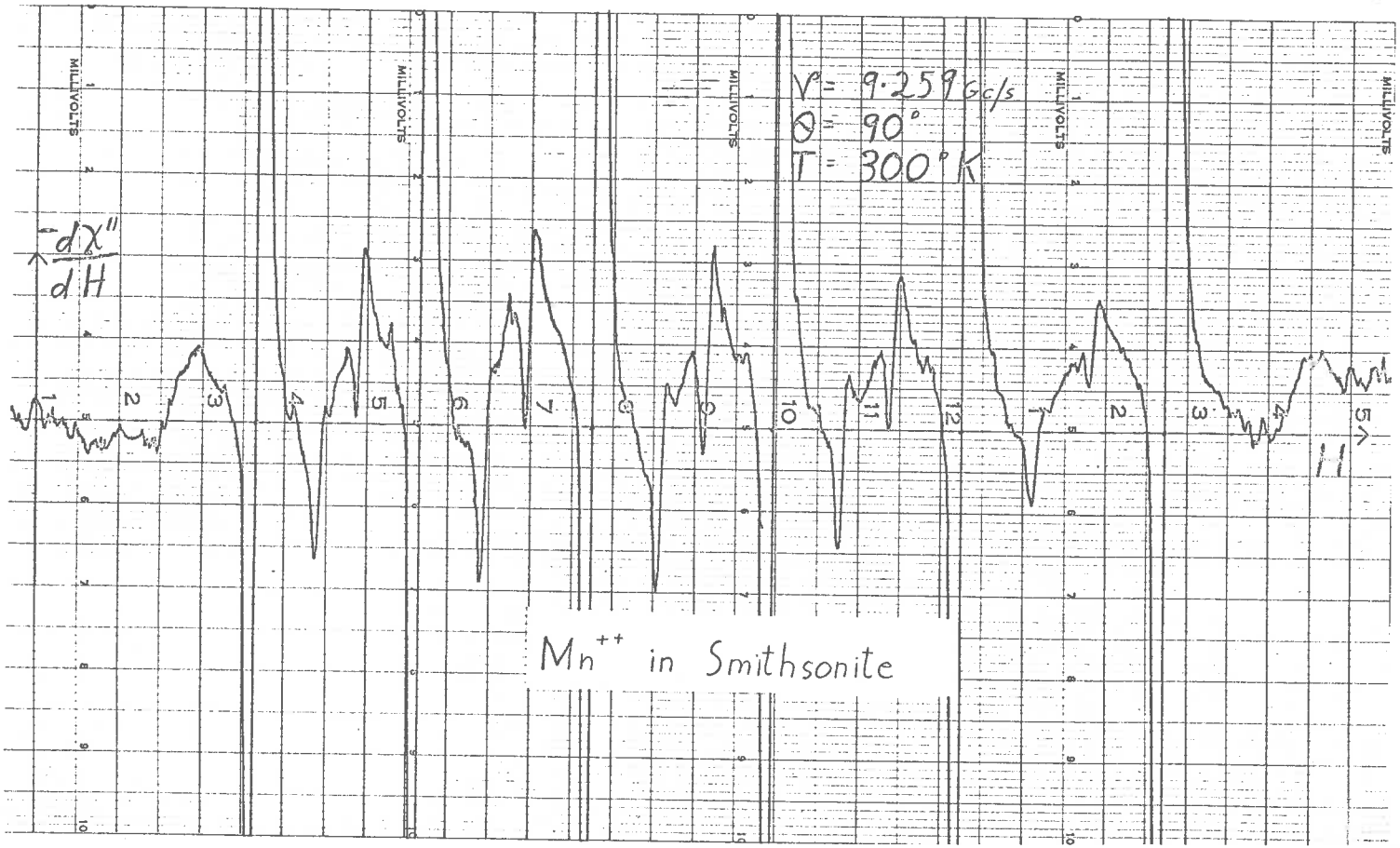
ν = 9.259 Gc/s
θ = 90°
T = 300°K
$\frac{-d\chi''}{dH}$
MILLIVOLTS
Mn++ in Smithsonite

Fig. 5·3

$$H_n = AS_zI_z+\tfrac{1}{2}B(S_+I_-+S_-I_+) - g_I\beta\underline{H}.\underline{I} + P\left[I_z^2 - \tfrac{1}{3}I(I+1)\right], \quad (1)$$

where the z axis is again taken as the trigonal axis, (Low (1960)). In equation (1), the first two terms represent the dipole-dipole interaction of the magnetic moment of the nucleus with that of the unpaired electrons; the third term corresponds to the effect of the applied magnetic field on the nucleus and the P term to the quadrupolar interaction discussed above.

5.4 Calculations Using Strong Magnetic Field States as Basic Vectors.

In the case of a strong magnetic field acting on a system having nuclear spin I as well as electronic spin S, each electron spin energy level splits into 2I + 1 levels. Hence the resulting secular determinant of the perturbations due to both electronic and nuclear spin will be of order (2S + 1)(2I + 1). This corresponds to a 36×36 determinant when S = 5/2 and I = 5/2 as for Mn^{++}.

Such large determinants are difficult to solve exactly and so perturbation procedures have been developed. These are reasonably accurate when the crystal field perturbations are small compared with those due to the magnetic field. However care must be exercised when this is not so. In the case of Apatite, to be studied later in this chapter, even a first order perturbation theory analysis indicates that the D term is comparable with the Zeeman splitting; so in considering higher orders of perturbation, it is necessary to take as the unperturbed operator $H_0 = g\beta\underline{H}.\underline{S} + D\left[S_z^2 - \tfrac{1}{3}S(S+1)\right]$

instead of the $H_o = g\beta \underline{H}.\underline{S}$, used by Bleaney and Ingram (1951) and subsequent workers in this field.

5.4.1 Energy Levels With H Parallel to the c Axis.

Here, using the fine structure Hamiltonian H_s of Section 4.3.2 and the nuclear terms in equation (1) of Section 5.3, the total effective Spin Hamiltonian representing the interactions of both the electronic and nuclear spins in an applied magnetic field can be written as :

$$H_S = g_{\parallel}\beta H S_z + D\left[S_z^2 - \tfrac{1}{3}S(S+1)\right] + \frac{(a-F)}{180}\left[35S_z^4 + 30S(S+1)S_z^2\right.$$

$$\left. + 25S_z^2 - 6S(S+1) + 3S^2(S+1)\right] \pm \frac{\sqrt{2}a}{36}\left[S_z\left\{S_+^3 \exp(-3i\phi)\right.\right.$$

$$\left.\left. + S_-^3 \exp(3i\phi)\right\} + \left\{S_+^3 \exp(-3i\phi) + S_-^3 \exp(3i\phi)\right\}S_z\right]$$

$$+ AS_zI_z + \tfrac{1}{2}B(S_+I_- + S_-I_+) - g_I\beta H I_z + P\left[I_z^2 - \tfrac{1}{3}I(I+1)\right] ,$$

(choosing the trigonal axis as the z axis).

To second order in the perturbation theory (and using $g_{\parallel}\beta H_z S_z + DS_z^2$ as the unperturbed operator) we obtain for the energy levels within the ground term :

$$E_{-5/2,m} = -\frac{5}{2}g_{\parallel}\beta H + \frac{10}{3}D - \tfrac{1}{3}(a-F) - \frac{20a^2}{27(g_{\parallel}\beta H - 2D)}$$

$$-\frac{5}{2}Am - \frac{5B^2}{4(g_{\parallel}\beta H - 4D)}\left[\frac{35}{4} - m(m+1)\right]$$

$$-g_I\beta H m + P\left(m^2 - \frac{35}{4}\right) ,$$

$$E_{-3/2,m} = -\frac{3}{2}g_{\parallel}\beta H - \frac{2}{3}D + (a-F)$$

$$-\frac{3}{2}Am - \frac{8B^2}{4(g_{\parallel}\beta H-2D)}\left[\frac{35}{4} - m(m+1)\right]$$

$$+ \frac{5B^2}{4(g_{\parallel}\beta H-4D)}\left[\frac{35}{4} - m(m-1)\right]$$

$$-g_I\beta Hm + P(m^2-\frac{35}{4}) \quad ,$$

$$E_{-1/2,m} = -\tfrac{1}{2}g_{\parallel}\beta H - \frac{8}{3}D - \frac{2}{3}(a-F) - \frac{20a^2}{27(g_{\parallel}\beta H+2D)}$$

$$-\tfrac{1}{2}Am - \frac{9B^2}{4g_{\parallel}\beta H}\left[\frac{35}{4} - m(m+1)\right]$$

$$+\frac{8B^2}{4(g_{\parallel}\beta H-2D)}\left[\frac{35}{4} - m(m-1)\right]$$

$$- g_I\beta Hm + P(m^2 - \frac{35}{4}) \quad ,$$

$$E_{1/2,m} = \tfrac{1}{2}g_{\parallel}\beta H - \frac{8}{3}D - \frac{2}{3}(a-F) + \frac{20a^2}{27(g_{\parallel}\beta H-2D)}$$

$$+\tfrac{1}{2}Am - \frac{8B^2}{4(g_{\parallel}\beta H+2D)}\left[\frac{35}{4}-m(m+1)\right]+\frac{9B^2}{4g_{\parallel}\beta H}\left[\frac{35}{4}-m(m-1)\right]$$

$$-g_I\beta Hm + P\left(m^2 - \frac{35}{4}\right) \quad ,$$

$$E_{3/2,m} = \frac{3}{2}g_{\parallel}\beta H - \frac{2}{3}D + (a-F)$$

$$+\frac{3}{2}Am - \frac{5B^2}{4(g_{\parallel}\beta H+4D)}\left[\frac{35}{4} - m(m+1)\right]$$

$$+\frac{8B^2}{4(g_{\parallel}\beta H +2D)}\left[\frac{35}{4} - m(m-1)\right]$$

$$-g_I\beta Hm + P\left(m^2 - \frac{35}{4}\right) \quad ,$$

$$E_{5/2,m} = \frac{5}{2}g_{\parallel}\beta H + \frac{10}{3}D - \tfrac{1}{3}(a-F) + \frac{20a^2}{27(g_{\parallel}\beta H+2D)}$$

$$+\frac{5}{2}Am + \frac{5B^2}{4(g_{\parallel}\beta H+4D)}\left[\frac{35}{4} - m(m-1)\right]$$

$$-g_I\beta Hm + P\left(\frac{35}{4} - m^2\right) \quad .$$

5.4.2 Energy Levels With H Perpendicular to the c Axis.

On transforming the effective Spin Hamiltonian of the last section into a coordinate system whose z axis corresponds to the x axis of the original system by means of the transformation given in Appendix C6, we obtain (with H along the x axis) :

$$H_{S'} = g_\perp \beta H S_z + D(S_+^2 + S_+S_- + S_-S_+ + S_-^2) - \frac{(a-F)}{2880}\Big[35(S_+^4 + S_+^2S_-S_+ + S_+^3S_- + S_+^2S_-^2 + S_-S_+^3 + S_-S_+S_-S_+ + S_-S_+^2S_- + S_-S_+S_-^2 + S_+S_-S_+^2 + S_+S_-^2S_+ + S_+S_-S_+S_- + S_+S_-^3 + S_-^2S_+^2 + S_-^3S_+ + S_-^2S_+S_- + S_-^4) - 950(S_+^2 + S_+S_- + S_-S_+ + S_-^2)\Big]$$
$$+ BS_zI_z + \frac{1}{4}(A+B)(S_+I_- + S_-I_+) + \frac{1}{4}(A-B)(S_+I_+ + S_-I_-)$$
$$- g_I\beta H S_z + P(I_+^2 + I_+I_- + I_-I_+ + I_-^2) \quad ,$$

(where we neglect the small off-diagonal component in "a" shown in Appendix C 7, and also some constant terms which affect all levels equally within the ground state). This transformation into the original x direction is chosen only for convenience; any other direction in the "perpendicular" plane could be used, as the spectrum is isotropic in this plane. Using $g_\perp \beta H_z S_z + D(S_+S_- + S_-S_+)$ as the unperturbed operator, second order perturbation theory gives the following energy levels within the ground state :

$$E_{-5/2,m} = -\frac{5}{2}g_\perp\beta H + D + (a-F) + \frac{10D^2}{4(2g_\perp\beta H+3D)}$$

$$- \frac{5}{2}Bm - \frac{5(A^2+B^2)}{8(g_\perp\beta H-2D)}\left[\frac{35}{4} - m(m+1)\right]$$

$$- g_I\beta Hm + \frac{1}{2}P\left(m^2 - \frac{35}{4}\right) ,$$

$$E_{-3/2,m} = -\frac{3}{2}g_\perp\beta H + 3D + \frac{3}{2}(a-F) + \frac{9D^2}{2(2g_\perp\beta H+D)}$$

$$- \frac{3}{2}Bm - \frac{3(A^2+B^2)}{8(g_\perp\beta H-D)}\left[\frac{35}{4} - m(m+1)\right]$$

$$+ \frac{5(A^2+B^2)}{8(g_\perp\beta H-2D)}\left[\frac{35}{4} - m(m-1)\right]$$

$$- g_I\beta Hm + \frac{1}{2}P\left(m^2 - \frac{35}{4}\right) ,$$

$$E_{-1/2,m} = -\frac{1}{2}g_\perp\beta H + 4D + \frac{7}{8}(a-F) + \frac{9D^2}{2(2g_\perp\beta H+D)}$$

$$- \frac{10D^2}{4(2g_\perp\beta H+3D)} - \frac{1}{2}Bm - \frac{3(A^2+B^2)}{8g_\perp\beta H}\left[\frac{35}{4} - m(m+1)\right]$$

$$+ \frac{3(A^2+B^2)}{8(g_\perp\beta H-D)}\left[\frac{35}{4} - m(m-1)\right] - g_I\beta Hm + \frac{1}{2}P\left(m^2 - \frac{35}{4}\right) ,$$

$$E_{1/2,m} = \tfrac{1}{2}g_\perp\beta H + 4D + \tfrac{7}{8}(a-F) - \frac{9D^2}{2(2g_\perp\beta H+D)}$$

$$+\frac{10D^2}{4(2g_\perp\beta H+3D)} + \tfrac{1}{2}Bm + \frac{9(A^2+B^2)}{8g_\perp\beta H}\left[\frac{35}{4} - m(m-1)\right]$$

$$-\frac{8(A^2+B^2)}{8(g_\perp\beta H-D)}\left[\frac{35}{4} - m(m+1)\right] - g_I\beta Hm+\tfrac{1}{2}P(m^2-\frac{35}{4}) \quad ,$$

$$E_{3/2,m} = \frac{3}{2}g_\perp\beta H + 3D + \frac{3}{2}(a-F) - \frac{9D^2}{2(2g_\perp\beta H+D)}$$

$$+\frac{3}{2}Bm - \frac{5(A^2+B^2)}{8(g_\perp\beta H+2D)}\left[\frac{35}{4} - m(m+1)\right]$$

$$+\frac{8(A^2+B^2)}{8(g_\perp\beta H+D)}\left[\frac{35}{4} - m(m-1)\right]$$

$$-g_I\beta Hm + \tfrac{1}{2}P(m^2 - \frac{35}{4}) \quad ,$$

$$E_{5/2,m} = \frac{5}{2}g_\perp\beta H + D + (a-F) - \frac{10D^2}{4(2g_\perp\beta H+3D)}$$

$$+\frac{5}{2}Bm + \frac{5(A^2+B^2)}{8(g_\perp\beta H+2D)}\left[\frac{35}{4} - m(m-1)\right]$$

$$-g_I\beta Hm + \tfrac{1}{2}P(m^2 - \frac{35}{4}) \quad ,$$

(where we neglect the small second order terms in P, a and (A-B)).

5.5 Fitting the Allowed Spectrum of Smithsonite.

Here we have an approximate "strong field spectrum" where the Zeeman effect is much greater than the zero field splitting, and so the allowed transitions are of the form $\Delta M = \pm 1$, $\Delta m = 0$. The physical reason for the selection rule $\Delta m = 0$ is that the nucleus may assume $2I + 1$ orientations in the magnetic field produced by the surrounding electrons. This field is $10^5 - 10^6$ oersteds, and therefore is much larger than the external field. The r.f. magnetic field causing transitions between the electronic levels does not effect the nuclear magnetic moment very much. Since each electronic level sets up different magnetic fields, the transition between two electronic levels differs for each of the $2I + 1$ nuclear orientations. Thus each electron's transition spectrum consists of $2I + 1$ lines. If, as usual, one observes the spectrum at fixed frequency and variable magnetic field, one finds $2I + 1$ approximately equally spaced lines associated with the cases in which the fixed microwave quantum equals the difference in energy between the levels, (Low (1960)).

Also in this "strong field" case we can use, as our zeroth order Hamiltonian in the perturbation calculations of Section 4.4.2 - 3, the usual operator $g\beta \underline{H}.\underline{S}$, since D is small. This simplifies the calculation of the appropriate constants as we can put D equal to zero in the second order corrections to the energy levels derived in the last section.

With the magnetic field parallel and perpendicular to the trigonal axis of the crystal, the allowed lines obtained at 300°K shown in Figs. 5.2 and

5.3 were accounted for by the parameters :

$g_{\parallel} = g_{\perp} = 2.003 \pm 0.001$,
$D = \mp 44.3$ (± 1) oersteds,
$(a-F) = \pm 12.2$ (± 1) oersteds,
$A = \mp 91.8$ (± 1) oersteds,
$B = \mp 92.7$ (± 1) oersteds,

where the relative signs are given by the spacing of the lines, (Bleaney and Ingram (1954)). The rather tedious algebra involved in the relevant calculations was carried out on the 1620 computor. Fortran statements of this programme are shown in Appendix B 9. One may notice, that for completeness, the programme includes third order terms in D and A which although not very significant in this case were useful in interpreting the forbidden lines, as is explained in the next section.

5.6 Fitting the Forbidden Spectrum of Smithsonite.

Forbidden hyperfine transitions ($\Delta m = 1$) have been observed in the e.s.r. spectra of Mn^{++} in various compounds by Bleaney and Ingram (1951), Friedman and Low (1960), Matarrese (1961), Folen (1962), Schneider and Sircar (1962) and Wolga and Tseng (1964).

The latter three authors show that, when making measurments to within a fraction of an oersted, third order perturbation theory terms become significant. However they make significant calculational errors : Folen omits an important third order correction to the energy levels involving B^3 and both Schneider and Sircar and Wolga and Tseng misinterpret its effect on the spacing

between the forbidden transition doublets. Hence the following independent treatment is given, in which allowance is also made for examining the effect of using $g\beta\underline{H}.\underline{S} + DS_z^2$ as the zeroth order Hamiltonian (instead of the more usual $g\beta\underline{H}.\underline{S}$) on the comparatively large second order terms.

Here we add to the second order perturbation theory energy levels derived in Section 5.4.1 all the significant third order terms (using for convenience in evaluating these terms, the unperturbed operator of $g\beta\underline{H}.\underline{S}$, which is valid since they are very small). We find a significant term in B^3 of the form suggested by Lacroix (1957), and another important term in B^2D derived by Bleaney and Rubins (1961).

Third order terms involving "a" have also been derived by Cavenett (1964); but these represent corrections much less than the experimental errors for all values of "a" encountered in this project. Also the third order term in D^2A derived by Wolga and Tseng (1964) had no effect at all on the "parallel" case, and in the "perpendicular" case, merely shifted the forbidden doublets together, and so had no effect on their spacing. Hence we obtain the following values for the $M = \pm\frac{1}{2}$ energy levels when $\underline{H}$ is parallel to the c axis :

$$E_{1/2,m} = \tfrac{1}{2}g_{\parallel}\beta H - \frac{8}{3}D - \frac{2}{3}(a-F) - \frac{20a^2}{27(g_{\parallel}\beta H+2D)}$$

$$+ \tfrac{1}{2}Am - g_I\beta Hm + P(m^2 - \frac{35}{12})$$

$$- \frac{8B^2}{4(g_{\parallel}\beta H+2D)}\left[\frac{35}{4} - m(m+1)\right] + \frac{9B^2}{4g_{\parallel}\beta H}\left[\frac{35}{4} - m(m-1)\right]$$

$$- \frac{B^3}{4(g_{\parallel}\beta H)^2}\left\{9\left[\frac{35}{4} - m(m+1)\right]\left[\tfrac{1}{2}+m\right] + 8\left[\frac{35}{4} - m(m-1)\right]\left[\frac{3}{2} - m\right]\right\}$$

$$- \frac{B^2D}{3(g_{\parallel}\beta H)^2}\left\{18\left[\frac{35}{4} - m(m+1)\right] + 4\left[\frac{35}{4} - m(m-1)\right]\right\} ,$$

$$E_{-1/2,m} = -\tfrac{1}{2}g_{\parallel}\beta H - \frac{8}{3}D - \frac{2}{3}(a-F) + \frac{20a^2}{27(g_{\parallel}\beta H-2D)}$$

$$- \tfrac{1}{2}Am - g_I\beta Hm + P(m^2 - \frac{35}{12})$$

$$- \frac{9B^2}{4g_{\parallel}\beta H}\left[\frac{35}{4} - m(m+1)\right] + \frac{8B^2}{4(g_{\parallel}\beta H-2D)}\left[\frac{35}{4} - m(m-1)\right]$$

$$- \frac{B^3}{4(g_{\parallel}\beta H)^2}\left\{8\left[\frac{35}{4} - m(m+1)\right]\left[\frac{3}{2}+m\right] + 9\left[\frac{35}{4} - m(m-1)\right]\left[\tfrac{1}{2} - m\right]\right\}$$

$$- \frac{B^2D}{3(g_{\parallel}\beta H)^2}\left\{4\left[\frac{35}{4} - m(m+1)\right] + 18\left[\frac{35}{4} - m(m-1)\right]\right\} .$$

Hence for the "parallel"case, the resonance condition corresponding to the transition $|\frac{1}{2},m) \longrightarrow |-\frac{1}{2}, m-1)$ is determined by the equation :

$$h\nu = g_{\parallel}\beta H + \frac{A}{2}(2m-1) - \frac{20a^2}{27(g_{\parallel}\beta H+2D)} - \frac{20a^2}{27(g_{\parallel}\beta H-2D)}$$

$$+ g_{\perp}\beta H - P(2m-1)$$

$$- \frac{8B^2}{4(g_{\parallel}\beta H+2D)}\left[\frac{35}{4} - m(m+1)\right] + \frac{9B^2}{4(g_{\parallel}\beta H)}\left[\frac{35}{4} - m(m-1)\right]$$

$$+ \frac{9B^2}{4(g_{\parallel}\beta H)}\left[\frac{35}{4} - m(m-1)\right] - \frac{8B^2}{4(g_{\parallel}\beta H-2D)}\left[\frac{35}{4} - (m-1)(m-2)\right]$$

$$+ \frac{B^3}{4(g_{\parallel}\beta H)^2}(2m-1)\left(m^2-m-\frac{195}{4}\right) + \frac{22B^2D}{3(g_{\parallel}\beta H)^2}(2m-1) \quad .$$

Similarly for the resonance corresponding to the transition $|\frac{1}{2}, m-1) \longrightarrow |-\frac{1}{2}, m)$, we obtain an analogous equation :

$$h\nu = g_{\parallel}\beta H + \frac{A}{2}(2m-1) - \frac{20a^2}{27(g_{\parallel}\beta H+2D)} - \frac{20a^2}{27(g_{\parallel}\beta H-2D)}$$

$$- g_{\perp}\beta H - P(2m-1)$$

$$- \frac{8B^2}{4(g_{\parallel}\beta H+2D)}\left[\frac{35}{4} - m(m-1)\right] + \frac{9B^2}{4g_{\parallel}\beta H}\left[\frac{35}{4} - (m-1)(m-2)\right]$$

$$+ \frac{9B^2}{4g_{\parallel}\beta H}\left[\frac{35}{4} - m(m+1)\right] - \frac{8B^2}{4(g_{\parallel}\beta H-2D)}\left[\frac{35}{4} - m(m-1)\right]$$

$$+ \frac{B^3}{4(g\,\beta H)^2}(2m-1)\left(m^2-m+\frac{73}{4}\right) \quad .$$

On dividing both these equations by $g_{\parallel}\beta$ and subtracting the second from the first, then on putting $H_o = h\nu/g_{\parallel}\beta$, we obtain as an estimate of the difference between the magnetic fields corresponding to these two resonances :

$$\Delta H = \left[\frac{9B'^2}{2H_o} + \frac{8B'^2}{2H_o}\left(\frac{H_o^2}{H_o^2 - 2D'^2}\right) + \frac{2g_I}{g} H_o\right]$$

$$- \left[\frac{67B'^3}{4H_o^2} - \frac{22B'^2D'}{3H_o^2} + 2P'\right](2m-1) \quad , \qquad (1)$$

(where the primes indicate that the parameters are now measured in oersteds).

The terms in the first set of square brackets give the average spacing of the doublets, while those within the second set indicate the systematic change in spacing as m ranges from -3/2 to 5/2 in unit steps.

When D' is very small compared with H_o (as it is in the spectrum of Mn^{++} in Smithsonite) then equation (1) may be written :

$$\Delta H = \left[\frac{17B'^2}{2H_o} + 2\frac{g_I}{g} H_o\right] - \left[\frac{67B'^3}{4H_o^2} - \frac{22B'^2D'}{3H_o^2} + 2P'\right](2m-1). \qquad (2)$$

This is consistent with the expressions derived by Folen (1962), except that he omits the term in B'^3/H_o^2. It also compares with the expressions used by Schneider and Sircar (1962) and Wolga and Tseng (1964), except that these authors incorrectly use $\frac{25}{2}$ instead of $\frac{67}{4}$ as the coefficient of the term in $B'^3/H_o 2$.

In addition to this expression for the spacing of the forbidden doublets in the "parallel" case, it was found useful to derive an analogous expression for the "perpendicular" case. This was found to be :

$$\Delta H = \left[\frac{17(A'^2+B'^2)}{4H_o} + 2\frac{g_I}{g}H_o\right] - \left[\frac{67B'^3}{4H_o^2} - \frac{22B'^2D'}{6H_o^2} + P'\right](2m-1). \qquad (3)$$

Using the parameters found from the allowed spectrum, it was possible to obtain good fits to both the "parallel" and "perpendicular" forbidden spectra without involving the use of any observable quadrupole interaction. A comparison between the experimental values and the theoretical values (with P' = 0) is given below :

Parallel Case.

ΔH (experimental)	ΔH (theoretical, P' = 0)
——	31.8 oersteds
*27.2(±1.0) oersteds	27.8 "
24.8(±0.4) "	24.7 "
22.0(±0.4) "	21.6 "
19.2(±0.4) "	18.6 "

(* This doublet was difficult to measure accurately being partially obscured by a pair of allowed lines).

Perpendicular Case.

ΔH (experimental)	ΔH (theoretical, P' = 0)
29.8(±0.4) oersteds	29.9 oersteds
27.1(±0.4) "	27.2 "
24.5(±0.4) "	24.5 "
22.3(±0.4) "	21.8 "
19.6(±0.4) "	19.1 "

The very small discrepancy between theory and experiment shown by these tables could be explained either by invoking a very small quadrupolar term ($P' \doteq 0.03$ oersteds), or as seems more likely, by the fact that, experimentally, we did not have pure "parallel" or "perpendicular" spectra because of the imperfect nature of the crystals. This latter suggestion accords with the appearance of the "crystals", which seemed to be a bundle of long crystallites arranged in a wedge formation converging to an angle of about 15°. It is also in agreement with the abnormally high intensity of the forbidden lines. Their intensity would be zero in both the "parallel" and "perpendicular" cases, according to the theory of Bleaney and Rubins (1961),(which considers only state mixing by the third order term containing A^2D); however Cavenett (1964) has found additional mixing effects from third order terms in A^2a which do not lead to zero intensities in the " parallel"

and "perpendicular" cases. But even this effect would be inadequate to explain the very large intensities actually observed. In fact these lines appear to be due to the superposition of many lines from separate crystallites whose axes lie within ±7° of the "parallel" and "perpendicular" cases; and hence their spacings, as well as their intensities, would be expected to differ from those exactly in the "parallel" and "perpendicular" directions.

5.7 The Apatite Spectrum.

Some large single crystals of Apatite ($Ca_{10}(PO_4)_6(F,Cl)$) from Erenfriedersdorf, containing Mn^{++} in concentrations slightly less than 0.1%, were obtained. These made possible a study of the spectrum previously observed in polycrystalline samples by Kasai (1962). Kasai concluded, on the basis of his observations, that the manganese ions were (in the main) in trigonal sites which had a very strong axial field ($D' \doteq 428$ oersteds) and a much smaller cubic field.

It was possible to obtain a best fit at X band and at Q band frequencies to both the "parallel" and "perpendicular" spectra shown in Figs. 5.4 and 5.5 using the perturbation theory formulae derived in Sections 5.4.1 and 5.4.2 with the following parameters :

$$g_{\parallel} = g_{\perp} = 2.000(\pm 0.001) \ ,$$
$$D' = \mp 433(\pm 1) \text{ oersteds} \ ,$$
$$(a-F)' = \pm 3(\pm 1) \text{ oersteds} \ ,$$
$$A' = \mp 96.2(\pm 1) \text{oersteds} \ ,$$
$$B' = \mp 95.5(\pm 1) \text{oersteds} \ ,$$

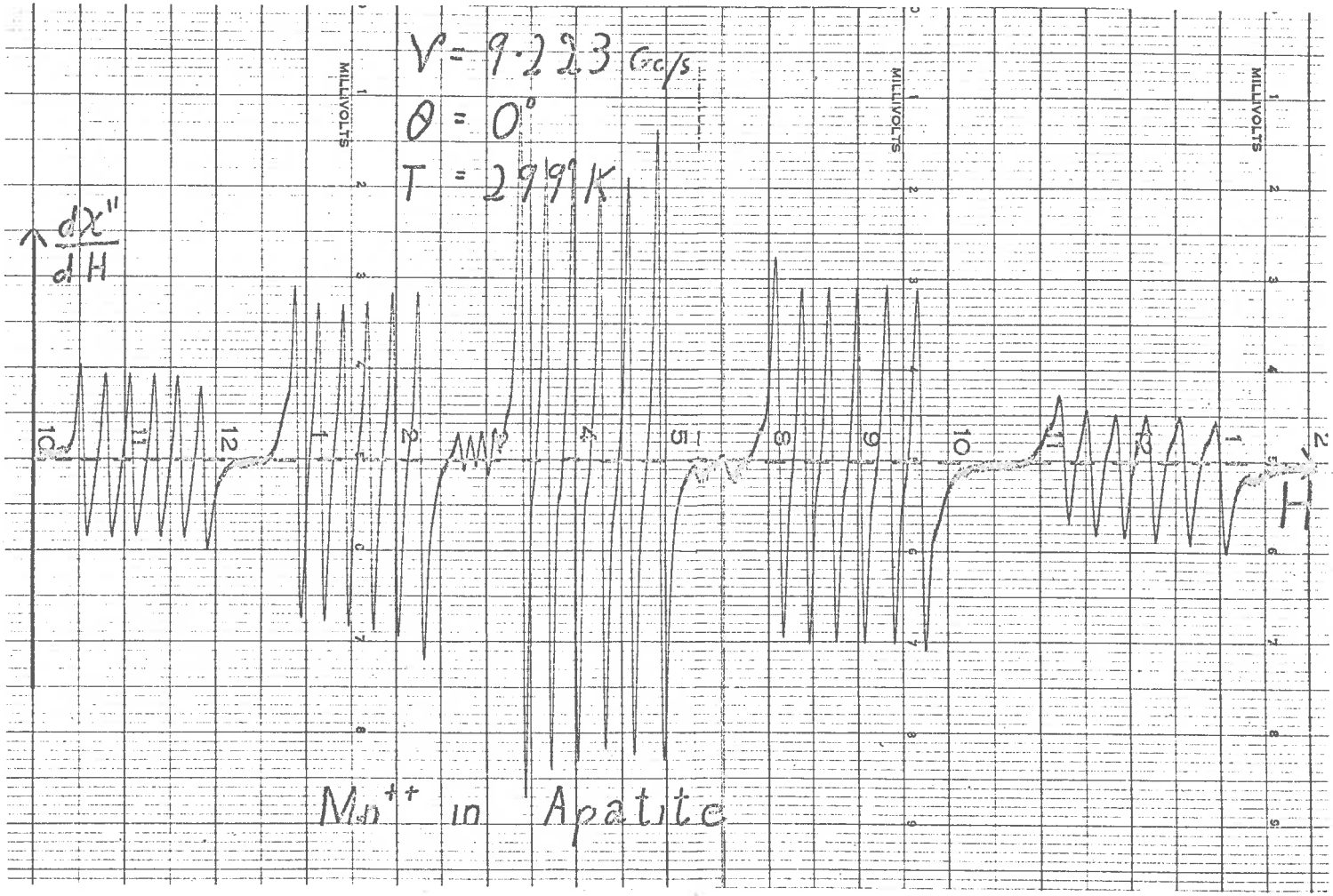

Fig. 5·4

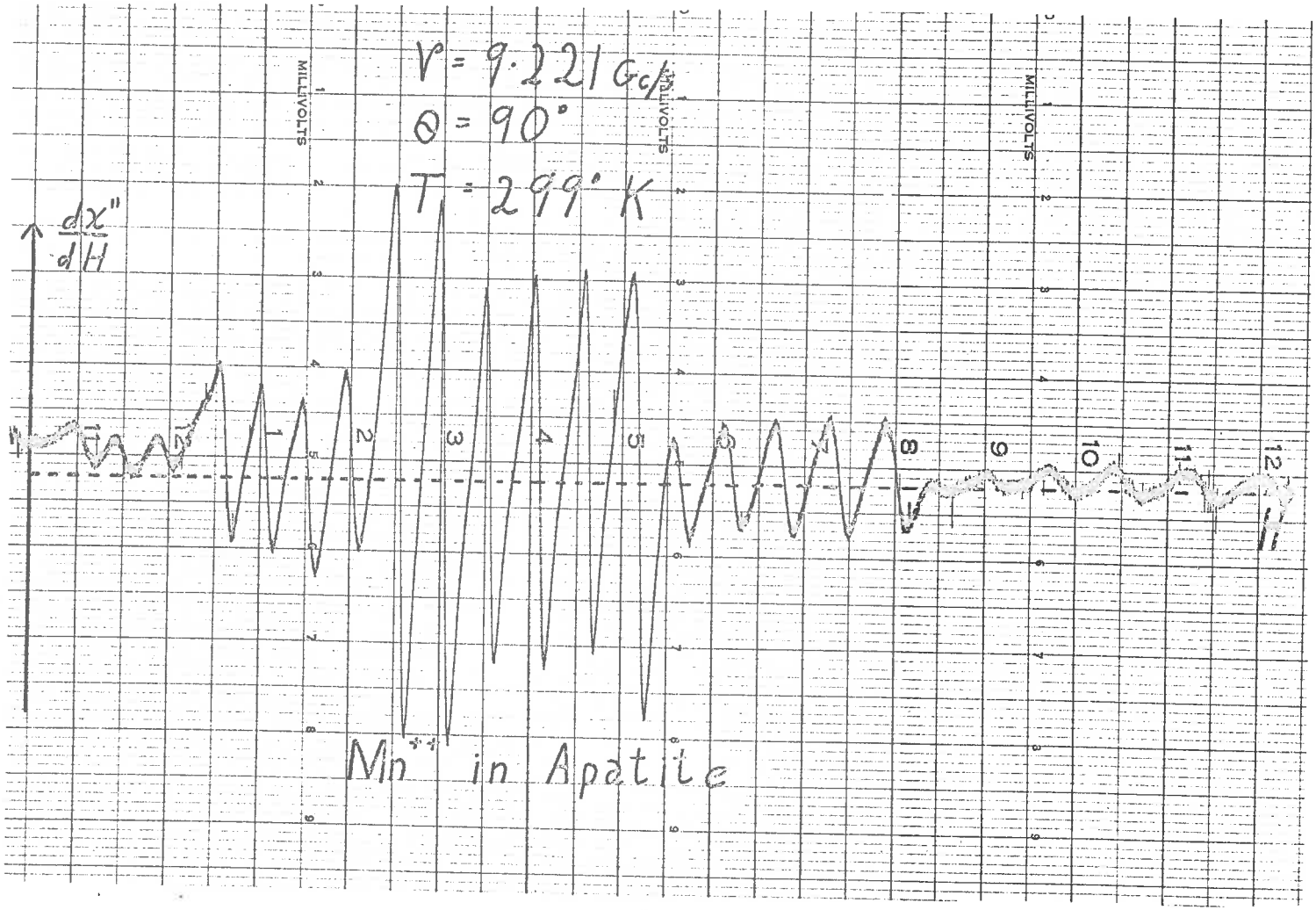

Fig. 5·5

(where the relative signs are given by considering the spacing of the lines in terms of arguments analogous to those of Bleaney and Ingram (1951)). However subsequent to the completion of this analysis, the author was informed of some similar results obtained by Bil'dyukevich et al. and reported to the Conference on Paramagnetic Resonance, Kazan 1960. The parameters communicated to the author by these workers are as follows :

$g = 2.003(\pm 0.001)$,
$|D|' = 433(\pm 1)$ oersteds ,
$|a|' = 3.5(\pm 1)$ oersteds ,
$|A|' = 96\ (\pm 1)$ oersteds ,
$|B|' = 93\ \ (\pm 1)$oersteds .

The differences between the two sets of results may be due to the use of specimens with different Fluorine and Chlorine contents; such variations are common and cause structural variations, (Thewlis et al. (1939)).

However the author was able to observe for the first time the forbidden $\Delta M = 2$, $\Delta m = 0$ transitions in the above sample (see Fig. 5.7), and also the forbidden $\Delta M = 1$, $\Delta m = \pm 1$ transitions in a rather more dilute sample from Ontario (see Fig. 5.6). This latter sample also included an axially symmetric defect centre line with 6 satelite lines; (presumably due to an electron in a trigonal Fluorine site and interacting with a nearby Mn^{++} centre, as has been suggested by Bil'dyukevich). This line could be removed by annealing the sample, after which the central pair of forbidden lines obscured in Fig. 5.6 became visible.

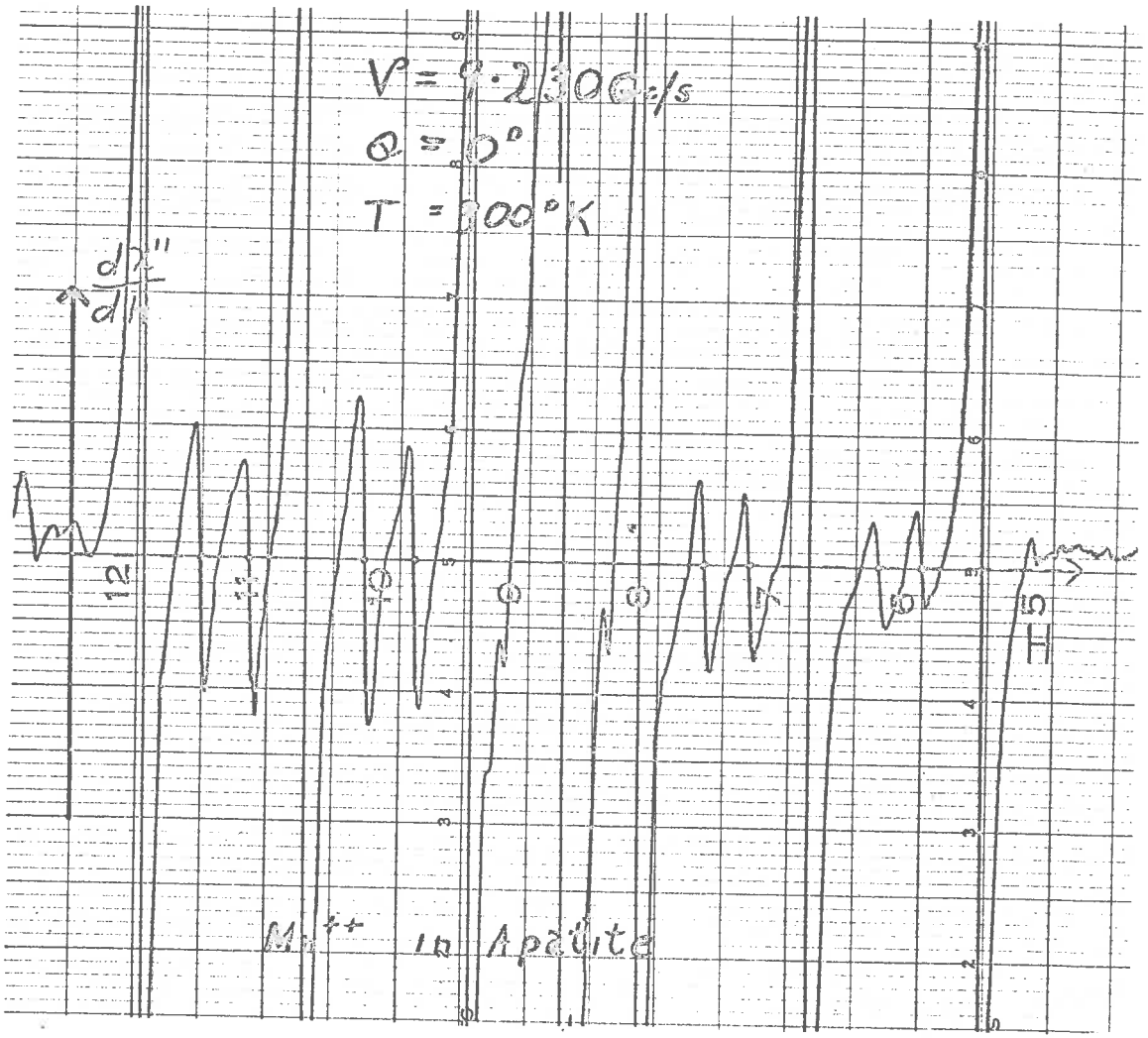

Fig. 5·6

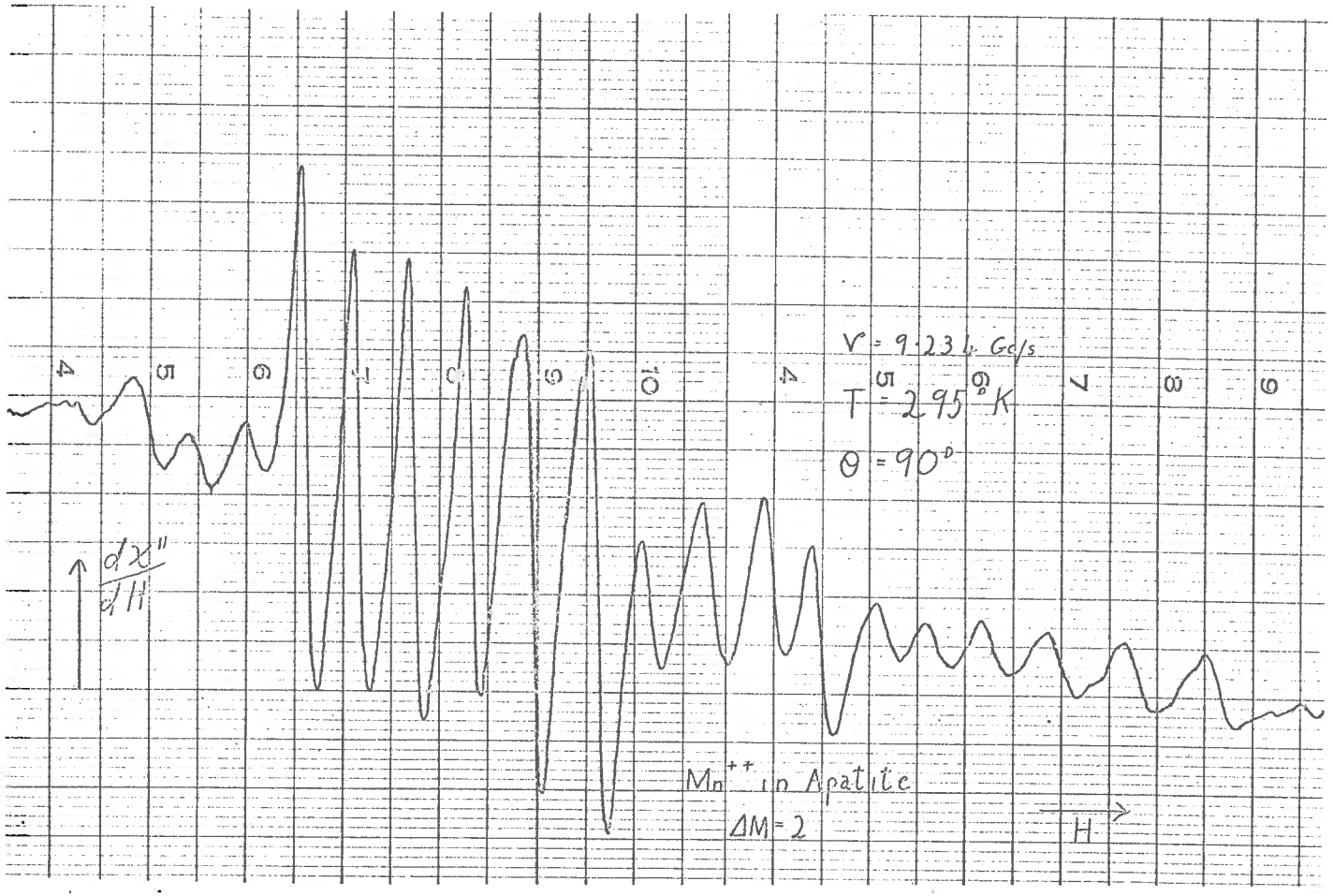

Fig. 5.7

A comparison between the experimental values of the spacing between the forbidden hyperfine transitions and the theoretical values given by equation (1) of Section 5.6 is indicated in the following table for the "parallel" spectrum :

ΔH(experimental)	ΔH(theoretical, P'=0)	ΔH(theoretical, P'=±0.2)
31.3(±0.4) oe.	31.8 oe.	31.1 oe.
29.2(±0.4) "	29.2 "	28.8 "
26.9(±0.4) "	26.5 "	26.5 "
24.6(±0.4) "	23.8 "	24.2 "
22.2(±0.4) "	21.2 "	21.9 "

The average experimental spacing of the doublets is 26.8 oersteds, which compares to within experimental error with the 26.5 oersteds predicted by equation (1) of Section 5.6; but it is not in agreement with the 26.1 oersteds predicted by equation (2) of that Section (which corresponds to the usual theoretical approach in which the D term is not used in the zeroth order of the perturbation treatment).

The forbidden $\Delta M = 2$, $\Delta m = 0$ transitions shown in Fig. 5.7 could not be accounted for in terms of the second order perturbation theory of Section 5.4.2. Discrepancies of the order of one hundred oersteds were noted, but in the light of the experience with such lines due to Fe^{+++} in Benitoite, such discrepancies were attributed to the poor convergence of the perturbation series.

It is therefore expected that a good fit could be obtained by exact diagonalisation of the 36×36 secular determinant.

5.8 Discussion of the Results.

The ambiguity in sign of the experimentally measured Spin Hamiltonian parameters of Mn^{++} in Apatite and Smithsonite can be removed by assuming, as in the case of Fe^{+++} in Benitoite, that "a" is positive and "F" is comparatively small.

Making these assumptions and converting the units to the conventional $cm.^{-1}$, we obtain, for the case of Mn^{++} in Apatite, an accurate fit to the Spin Hamiltonian, at room temperatures, with the parameters :

$$
\begin{aligned}
g &= 2.000(\pm 0.001) \quad \text{(isotropic)} , \\
D &= -404.3(\pm 1) \times 10^{-4} cm.^{-1} , \\
(a-F) &= +2.8(\pm 1) \times 10^{-4} cm.^{-1} , \\
A &= -89.8(\pm 1) \times 10^{-4} cm.^{-1} , \\
B &= -89.2(\pm 1) \times 10^{-4} cm.^{-1} , \\
P &= +0.19(\pm 0.05) \times 10^{-4} cm.^{-1} .
\end{aligned}
$$

Similarly we obtain for the parameters of the Spin Hamiltonian of Mn^{++} in Smithsonite, at room temperatures, in units of $cm.^{-1}$:

$$
\begin{aligned}
g &= 2.003(\pm 0.001) \quad \text{(isotropic)} , \\
D &= -41.4(\pm 1) \times 10^{-4} cm.^{-1} , \\
(a-F) &= +11.4(\pm 1) \times 10^{-4} cm.^{61} , \\
A &= -85.9(\pm 1) \times 10^{-4} cm.^{-1} , \\
B &= -86.7(\pm 1) \times 10^{-4} cm.^{-1} , \\
P &= +0.0(\pm 0.03) \times 10^{-4} cm.^{-1} .
\end{aligned}
$$

In both these cases, the negative sign predicted for "A" is in accord with all experience to date.

Following the theory of Van Wieringen (1955), we can obtain estimates of the percentage covalency of the Mn-O bonds as being about 3% for Apatite and 8% for Smithsonite.

The quadrupole coupling parameter (P) represents the interaction between the quadrupole moment of the ^{55}Mn nucleus and the gradient of the electric field acting on it. This gradient is zero in the case of a purely cubic field, so it is not surprising that evidence of such an interaction is obtained from the Apatite spectrum, where the axial distortion (represented by the "D" term) is large, but is not obtained in the Smithsonite spectrum, where the axial distortion is much less.

CHAPTER VI

Impurity Centres in Tetragonal Sites in Scheelite and Apophyllite.

6.1 The Manganese Spectrum in Scheelite.

The J band spectrum of Mn^{++} in synthetic Scheelite ($CaWO_4$) has been reported (Hempsted and Bowers (1960)), and it was found that at that frequency, "the effect of the applied field is so dominant over all the other interactions that only the $\Delta M = 1$, $\Delta m = 0$ transitions are observed". However some natural specimens from Yalgoo in Western Australia were studied in this project at X band frequencies where, in addition to the allowed lines previously observed, the forbidden $\Delta M = 1$, $\Delta m = 1$, and the $\Delta M = 2$, $\Delta m = 0$ transitions were visible.

The positions of 30 $\Delta M = 1$, $\Delta m = 0$ allowed transitions were measured with $\underline{H}$ parallel to the c axis, and the 45°variations of the line positions as $\underline{H}$ was rotated in the equatorial plane were also measured. Applying second order perturbation theory to the usual Spin Hamiltonain for Mn^{++} in a tetragonal site (Bleaney and Stevens (1953)) :

$$H_S = g\beta\underline{H}.\underline{S} + D\left(S_z^2 - \frac{35}{12}\right) + \frac{7}{36}\left[S_z^4 - \frac{95}{14}S_z^2 + \frac{81}{16}\right]$$

$$+ \frac{a}{6}\left(S_x^4 + S_y^4 + S_z^4 - \frac{707}{16}\right) + AS_zI_z + B(S_xI_x + S_yI_y)$$

$$- g_I\beta\underline{H}.\underline{I} + P\left(I^2 - \frac{35}{12}\right) ,$$

a fit to the experimental results was obtained with the parameters :

$g_{\parallel} = g_{\perp} = 2.000 \pm 0.001$,

$D' = -147.3\ (\pm 1)$ oersteds ,

$\frac{a'}{2} + \frac{F'}{3} = -2(\pm 1)$ oersteds ,

$\frac{5a'}{2} = -10(\pm 1)$ oersteds ,

$A' = -93.5(\pm 1)$ oersteds ,

$B' = -95.1(\pm 1)$ oersteds .

These parameters are in agreement with the values obtained by Hempstead and Bowers.

6.1.1 The Forbidden $\Delta m = 1$ Transitions.

The forbidden $M = \frac{1}{2} \longleftrightarrow -\frac{1}{2}$, $\Delta m = \pm 1$ transitions were easily observed with the magnetic field at all angles off the c axis and the equatorial plane (on the c axis and in the equatorial plane the lines, unlike those in Smithsonite and Apatite, vanished). A trace of the spectrum taken with the magnetic field at 5° to the c axis is shown in Fig. 6.1. Here the ten $M = \frac{1}{2} \longleftrightarrow -\frac{1}{2}$, $\Delta m = \pm 1$ lines are clearly visible, (the two very weak lines on the left are $M = -3/2 \leftrightarrow -\frac{1}{2}$, $\Delta m = \pm 1$ transitions).

In this spectrum, the forbidden $M = \frac{1}{2} \longleftrightarrow -\frac{1}{2}$, $\Delta m = \pm 1$ lines are accurately predicted by equation (1) of Section 5.6 even though this formula was derived for the trigonal and not the tetragonal case. This is due to that fact that this equation does not include the cubic field terms, whose forms represent the only difference between the two cases.

The table below indicates the comparison between the measured spacing at 77°K between the $\Delta m = \pm 1$ doublets (ΔH) and the calculated values, predicted by this theory, for the "parallel" spectrum. (Actually the measurements were taken about 2° from the "parallel"

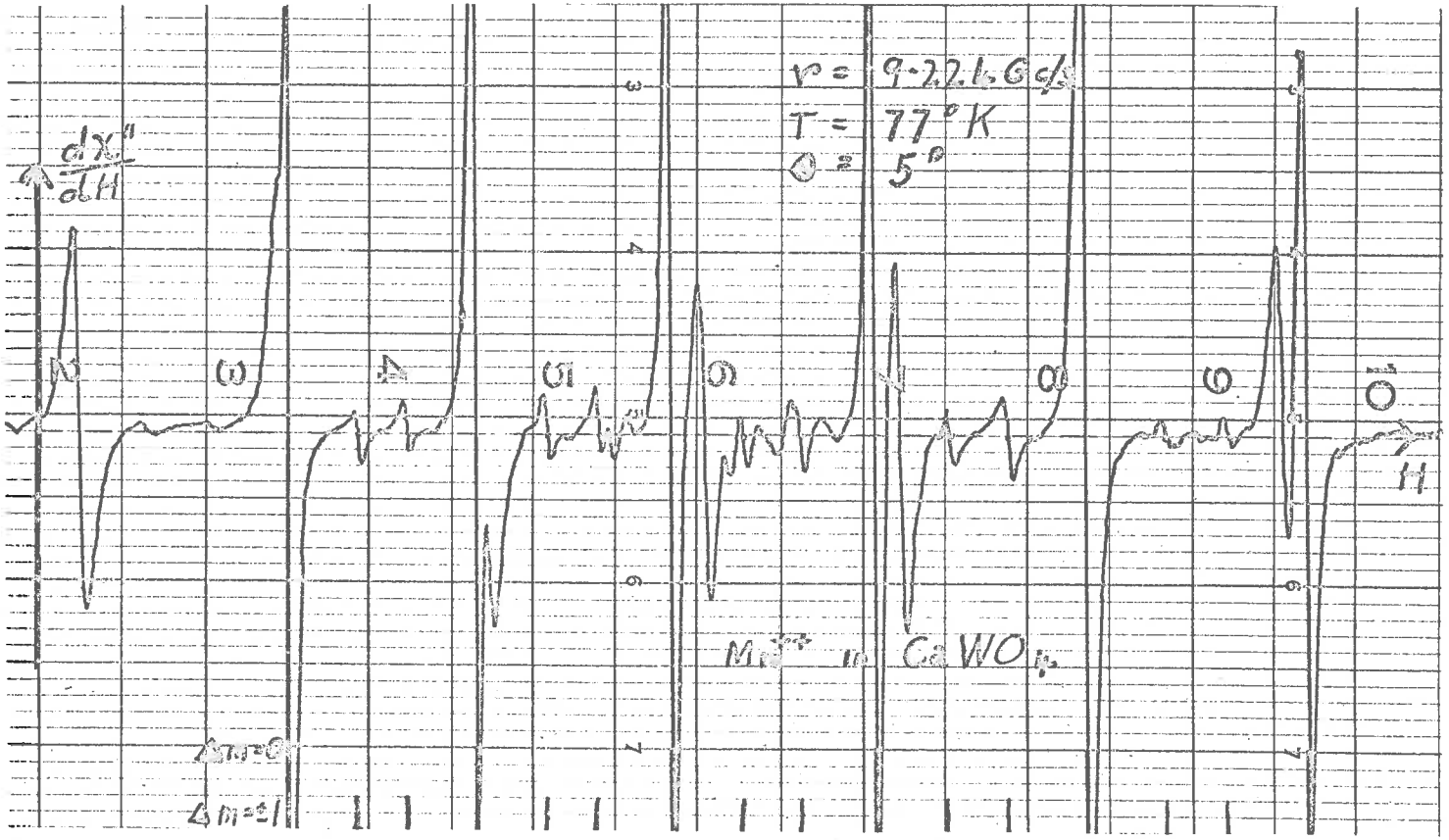

Fig. 6-1

case since in the "parallel" case the lines are forbidden; but this procedure did not lead to any significant error), (c.f. Schneider and Sircar (1962)).

ΔH (experimental)	ΔH(theoretical, P=0)	ΔH(theoretical, P±0.25)
28.9(±0.5) oersteds	27.6 oersteds	28.6 oersteds
27.6(±0.5) "	26.8 "	27.3 "
26.4(±0.5) "	25.9 "	25.9 "
24.9(±0.5) "	25.0 "	24.5 "
23.4(±0.5) "	24.2 "	23.2 "

Again in order to account for the observed widening of the doublets towards high fields, it was necessary to invoke a quadrupolar interaction, this time given by $P' = 0.25 \pm 0.05$ oersteds. Also there was a small improvement (0.15 oersteds) in fitting the observed lines when the D term was included in the zeroth order Hamiltonian.

6.1.2 Low Field Lines.

At fields between 1,400 and 1,800 oersteds, the characersitic $\Delta M = 2$, $\Delta m = 0$ forbidden lines of Mn^{++} were seen. Also in this region and at lower fields a large number of other weak lines were observed which did not occur in the sextets characteristic on Mn^{++}. Their positions and intensities were strongly dependent on the direction of the magnetic field; however they were too weak for detailed analysis.

In another sample of black Scheelite from the

Larkin Mine in North Queensland, much stronger versions of these lines were seen without the complicating Mn^{++} spectrum. Many other lines were observed at fields extending up to 9,600 oersteds. In all, some 23 lines were noted. As these were plainly due to an ion (or ions?) with a large zero field splitting, it was decided to investigate this spectrum on the Monash University Q band spectrometer. Here the seven line Gd^{+++} spectrum observed by Hempstead and Bowers (1960) was resolved out, together with three other weak lines near g = 2 which had different angular properties. These latter lines have not yet been given a definite assignment.

With the c axis identified by the Q band measurements, the X band transitions were again studied with the magnetic field now along this direction. Using the eigenvalues of the factorised secular determinant of the Spin Hamiltonian for Gd^{+++} in a tetragonal field, which were evaluated on the Weapons Research Establishment 7090 computor (see Programme in Appendix B10) the observed spectrum at room temperature was accounted for by the parameters :

$$g = 1.999 \quad ,$$
$$b_2^0 = -939 \times 10^{-4} \text{cm.}^{-1} \quad ,$$
$$b_4^0 = -24 \times 10^{-4} \text{cm.}^{-1} \quad ,$$
$$b_4^4 = -145 \times 10^{-4} \text{cm.}^{-1} \quad ,$$
$$b_6^0 = -0.5 \times 10^{-4} \text{cm.}^{-1} \quad .$$

See Fig. 6.2 for the consequent explanation of the X band and Q band transitions observed in the "parallel" case.

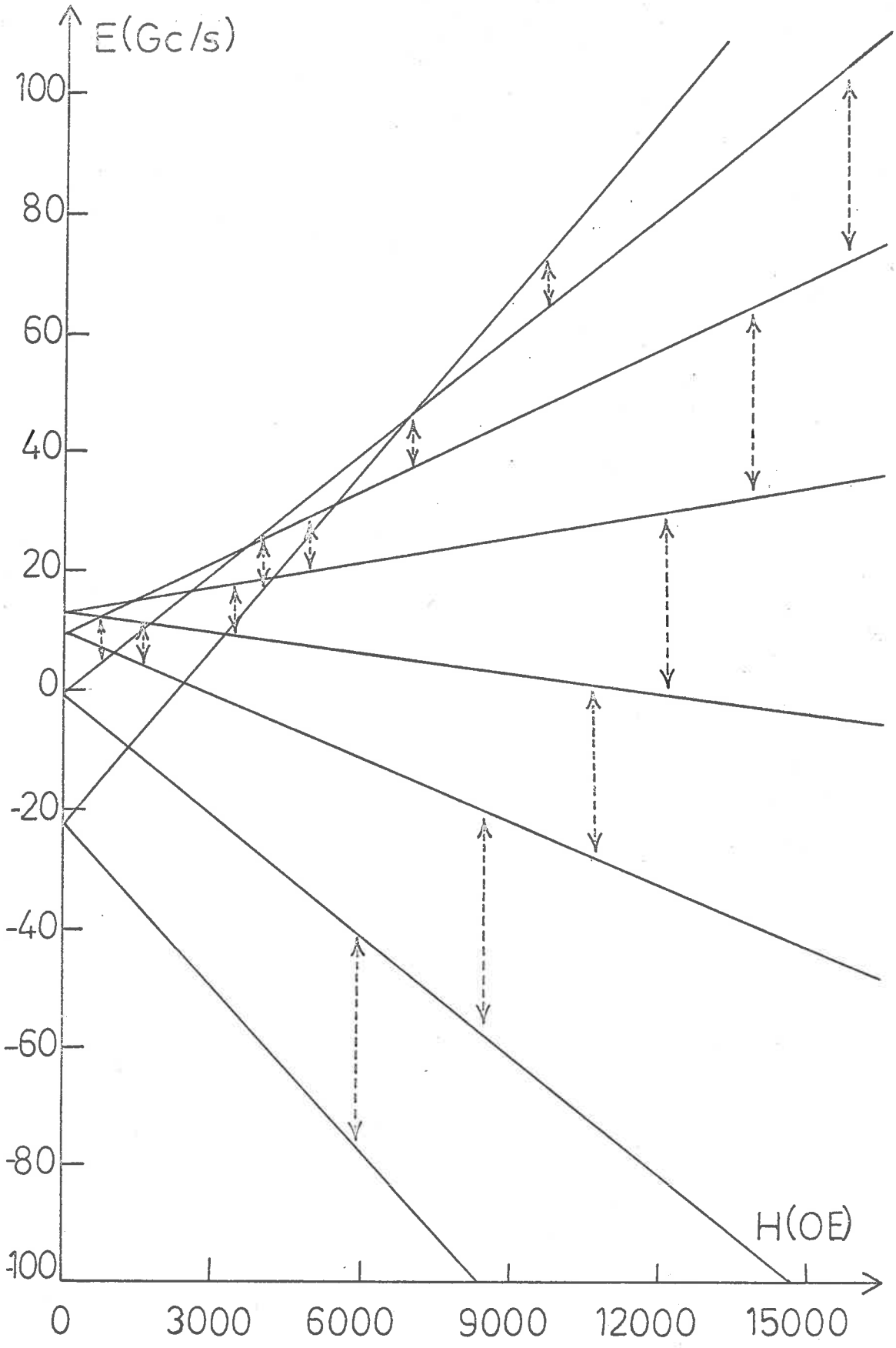

Fig. 6-2 The energy level scheme for the "parallel" spectrum of Gd^{+++} in Scheelite.

The above parameters are in agreement with the values obtained by Hempstead and Bowers when they used second order perturbation theory to account for the J band spectrum at liquid air temperature (77°K), but with an exception in the case of b_2^0, which we found to be 2.5% greater at room temperature (300°K). Such a variation of the axial b_2^0 term with temperature is in accordance with other experience (e.g. the case of Fe^{+++} in Benitoite in Chapter IV). The numerous low field lines vanished for $\underline{H}$ parallel to the c axis, and were apparently the $\Delta M \neq 1$ transitions. All lines were too broad to display the characteristic Gd^{+++} hyperfine structure.

6.2 The Lines in Apophyllite.

Large tetragonal crystals of the sheet silicate Apophyllite $KFCa_4(Si_2O_5)_4 \cdot 8H_2O$ were studied at X band at room temperature. The morphological c axis is easily determined by the perfect c(001) cleavage. One large clear crystal from Kimberly, South Africa showed a strong line near g = 2 which was angle dependent, having turning values when the magnetic field was either in the equatorial plane (where it was isotropic), or when it was along the c axis. No other lines were seen for fields up to 10,000 oersteds. Similar results were obtained for fields up to 15,000 oersteds at Q band.

This might perhaps suggest a simple Spin Hamiltonian of the form :

$$H_s = g_{\parallel}\beta H_z S_z + g_{\perp}\beta (H_x S_x + H_y S_y) ,$$

with $S = \frac{1}{2}$

$g_{\parallel} = 2.0032 \pm 0.0005$,

$g_{\perp} = 2.0435 \pm 0.0005$.

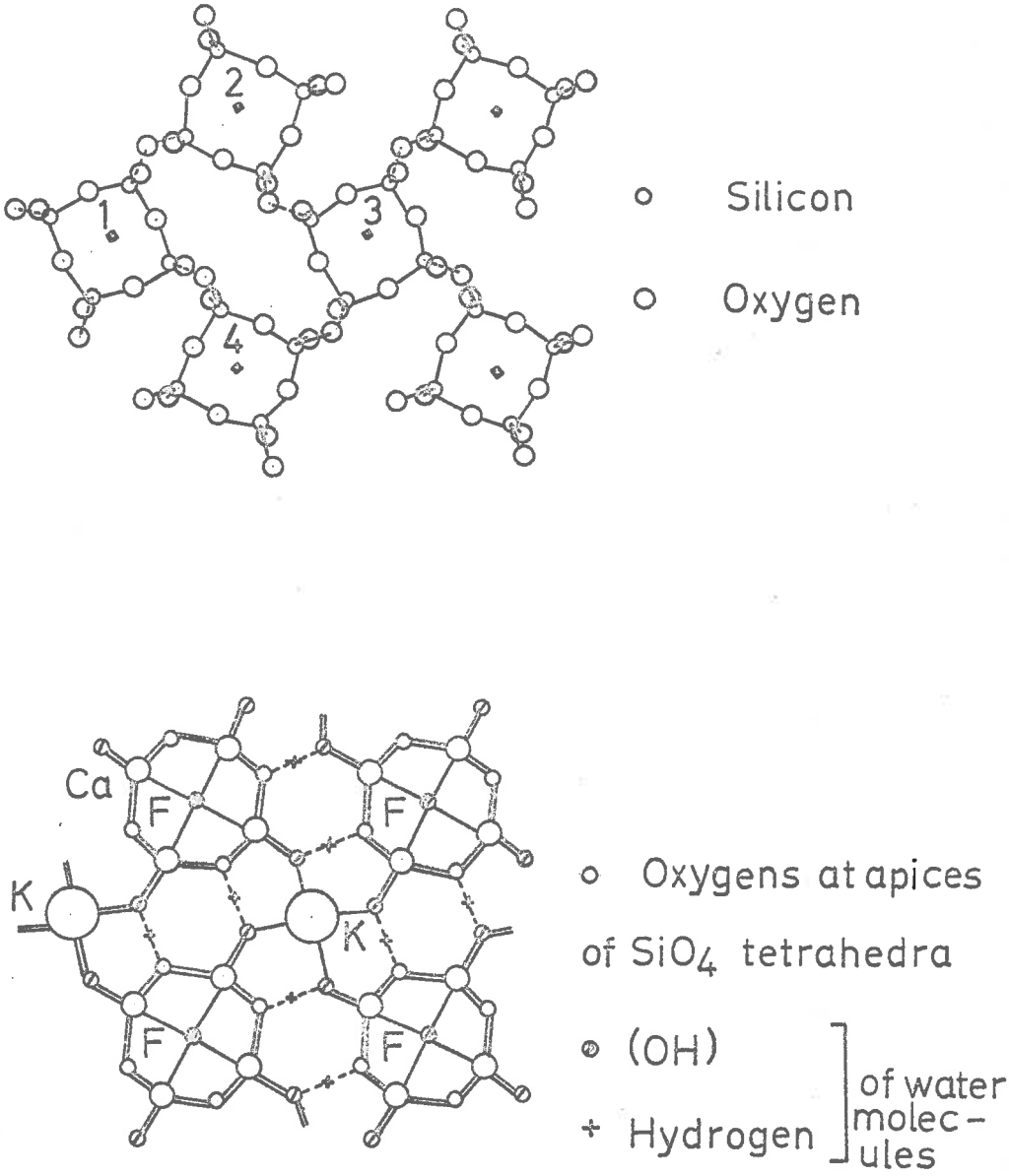

Fig. 6·3 Projection of the Apophyllite structure on the plane 001.

(After Deer et al. (1962)).

Such should occur for an electron or a hole in a trigonal or tetragonal site. An inspection of the crystal structure (see Fig. 6.3) shows no trigonal sites, but there are apparently tetragonal sites ordinarily occupied by F or K ions. Since the sites are tetragonal, we may conclude from the axial symmetry of the spectrum that $S \leq 3/2$. Annealing studies were prevented by the very low decomposition temperature of Apophyllite.

A greenish crystal from Poona, India was also observed to have sets of very weak lines near $g = 2$, probably due to Mn^{++} in the inequivalent rhombic Ca sites. However no fine structure was observed for magnetic fields up to 10,000 oersteds.

Beautiful amethyst pink, yellow and brown crystals reported in other localities (Dana (1932)) may include more interesting paramagnetic centres.

CHAPTER VII

Electron Spin Resonance in Glassy Systems

7.1 Introduction.

Very broad lines (over 1,000 oersteds wide) near g = 2 were found in some Opals (amorphous silica) studied in this project. Also several Australites (glassy silica meteorites) were found to have even wider lines near g = 2. These latter lines were eventually attributed to ferromagnetic resonance effects from included particles of nickel-iron alloy. However the uncertain composition of these glasses did not make them very useful materials to investigate. It was therefore decided to follow a suggestion of Huggins (1958) "that in studying the variations of properties resulting from the substitution of small amounts of other components for a corresponding amount of a given component in a base glass, it should help to use a base glass of known composition, such as a simple sodium silicate or sodium borate glass".

A considerable amount of work has been done on paramagnetic centres in sodium silicate glasses, so it was decided to work with Borax glasses, made in accordance with the method of the well-known "Borax bead" test.

7.2 The Structure of Glasses.

In the classical theory of glasses due to Zachariasen (1932), the oxides in glassy substances were divided into "network formers" and "network modifiers", and only a few compounds were held to satisfy the theoretical requirements of a glass. The "network modifiers" included oxides of uni, bi and some trivalent metals. The "network formers" were supposed to be covalently coordinated to 3 or 4 oxygen atoms. The network

modifying cations located in the interstices of the network were usually Na^+, K^+, Ca^{++} etc., the bonds between these and the oxygens being almost purely ionic. Fig. 7.4 (A) shows how this theory represented the effect of adding a small amount of Na_2O to a B_2O_3 network. According to Warren (1941), "all of the borons remain in the three-fold coordination and there will be two kinds of oxygens, namely, those bonded to two borons and those bonded to only one boron. The sodium ions will try to surround themselves by unsaturated single-bonded oxygens. The number of sodium atoms and of unsaturated oxygens is too small at small sodium oxide content, and they are consequently too widely separated for this to be accomplished effectively".

However, Douglas (1958) has pointed out that, although the "network-former-modifier hypothesis can be regarded as a convenient first approximation to be used in relating the physical properties of silicate-type glasses to their chemical compositions ..., as a second approximation the nature of the chemical bonding of a given atom in a glass must be considered. In some cases this may be conveniently described in terms of coordination number and ionic field strength".

More recent optical work by Bamford (1962) indicates that, as a transition metal (M) is introduced into a series of $Na_2O.XB_2O_3$ glasses with a very high B_2O_3 content, the number of oxygens surrounding the M^{n+} ion is dictated by the network; but with more soda present, the network is broken up and the M can then dictate its surroundings, giving probably a true octahedral $[M\ O_6]^{n+}$ complex ion.

The author's observations of the e.s.r. spectra of Cu^{++} and Ti^{+++} in $Na_2O.2B_2O_3$ glasses is in close

agreement with this model. These ions were studied in some detail because, with their effective spin of one half, they had simple spectra (just one line) which made for simple analysis.

7.3.1 The Spectrum of Cu^{++} in $Na_2O.2B_2O_3$.

The spectrum of Cu^{++} in $Na_2O.2B_2O_3$ glass fused under oxidizing conditions is shown in Fig. 7.1.

The line shape is similar to that observed for Cu^{++} in sets of similar axially symmetric sites which are randomly orientated, as in powders and liquids, (Kneubuhl (1960)). It is also similar to that observed in soda lime silica glass by Sands (1955). The Spin Hamiltonian is obtained by generalising that obtained by Bleaney et al. (1949) for the Tutton salts giving :

$$H_s^i = g_{\parallel}^i \beta H_z S_z + g_{\perp}^i \beta (H_x S_x + H_y S_y) + A^i S_z I_z + B^i (S_x I_x + S_y I_y) ,$$

where $S = \frac{1}{2}$, $I = 3/2$, i ranges over all the different sites, and z is the direction of the axial component of the electric field at a given site. Hence the line width can be attributed to the combined effect of the dispersion of the values of the parameters and their anisotropy.

Following essentially the method of Sands (1955), the average values of $g_{\parallel}^i$, $g_{\perp}^i$, A^i , and B^i were found from the line shape of Fig. 7.1 by ignoring any effect due to differences between the sites, and considering the broad line shape as resulting from the random orientation of uniform tetragonal sites with respect to the direction of $\underline{H}$. This turned out to be a reasonable assumption, as it explained how the asymmetry of the line shape resulted from there being twice as many sites

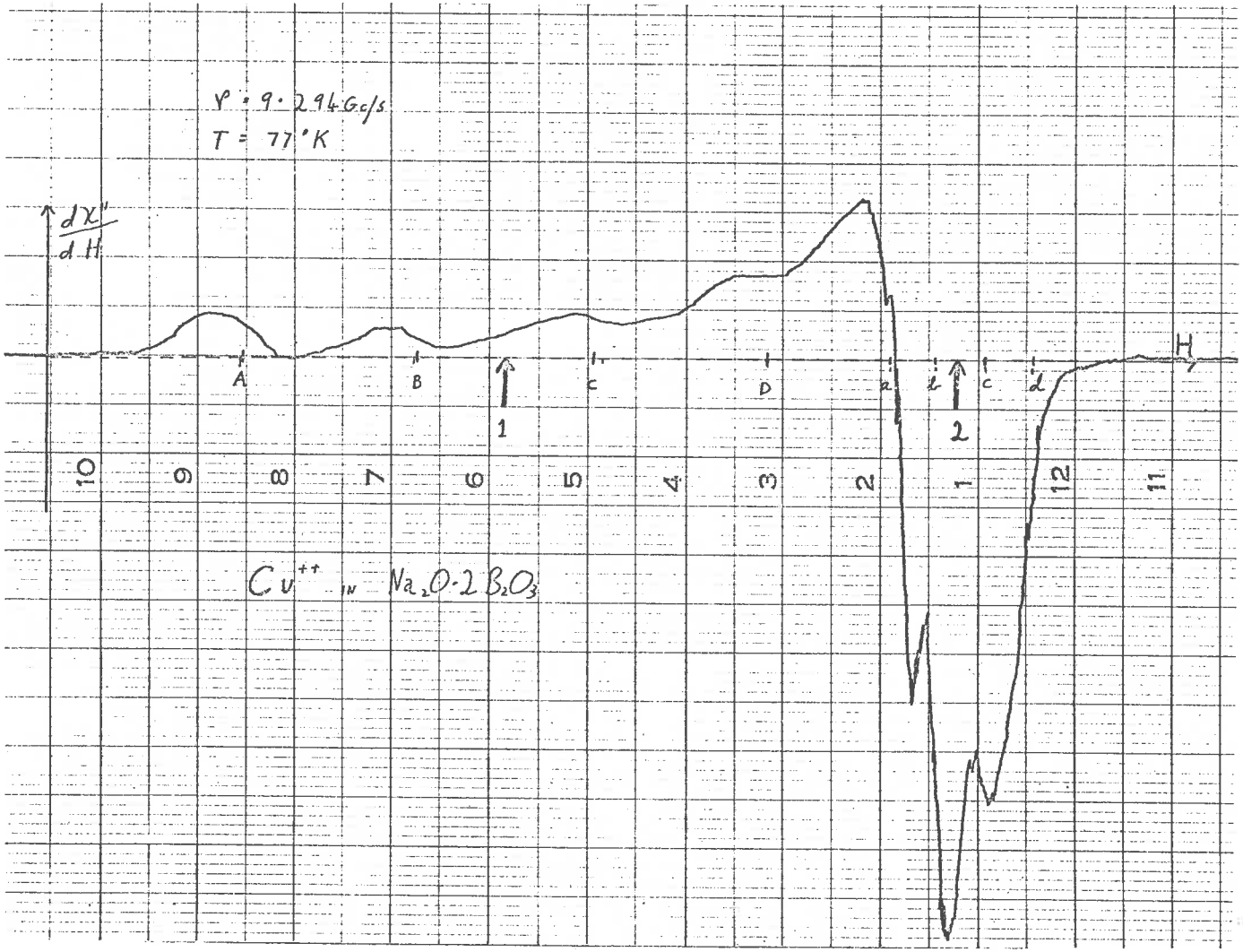
ν = 9·294 Gc/s
T = 77 °K
dχ''/dH
A
B
1
C
D
a
b
2
c
d
H
10
9
8
7
6
5
4
3
2
1
12
11
Cu++ in Na2O·2B2O3

Fig. 7·1

aligned with $\underline{H}$ near the equatorial plane as with $\underline{H}$ near the tetragonal axis.

This analysis indicates that the upper four lines (a, b, c, d, in Fig. 7.1) are given by :

$$\frac{h\nu}{g_{\perp}\beta} = H + \frac{Bm}{g_{\perp}\beta} \quad , \quad (m = \pm 3/2, \pm \tfrac{1}{2})$$

and the lower four lines (A, B, C, D, in Fig. 7.1) are given by :

$$\frac{h\nu}{g_{\parallel}\beta} = H + \frac{Am}{g_{\parallel}\beta} \quad , \quad (m = \pm 3/2, \pm \tfrac{1}{2})$$

(corresponding to the allowed $\Delta M = 1$, $\Delta m = 0$ transitions).

These formulae fit the experimental results for the parameters :

$$g_{\parallel} = 2.330 \pm 0.010 \ ,$$
$$g_{\perp} = 2.040 \pm 0.003 \ ,$$
$$A = 146(\pm 1) \times 10^{-4} cm^{-1} \ ,$$
$$B = 33(\pm 1) \times 10^{-4} cm^{-1} \ .$$

There was no significant temperature dependence of these parameters between 77°K and 300°K.

7.3.2 Theory of Cu^{++} in $Na_2O.2B_2O_3$.

The parameters obtained above are in close agreement with those obtained for the known octahedral Cu^{++} complexes in the Tutton salts (Bleaney et al. (1949)). Also Bamford (1962) has shown that Cu^{++} in Borax has the broad absorption band near 12,500cm.$^{-1}$ characteristic of the $Cu(OH_2)_6^{++}$ complex. He attributes this to the splitting by the cubic field of the $3d^9$, ^2D

ground state of Cu^{++} into a low lying doublet Γ_3 and a higher triplet Γ_5. However this seems arguable (Orgel (1959)), and here we follow Polder (1942) in attributing this band to transitions between the orbital singlets produced by a tetragonal Jahn-Teller distortion acting on the low lying Γ_3 doublet.

According to Polder, the effect of cubic and tetragonal fields on the ^2D state may be shown as follows :-

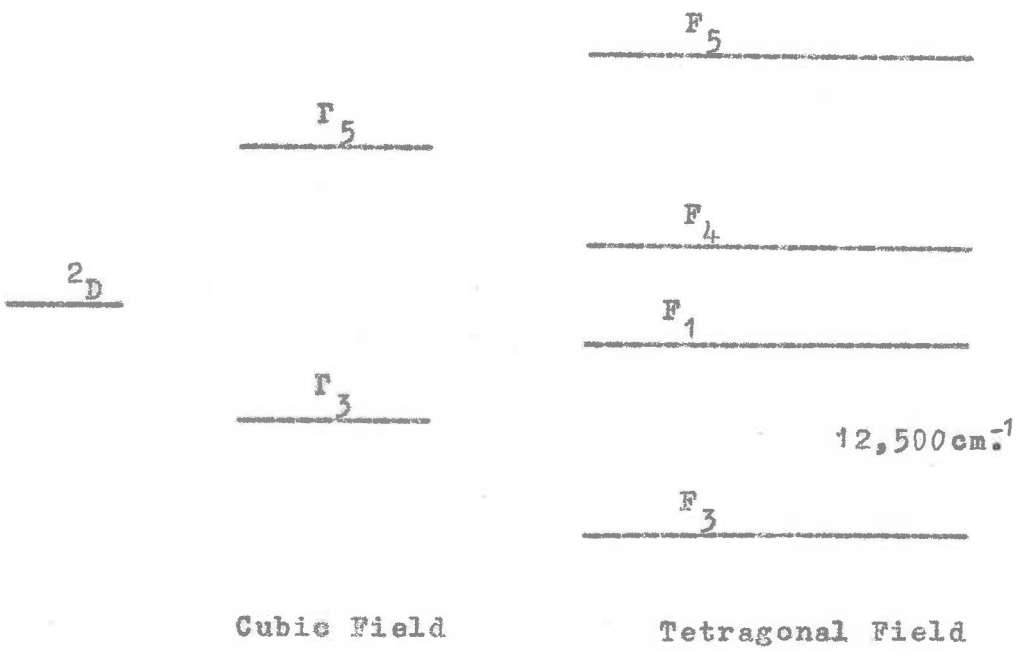

Polder concluded that the terms describing the tetragonal splitting were not small compared with the cubic term in the Cu Tutton salts. Also he showed that the g values were given by :

$$g_{\parallel} = 2\left(1 - \frac{4\lambda}{F_4 - F_3}\right),$$

$$g_{\perp} = 2\left(1 - \frac{\lambda}{F_5 - F_3}\right),$$

where λ is the spin orbit coupling constant, which is taken as that of the free ion.

Substituting in the experimental values of $g_{\parallel}$ and $g_{\perp}$ obtained above for Cu^{++} ions in Borax glass, this indicates that, in that case, $F_4 - F_3 = 21,000 \pm 1,000 cm.^{-1}$ and $F_5 - F_3 = 44,000 \pm 4,000 cm.^{-1}$. The former value may prove interesting in the light of the transition near $22,000 cm.^{-1}$ observed optically by Bamford (1962), but for which he was unable to offer any explanation.

The g values are in close agreement with those obtained by Sands (1955) for silicate glasses. The significantly smaller value of $g_{\perp}$ obtained in the Borax case is in accordance with the expectation of higher ligand field strengths in sodium borate glasses than in the sodium silicates, (Bamford (1962)).

7.4.1 The Spectrum of Ti^{+++} in $Na_2O.2B_2O_3$.

The e.s.r. spectra of Ti^{+++} ions in lithium, sodium and potassium silicate and phosphate glasses have been studied by Yafaev and Yablokov (1962). However, they report that " in all the borate glass samples, an e.s.r. signal could not be detected. Nor did the borate glasses used have discolourations".

However, on adding TiO_2 to Borax and fusing under the strongly reducing conditions in the centre of a bunsen flame, the author obtained beads which gave the e.s.r. spectra shown in Fig. 7.2. These were similar to the spectra obtained by Yafaev and Yablokov for Ti^{+++} in silicate glasses.

Here, as in the Cu^{++} case, the asymmetric line shape would suggest an approximately axially symmetric

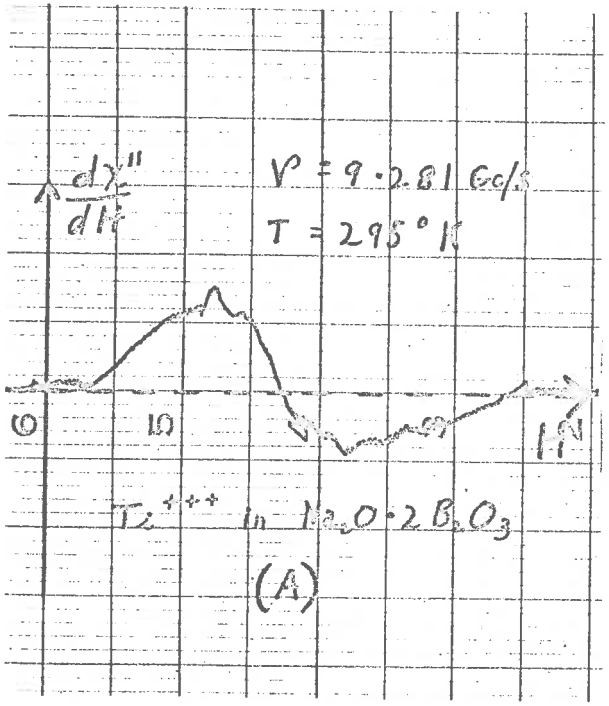
$\frac{dx''}{dH}$
V = 9·2.81 Gc/s
T = 295° K
0
10
H
Fe^{+++} in Na_2O·2B_2O_3
(A)

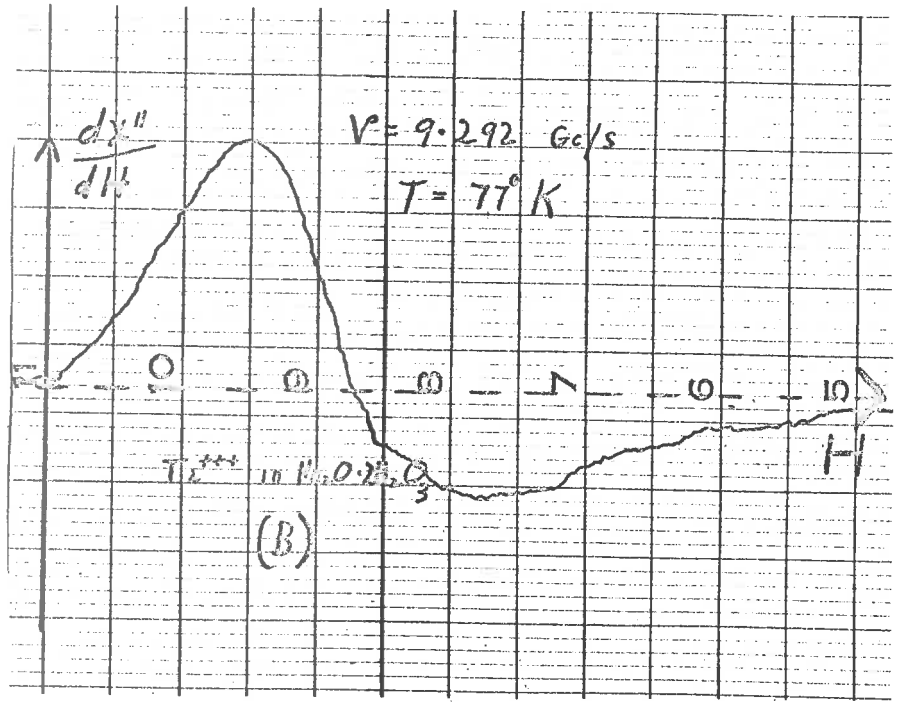
$\frac{dx''}{dH}$
V = 9·292 Gc/s
T = 77° K
0
10
H
Fe^{+++} in Na_2O·2B_2O_3
(B)

Fig. 7·2

site (but in this case, $g_{\parallel}$ is less than $g_{\perp}$ and there is no observed nuclear interaction). We shall accordingly use the Spin Hamiltonian :

$$H_s^i = g_{\parallel}^i \beta H_z S_z + g_{\perp}^i \beta (H_x S_x + H_y S_y) ,$$

where $S = \frac{1}{2}$ and i ranges over all sites.

In the absence of hyperfine structure, it is difficult to obtain useful measures of the average values of $g_{\parallel}$ and $g_{\perp}$ and so the lines are described in terms of an effective g ($g_{eff.}$), whose value indicates the field position where the derivative trace is zero, and ΔH, which measures the distance between the points of the maximum slope. The results obtained at 300°K and 77°K are shown in the table below (where they are compared with the values obtained for silicate glass by Yafaev and Yablokov).

Composition by synthesis.	300°K		77°K	
	ΔH (oersteds)	$g_{eff.}$	ΔH (oersteds)	$g_{eff.}$
$20Na_2O$ $\cdot 79SiO_2$ $\cdot 5TiO_2$	79 ± 4	1.926±0.002	165 ± 8	1.894±0.001
$20Na_2O$ $\cdot 40B_2O_3$ $\cdot 5TiO_2$	67 ± 4	1.944±0.008	122 ±10	1.875±0.008

7.4.2 Theory of Ti^{+++} in $Na_2O.2B_2O_3$.

The violet colouration observed in the beads is in accordance with the absorption band at 20,000cm.$^{-1}$ seen in octahedral $Ti(H_2O)_6^{+++}$, (Hartmann and Schlafer (1951)). We expect also a trigonal Jahn-Teller distortion, splitting the threefold orbital degeneracy of the ground state Γ_5 (given by the action of an octahedral field on the $3d^1$, ^2D ground state of Ti^{+++}), (Van Vleck (1940)). Hence an axially symmetric g factor is to be expected. However this would require g values close to 2 and with $g_\perp > g_{//}$. This could only occur with a very strong trigonal field and/or with a large amount of covalent bonding, (Rei (1962)). Results of a similar character were obtained by Bowers for Ti^{+++} in $KTi(C_2O_4)_2.2H_2O$, but the structure of this compound is not known and so no theoretical account has been given of its g values, (Bowers and Owen (1955)).

Following Yafaev and Yablokov, we note that the temperature dependence of the observed broad lines can be explained by supposing that they represent a superposition of lines from many centres having different relaxation times and g values. Further, we suppose that some centres with small trigonal splittings (and consequently small relaxation times and g values) become visible only at low temperatures. This then explains the broadening of the lines towards high fields as the temperature is lowered.

7.5 Damage Centres in Borax Glass.

Optical studies of X-ray damage in silicate and borate glass by Yokota (1954) showed a bluish absorption band near 5,000A.U. and an ultra-violet band near

3,000A.U.. Yokota concluded that the visible absorption peak was due to electrons trapped by oxygen vacancies neighbouring alkali ions in a manner similar to the case of the F centres found in alkali halides by Pohl (1937). The ultra-violet peak was attributed to holes trapped in sodium vacancies.

7.5.1 The Spectrum of Damage Centres in $Na_2O.2B_2O_3$.

Similar blue bands were induced in Borax beads during the course of this project by exposing them to X-rays for several hours. These beads were observed to give a symmetric e.s.r. absorption line near g = 2 displaying a fourfold hyperfine splitting (see Fig. 7.3).

This spectrum can be described by a Spin Hamiltonian of the form :

$$H_s^i = g^i \beta \underline{H}.\underline{S} + A^i \underline{S}.\underline{I} \quad ,$$

where $S = \frac{1}{2}$, $I = 3/2$,
and i varies over all sites.
For X band measurements at 300°K, the following average values of the constants were obtained :

$$g = 2.010 \pm 0.002 \quad ,$$
$$A = 12.2(\pm 1.0) \times 10^{-4} cm.^{-1} \quad ,$$

and at 77°K these became :

$$g = 2.027 \pm 0.002 \quad ,$$
$$A = 12.2(\pm 1.0) \times 10^{-4} cm.^{-1} \quad .$$

Comparisons with a standard copper sulphate sample indicated that a Borax bead 3mm. in diameter showed a maximum of 10^{17} centres, after thirty hours of

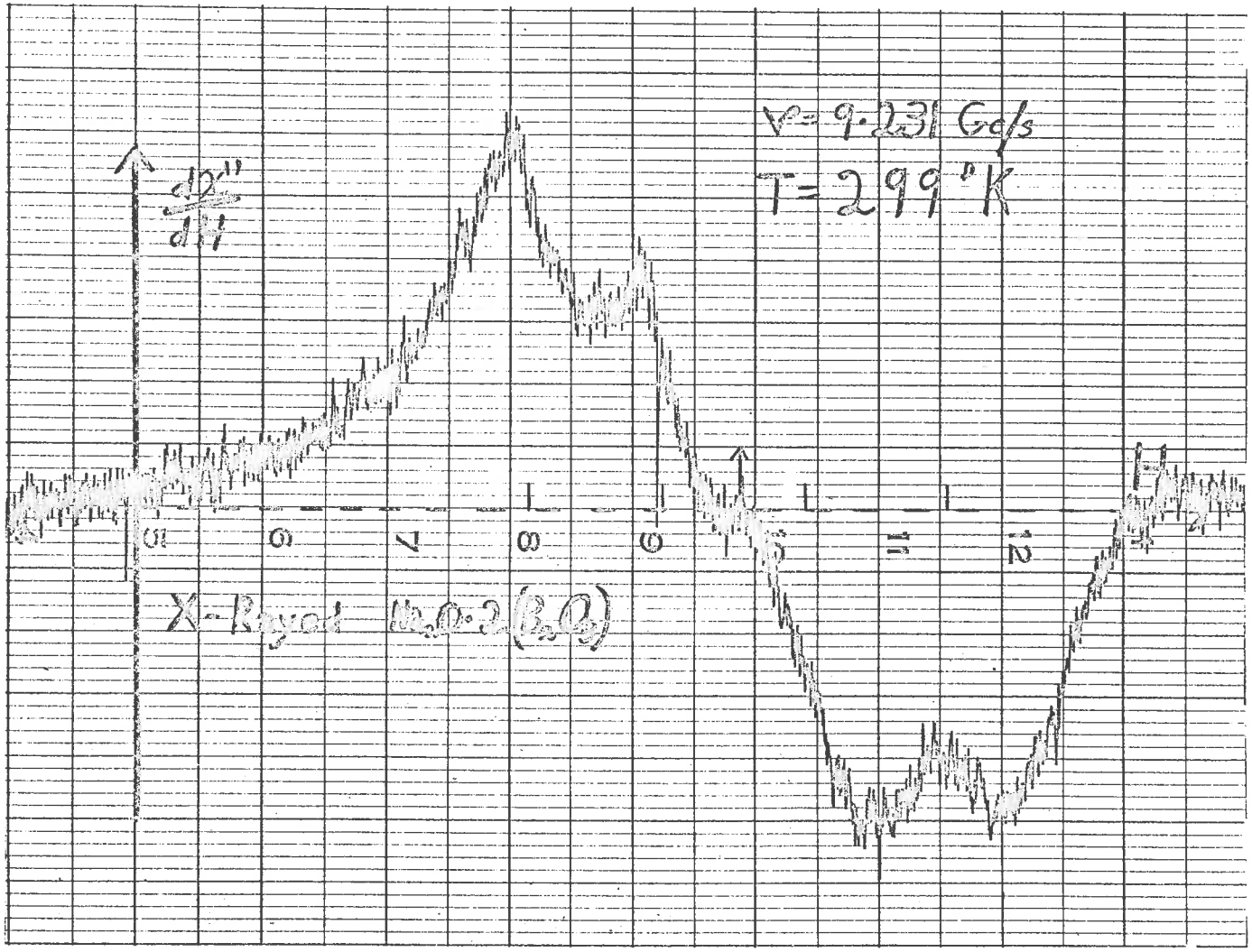

Fig. 7-3

irradiation by X-rays from a 34 kilovolt, 25ma. source, when the sample was situated 3.3cms. from the focal spot. Further irradiation gave no increase.

7.5.2 Theory of Damage Centres in $Na_2O.2B_2O_3$.

Following the treatment of Kats and Stevels (1956) for radiation damage in sodium silicate glass, we postulate that the X-rays remove the oxygen ion of a Na^D centre in Borax (Fig. 7.4A). The remaining oxygen with one electron hole (a Q_+ centre) is responsible for the absorption band near 3,000A.U.. This band is independent of the nature of the network modifiers present.

Once an electron has been removed from an oxygen atom, the network modifier will tend to recede until it lodges in an interstice together with a trapped electron, thus creating a P centre (see Fig. 7.4B). The position of the absorption band belonging to the P centre depends on the nature of the network modifier. In this case, one finds an absorption band near 5,000A.U. for the Na^{P_-} centre.

The behaviour of the P_- and Q_+ centres in glass is analogous with that of F and V centres in alkali halides. These centres can be made to disappear simultaneously by thermal bleaching or by irradiation with rays having the wavelength of one of the two absorption bands.

The fourfold splitting of the e.s.r. spectrum suggests that it may be due to the Q_+ centre --- a hole in the orbitals of a nonbridging oxygen ion attached to a single boron atom, (the I = 3/2 hyperfine interaction being due to the 81% B^{11} nuclei found in natural B). This hypothesis is consistent with the fact that, although optical evidence suggests that analogous centres

(A)

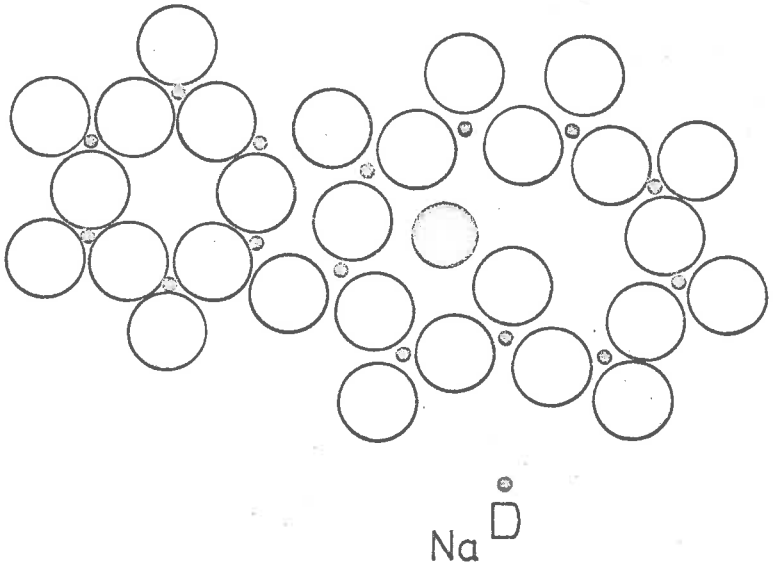

(B)

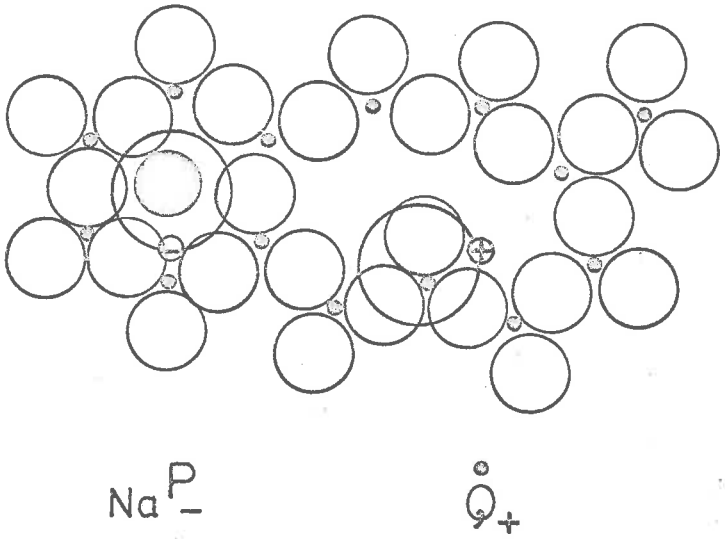

Fig. 7·4 Defect centres due to sodium in B_2O_3 structure.

(After Kats and Stevels (1956)).

are formed by irradiation of silicate glasses (Yakota (1954)), the e.s.r. spectra in the silicate case show no evidence of hyperfine splitting (Van Wieringen and Kats (1957)), the nuclear spin of the 95% abundant Si^{28} being zero.

7.6 Discussion of the Results.

Further e.s.r. studies on damage centres in borate glasses containing different percentages of alkali may shed more light on the "boric oxide anomaly" (Krogh-Moe (1962)), and the associated changes in the boron coordination number. The similarity between the spectra obtained in this project and those obtained by Yasaitis and Smaller (1953) for boron in silicate glasses (where boron is known to be tetrahedrally coordinated), (Weyl (1959)), may be taken as evidence of the tetrahedral coordination of boron in Borax glass.

The spectra of both Cu^{++} and Ti^{+++} in Borax glass are those which would be expected from these ions in octahedral complexes having very strong axial distortions, (stronger than have been observed in crystals containing these ions). Such distortions might be due to the Jahn-Teller effect, which could be expected to cause greater distortions in glasses than in crystals, since, in the case of glasses, it would not have to compete with strong crystal field forces in determining its surroundings.

Mo^{5+} can also be obtained in Borax beads (fused under reducing conditions), giving them a greenish colour (Weyl (1959)). This ion, like Cu^{++} and Ti^{+++} has $S = \frac{1}{2}$ and so should be interesting to study by means of e.s.r. (especially as it has a nuclear spin of $I = 5/2$).

APPENDIX A

Circuit Diagrams of Spectrometer Units.

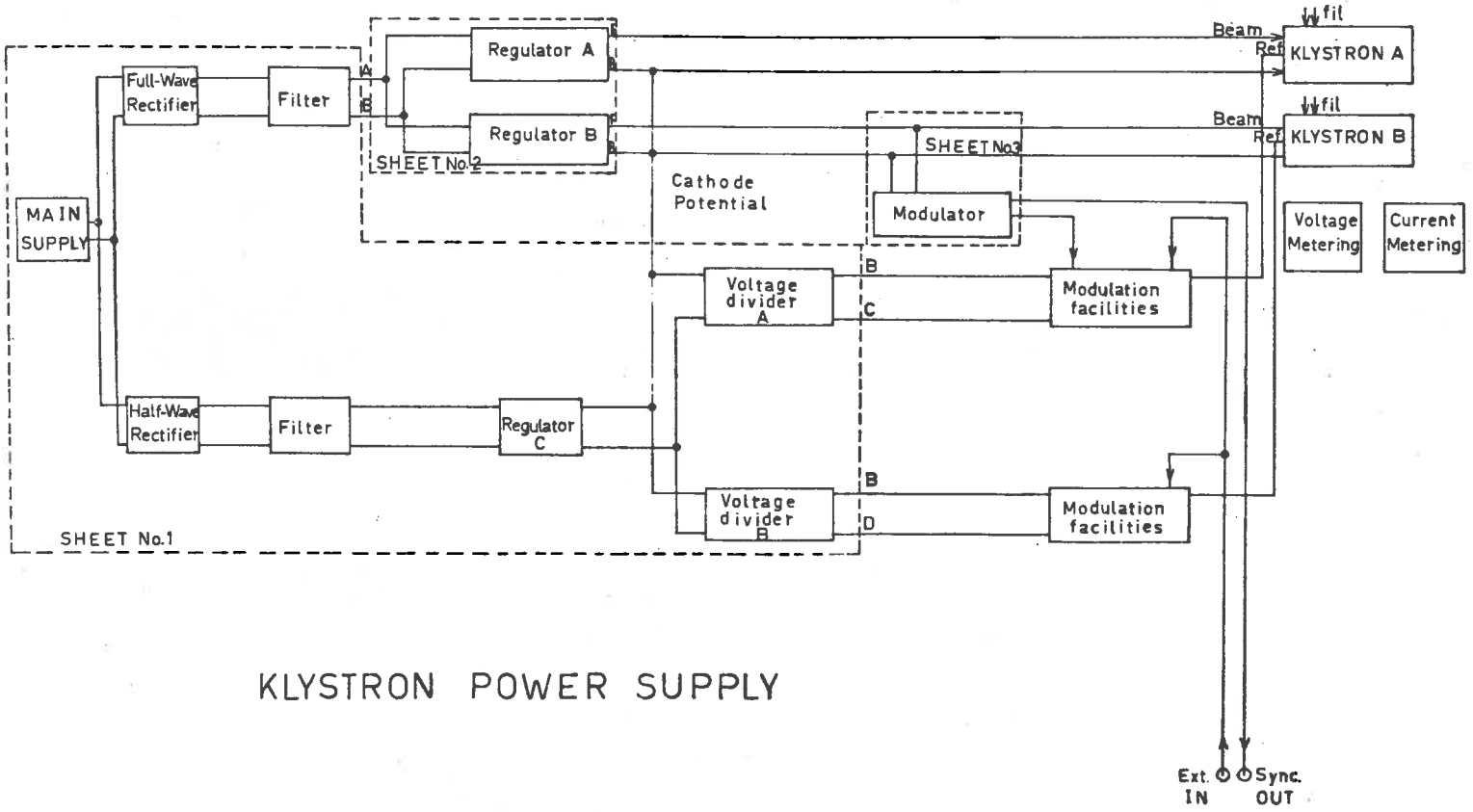

KLYSTRON POWER SUPPLY

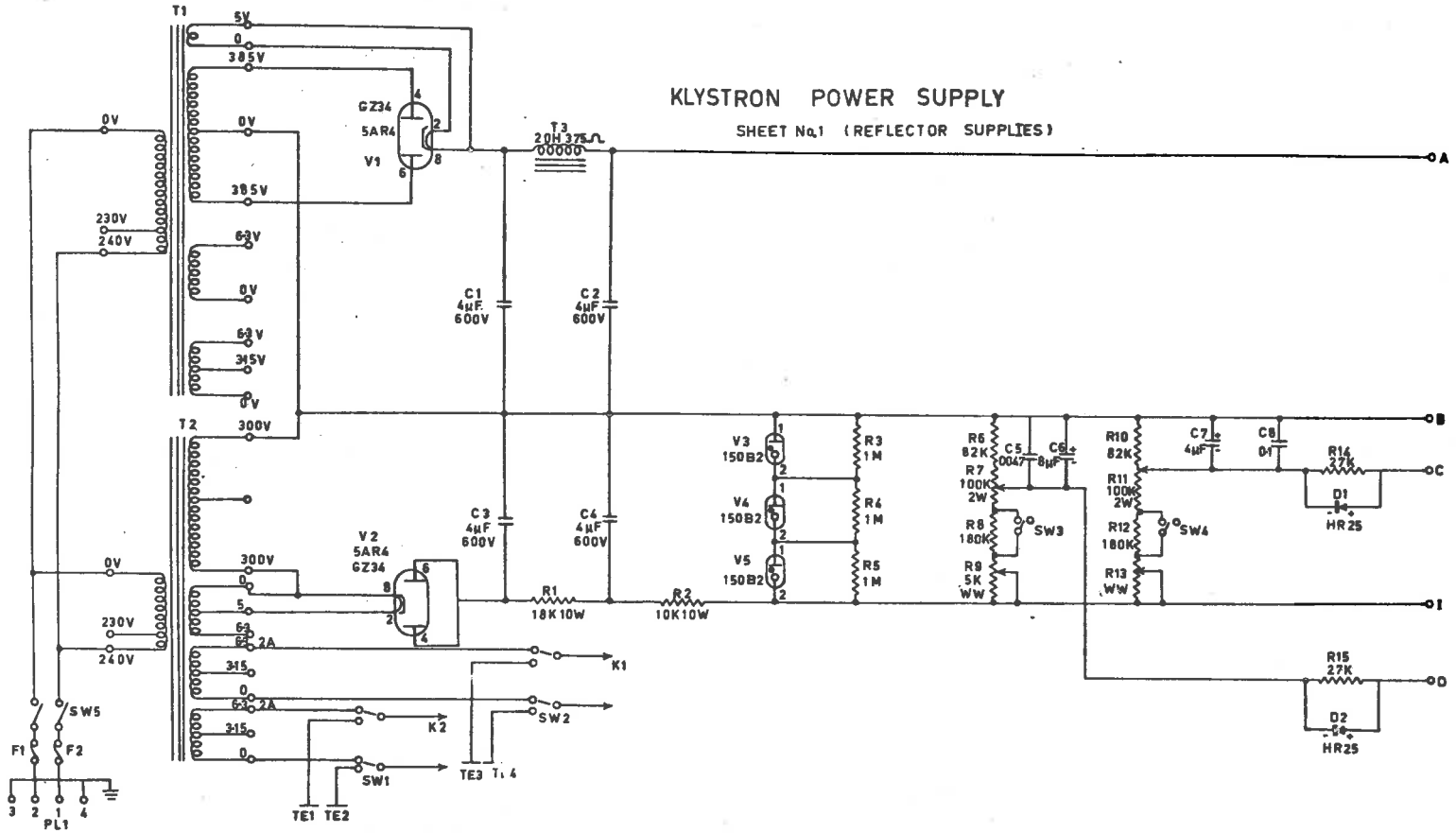
KLYSTRON POWER SUPPLY
SHEET No.1 (REFLECTOR SUPPLIES)
T1
5V
0
385V
0V
385V
230V
240V
6.3V
0V
6.3V
315V
0V
T2
300V
0V
300V
0
5
6.3
6.3 2A
315
0
6.3 2A
315
0
230V
240V
SW5
F1
F2
PL1
3 2 1 4
GZ34
5AR4
V1
T3
20H 375
C1
4μF
600V
C2
4μF
600V
C3
4μF
600V
C4
4μF
600V
V2
5AR4
GZ34
R1
18K 10W
R2
10K 10W
V3
150B2
V4
150B2
V5
150B2
R3
1M
R4
1M
R5
1M
R6
82K
R7
100K
2W
R8
180K
R9
5K
WW
C5
.0047
C6
8μF
SW3
R10
82K
R11
100K
2W
R12
180K
R13
WW
SW4
C7
4μF
C8
.01
R14
27K
D1
HR25
R15
27K
D2
HR25
K1
K2
SW2
SW1
TE1
TE2
TE3
TE4
A
B
C
I
D

A2.

KLYSTRON POWER SUPPLY

SHEET No. 2 (PLATE POWER SUPPLIES)

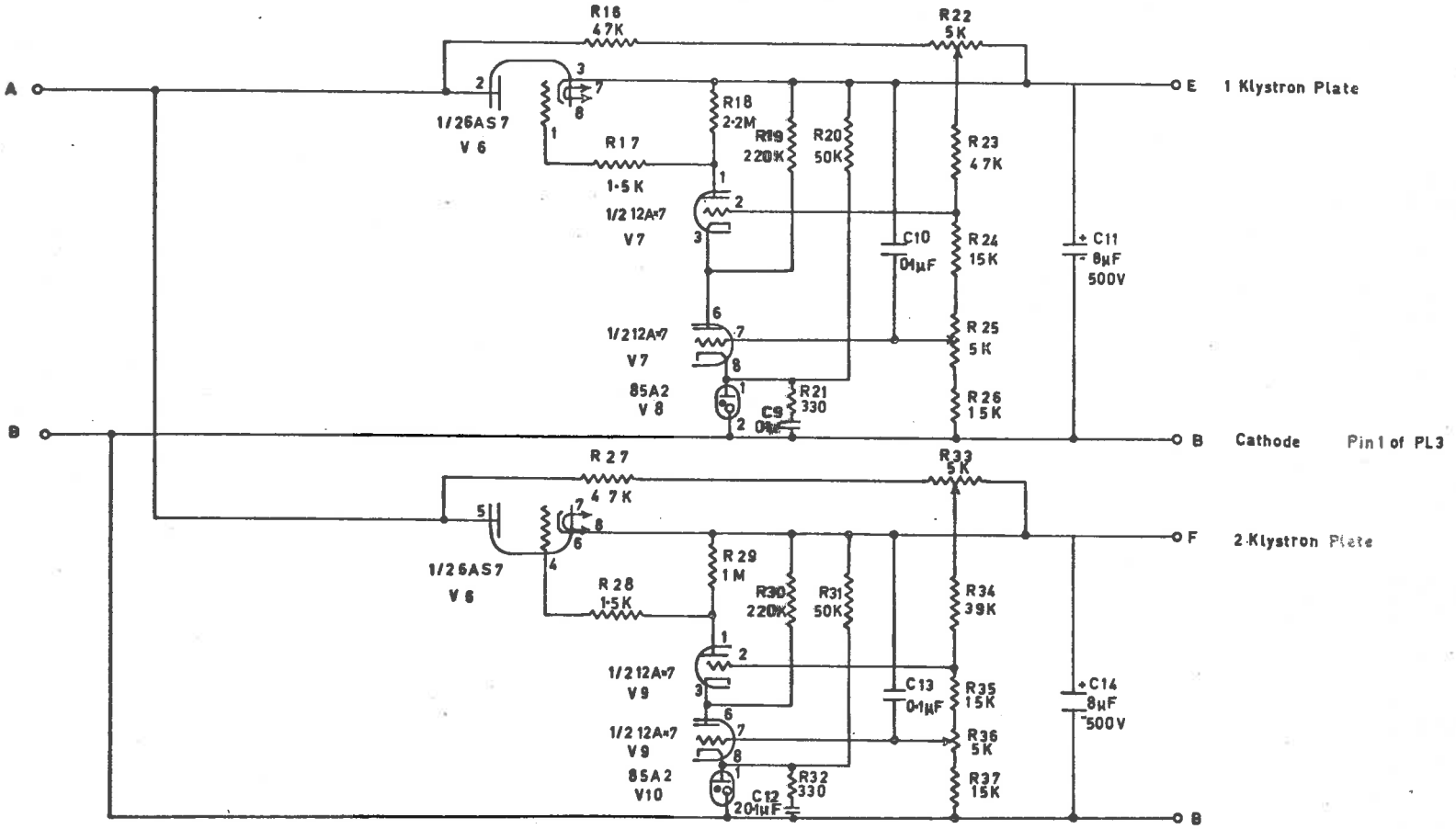

A3

KLYSTRON POWER SUPPLY

SHEET No. 3 (⎍ OSCILLATOR)

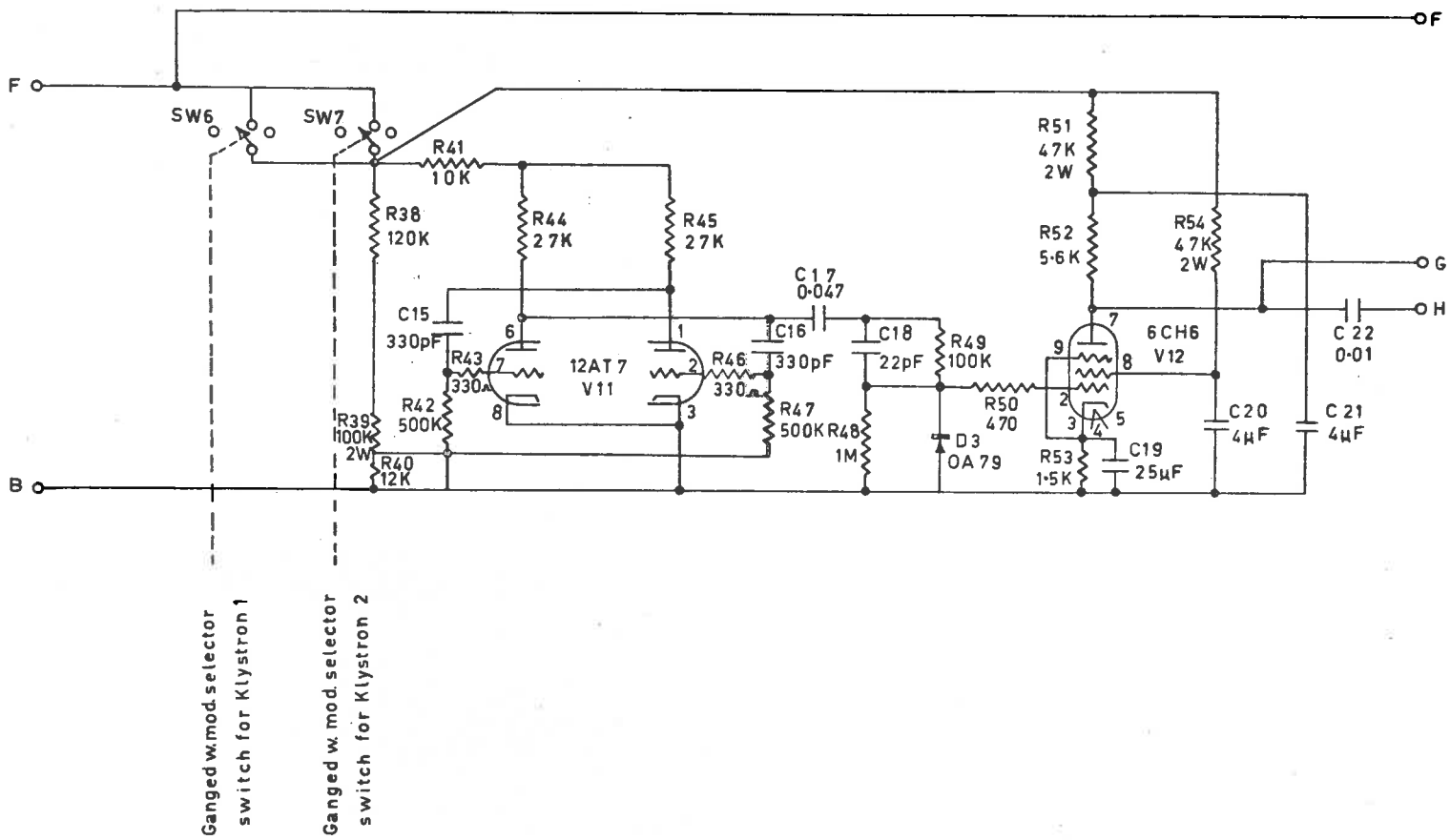

A4

KLYSTRON POWER SUPPLY

SHEET No. 4

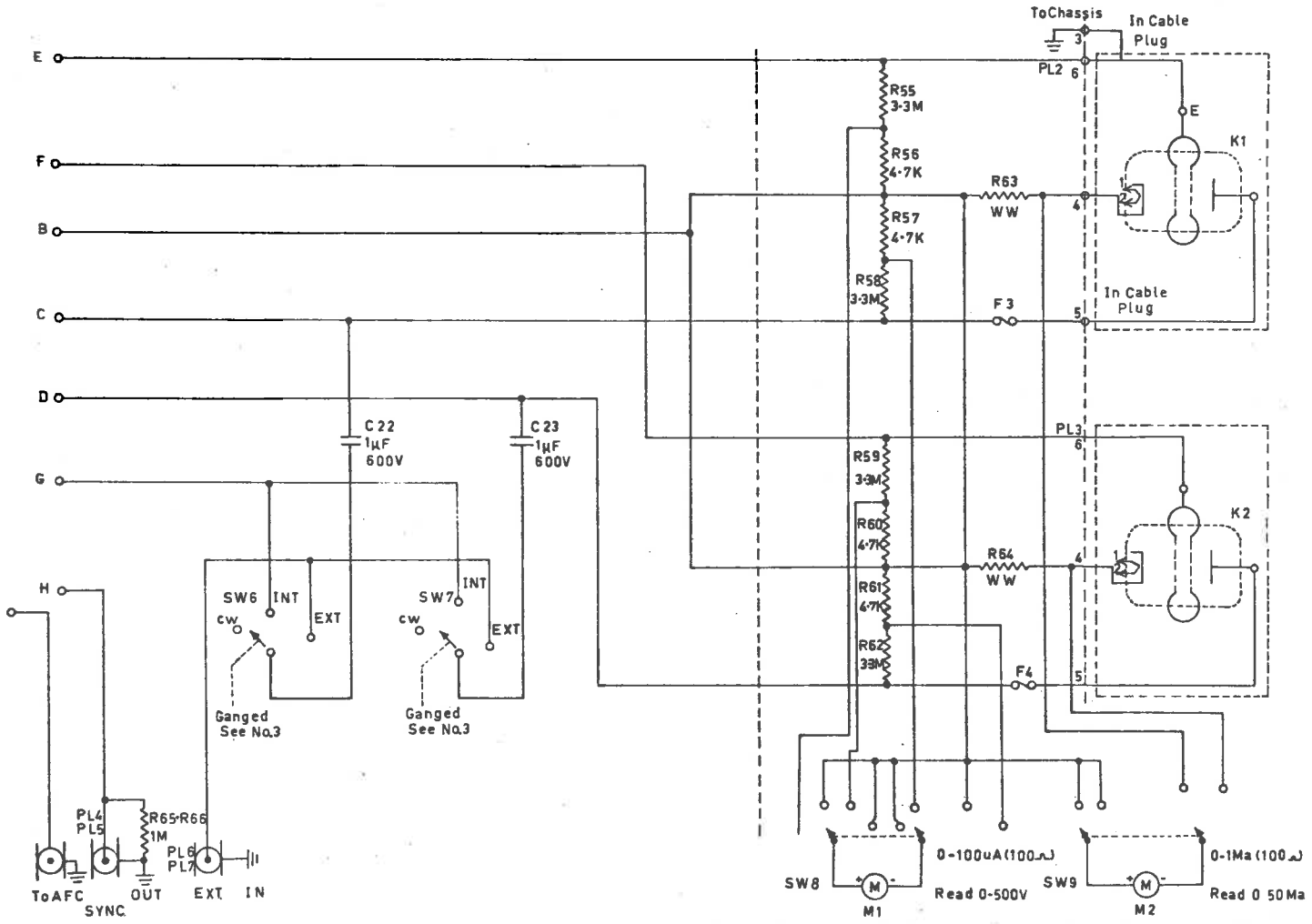

KLYSTRON FREQUENCY CONTROLLER

PRE-AMPLIFIER

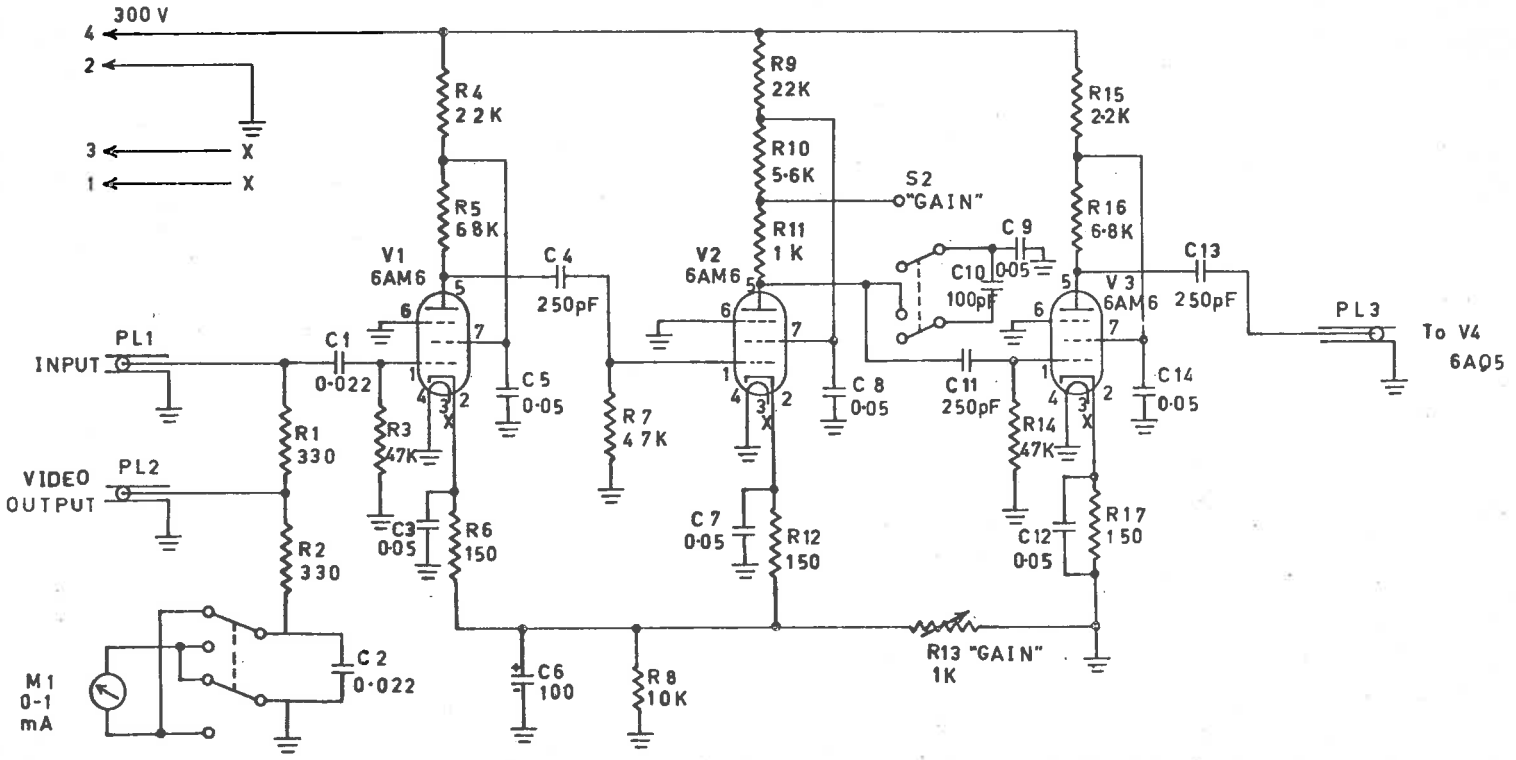

A6

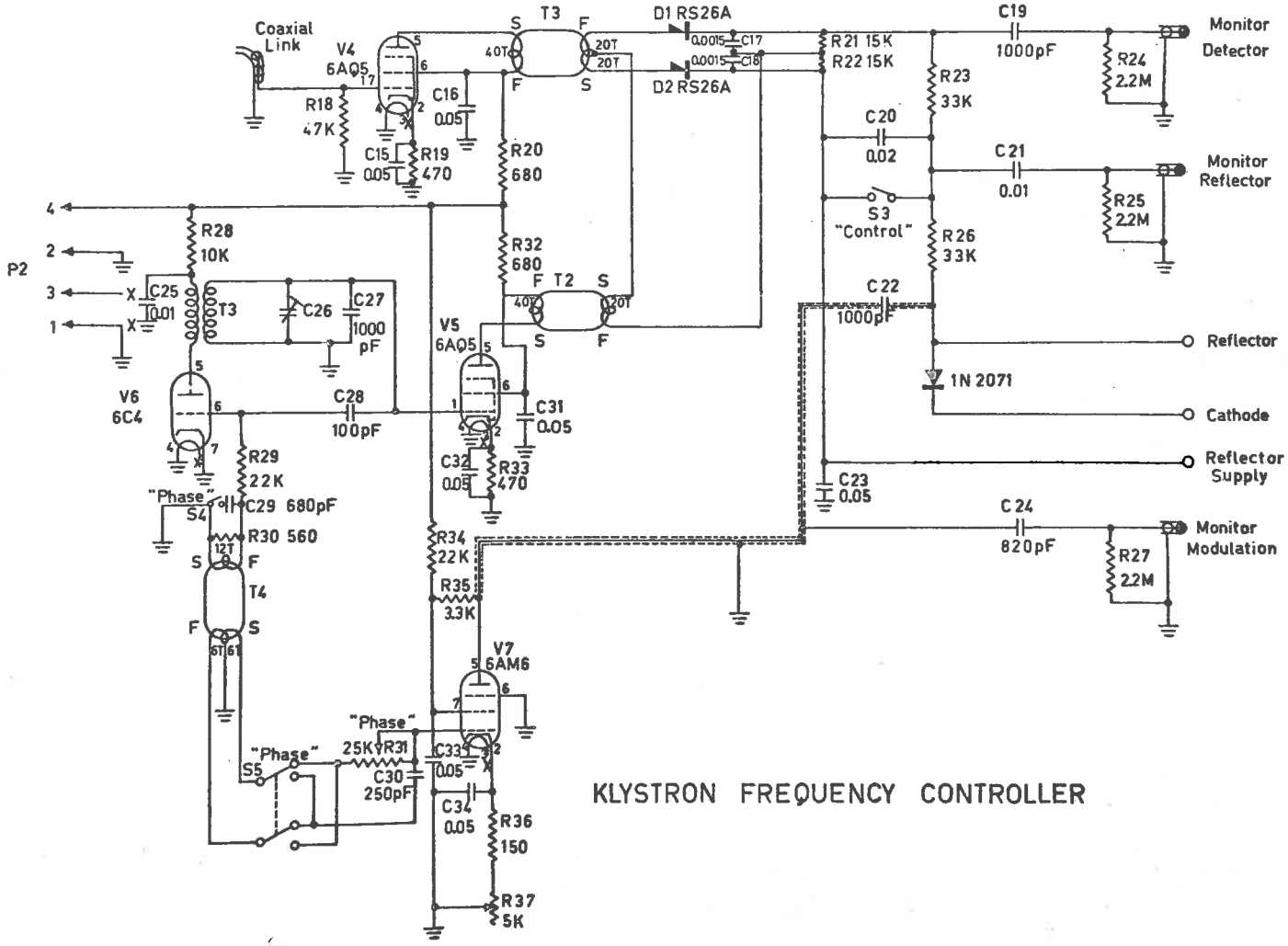

KLYSTRON FREQUENCY CONTROLLER

BALANCED MIXER (9375 kmc/s, $\lambda g = 4.45$ cms)

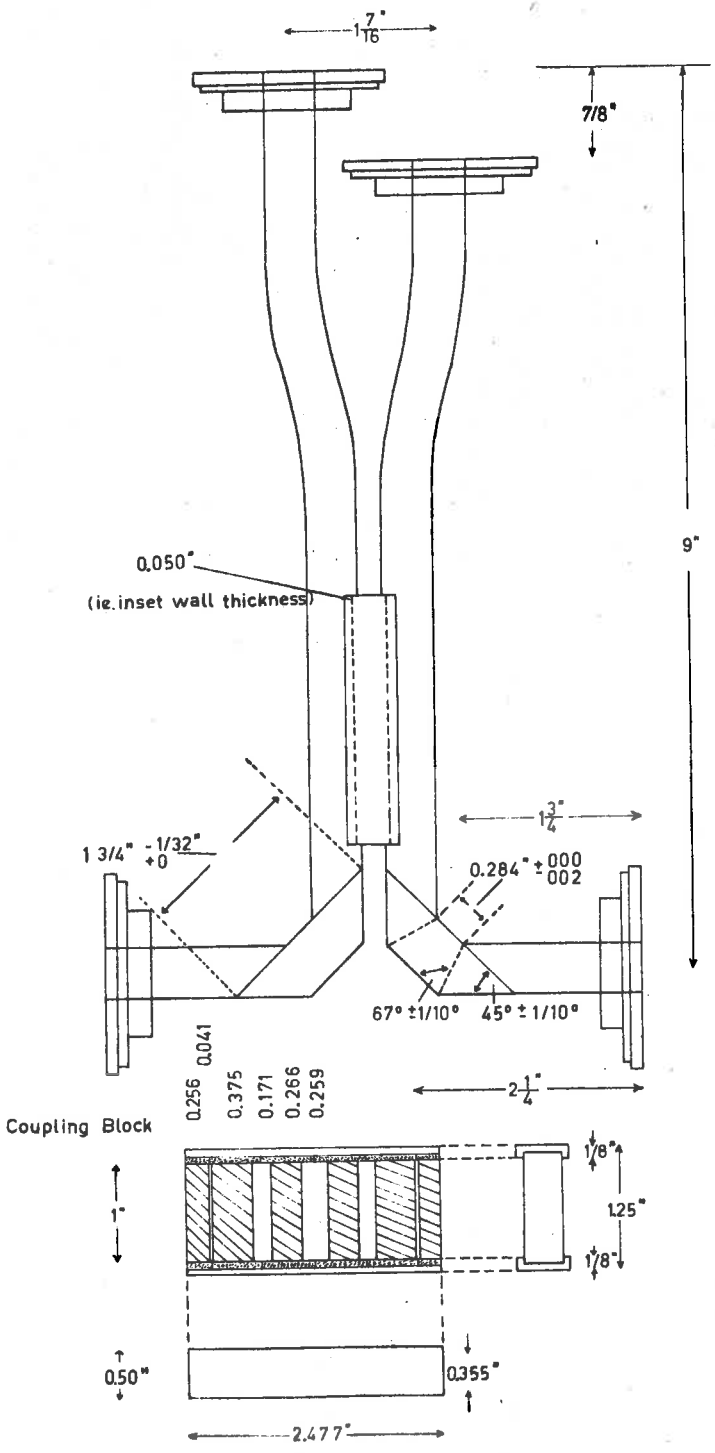

I.F. AMPLIFIER 45Mc/s

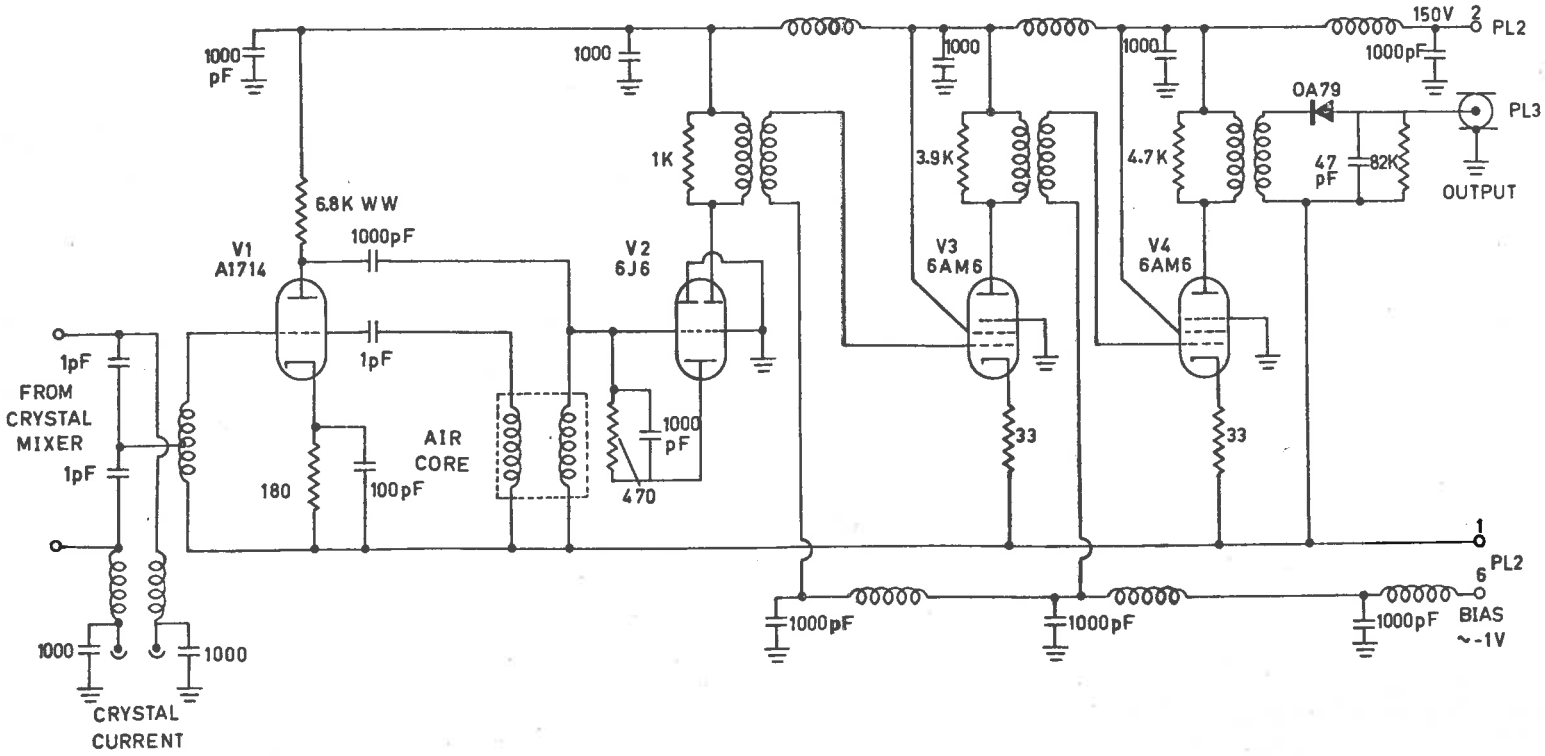

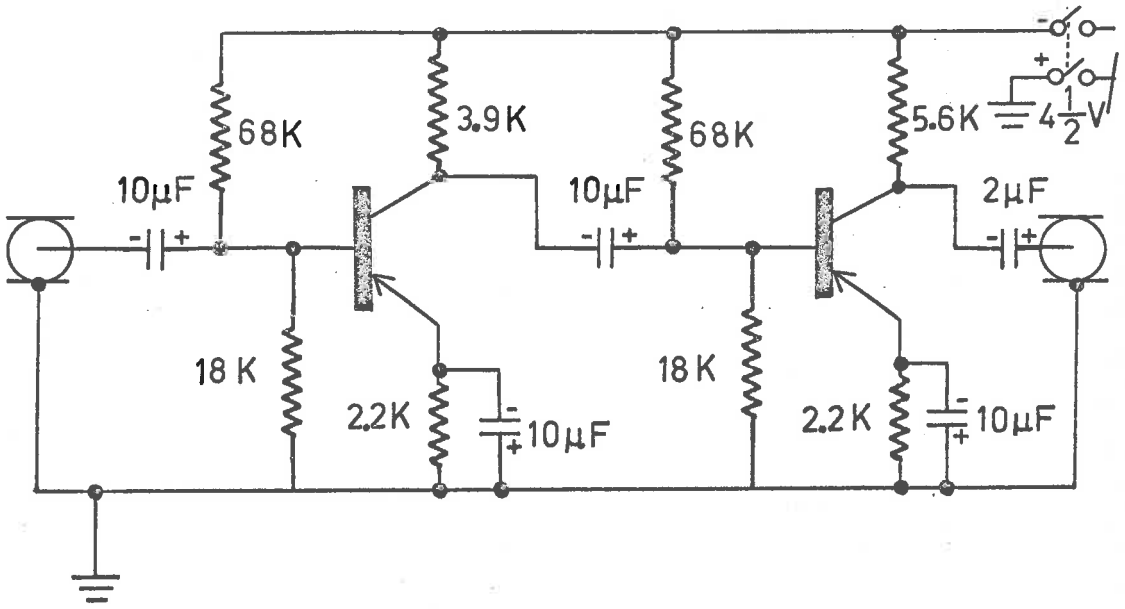

PREAMPLIFIER

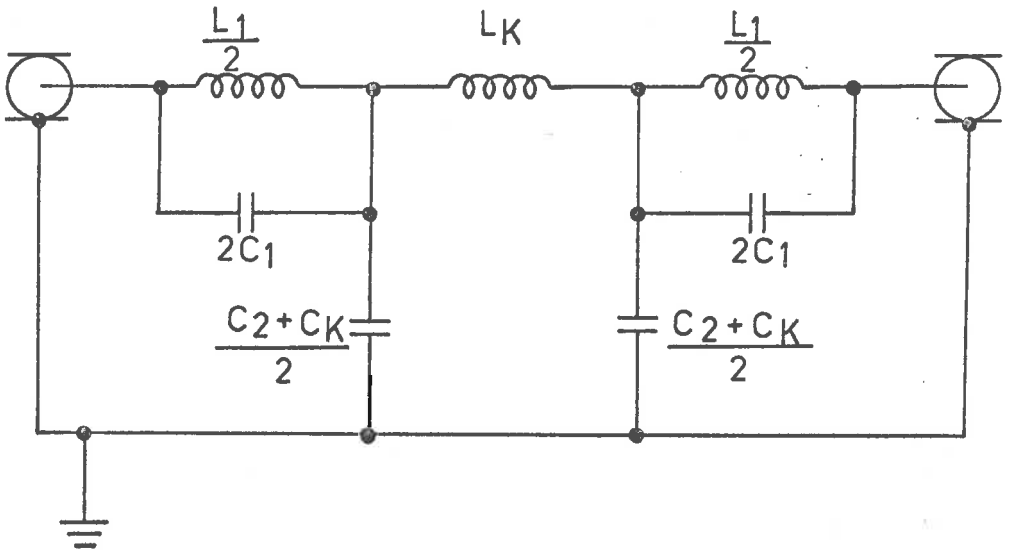

SHARP CUTOFF FILTER

SELECTIVE AMPLIFIER 135c/s I

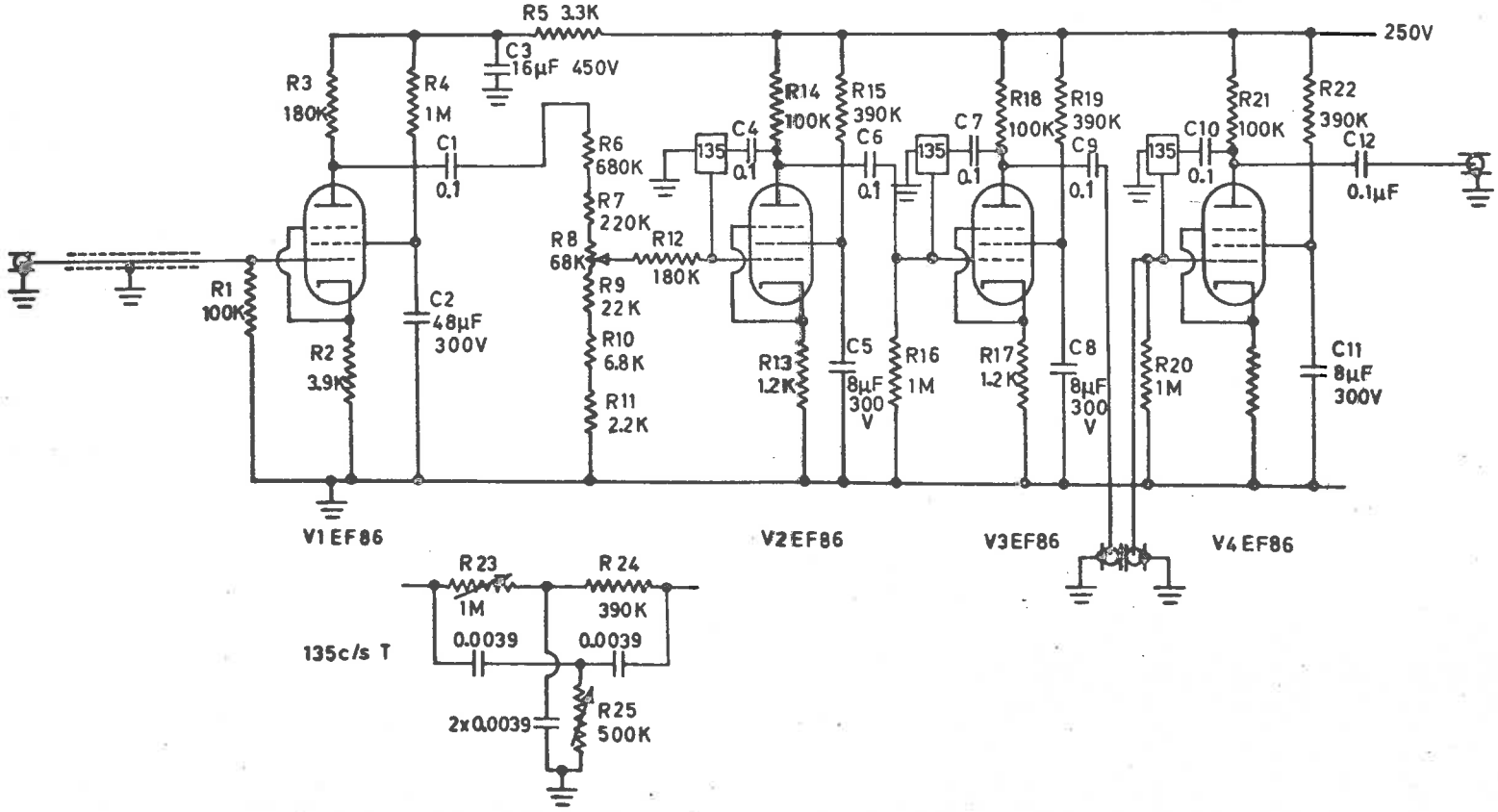

SELECTIVE AMPLIFIER 135c/s II

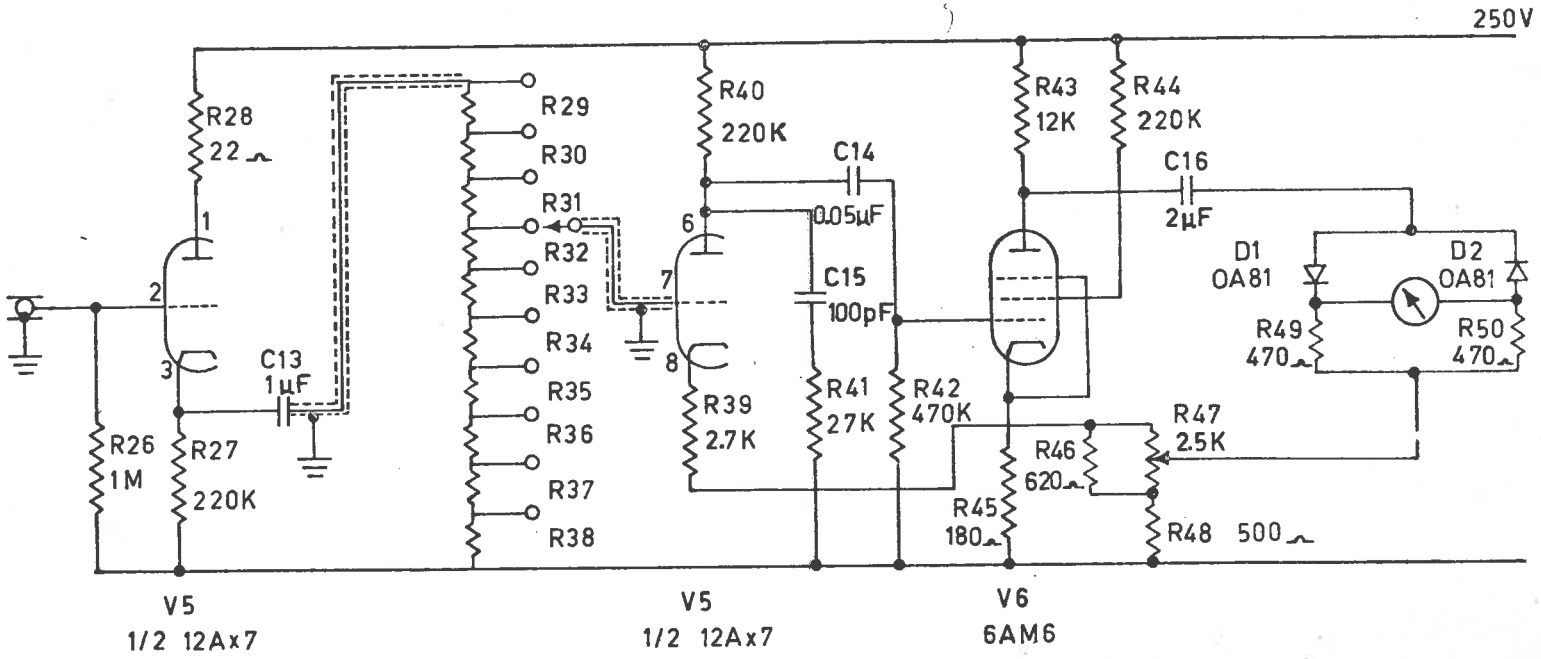

PHASE SENSITIVE DETECTOR

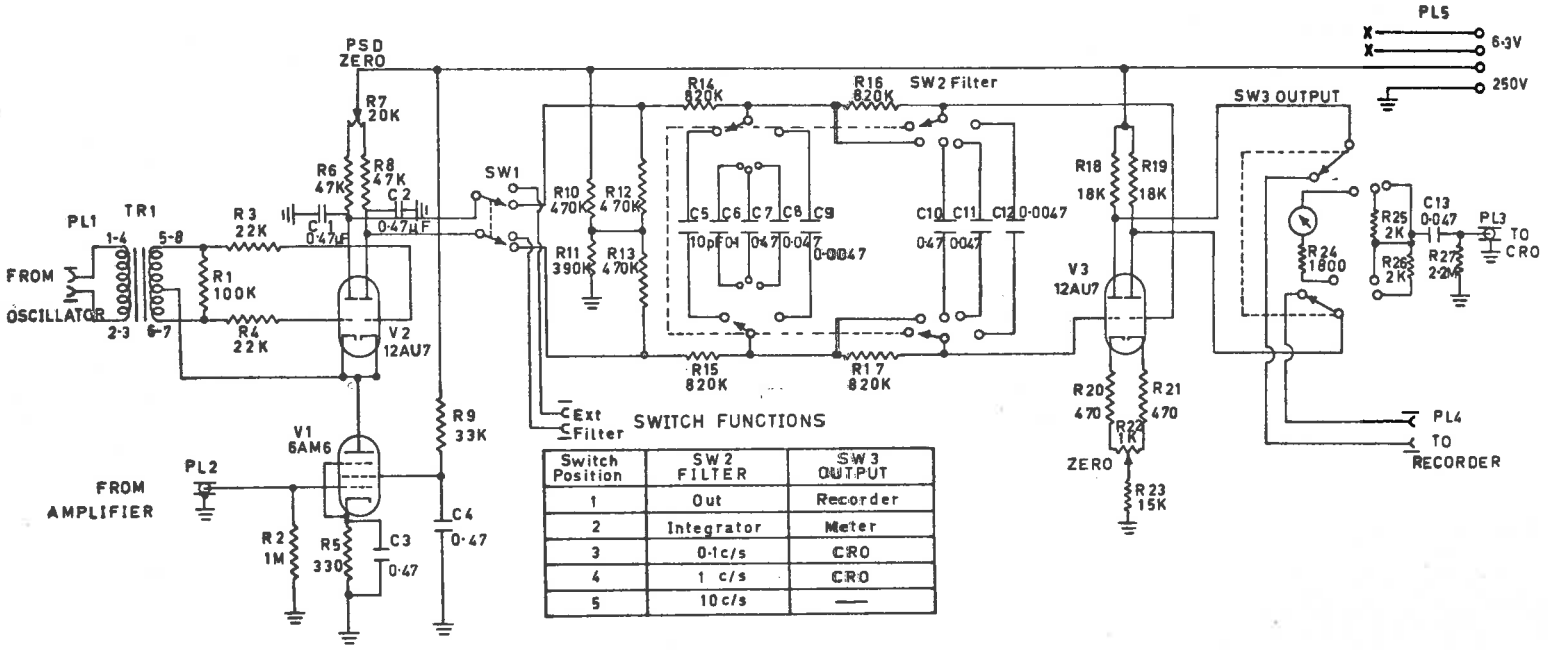

Switch Position	SW2 FILTER	SW3 OUTPUT
1	Out	Recorder
2	Integrator	Meter
3	0·1c/s	CRO
4	1 c/s	CRO
5	10c/s	—

OSCILLATOR AND REFERENCE I (135c/s)

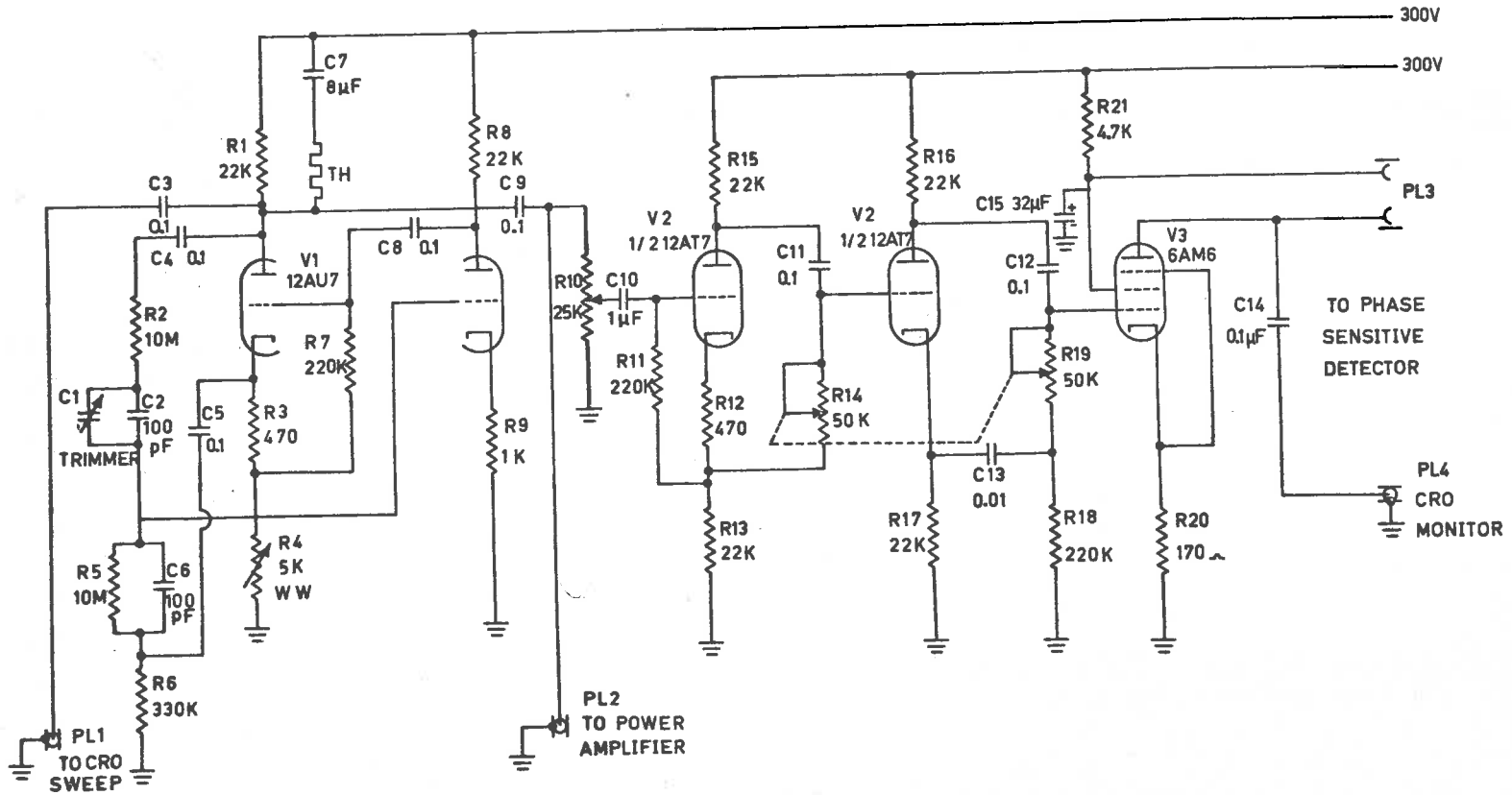

100 WATT PA AMPLIFIER

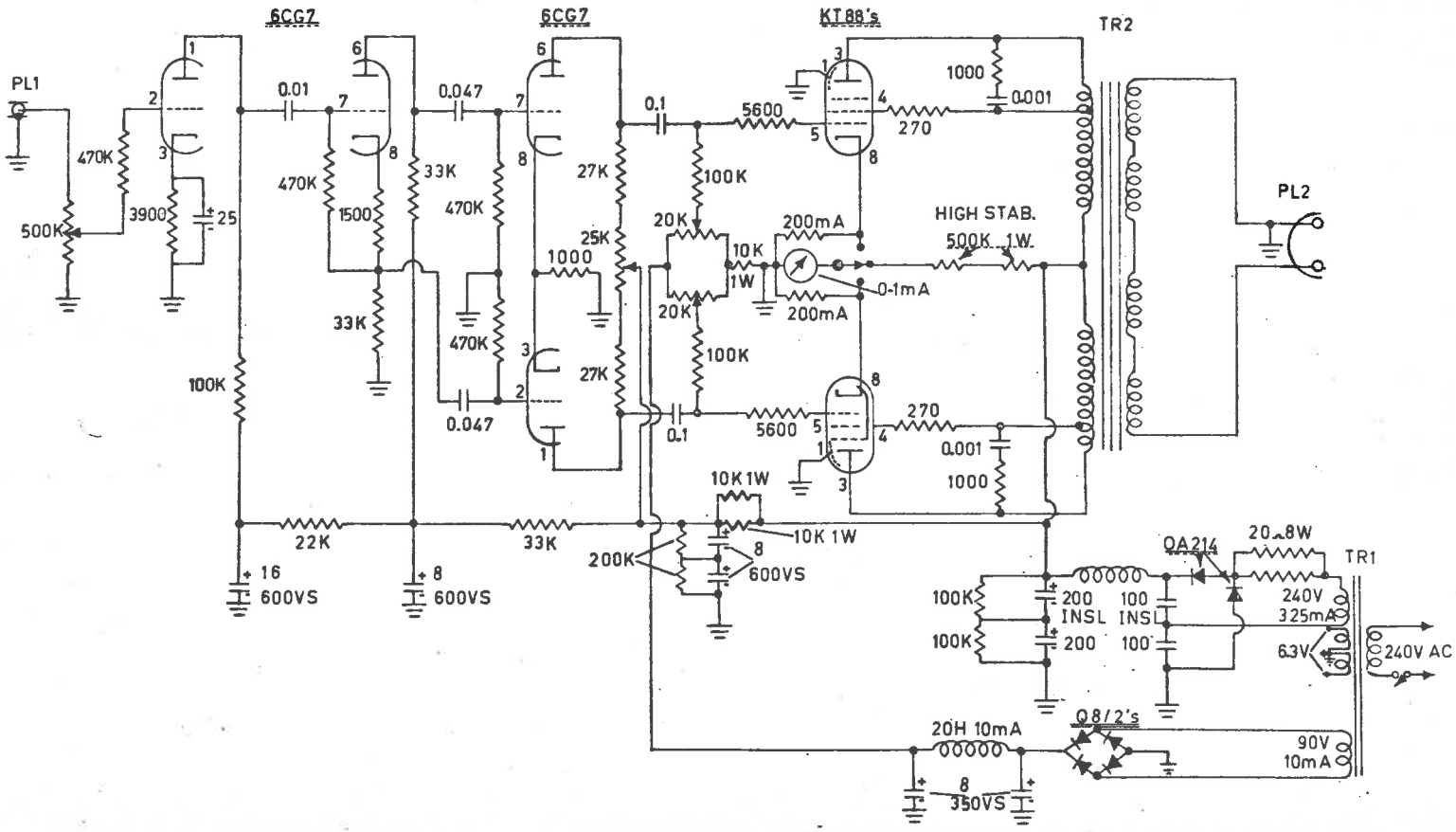

AFC DISCRIMINATOR - 45 Mc/s

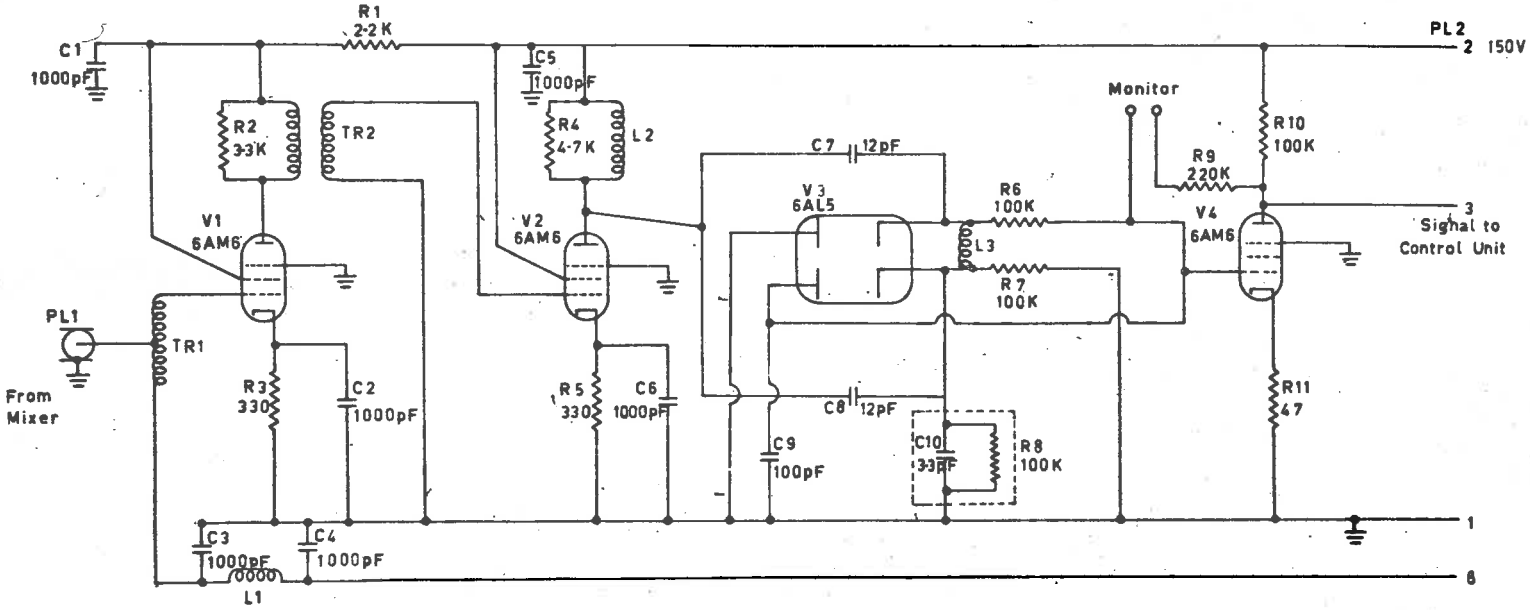

AFC KLYSTRON CONTROLLER

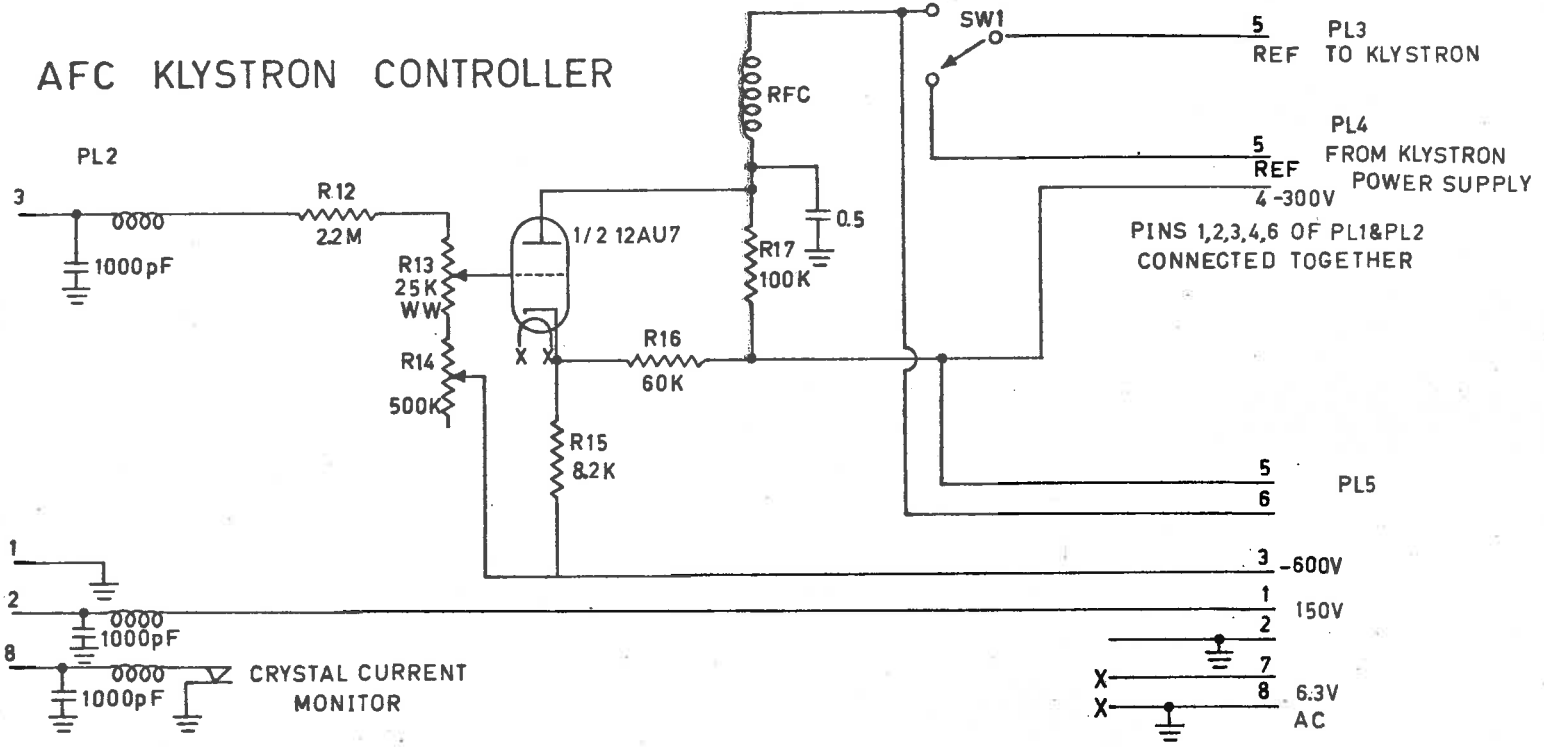

POWER SUPPLY

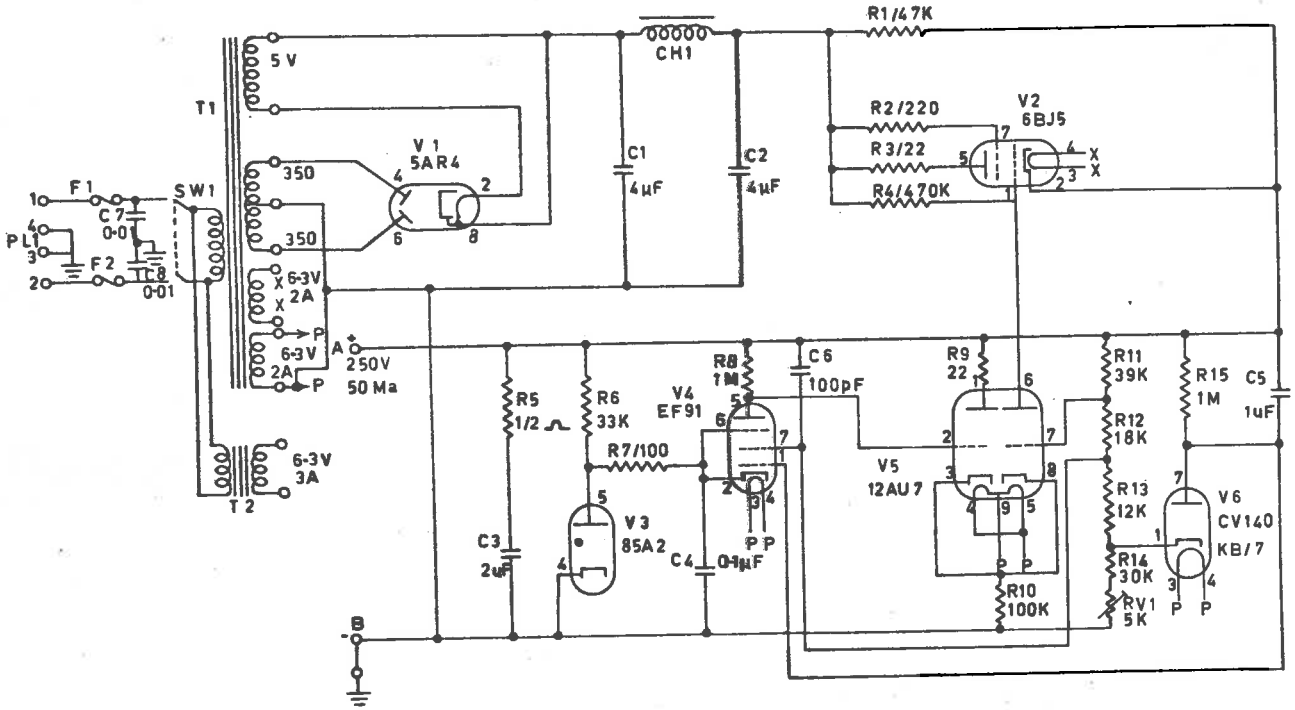

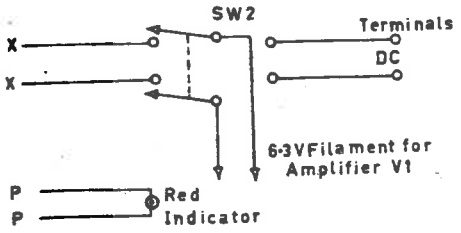

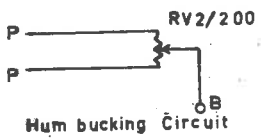

N.M.R. MAGNETOMETER

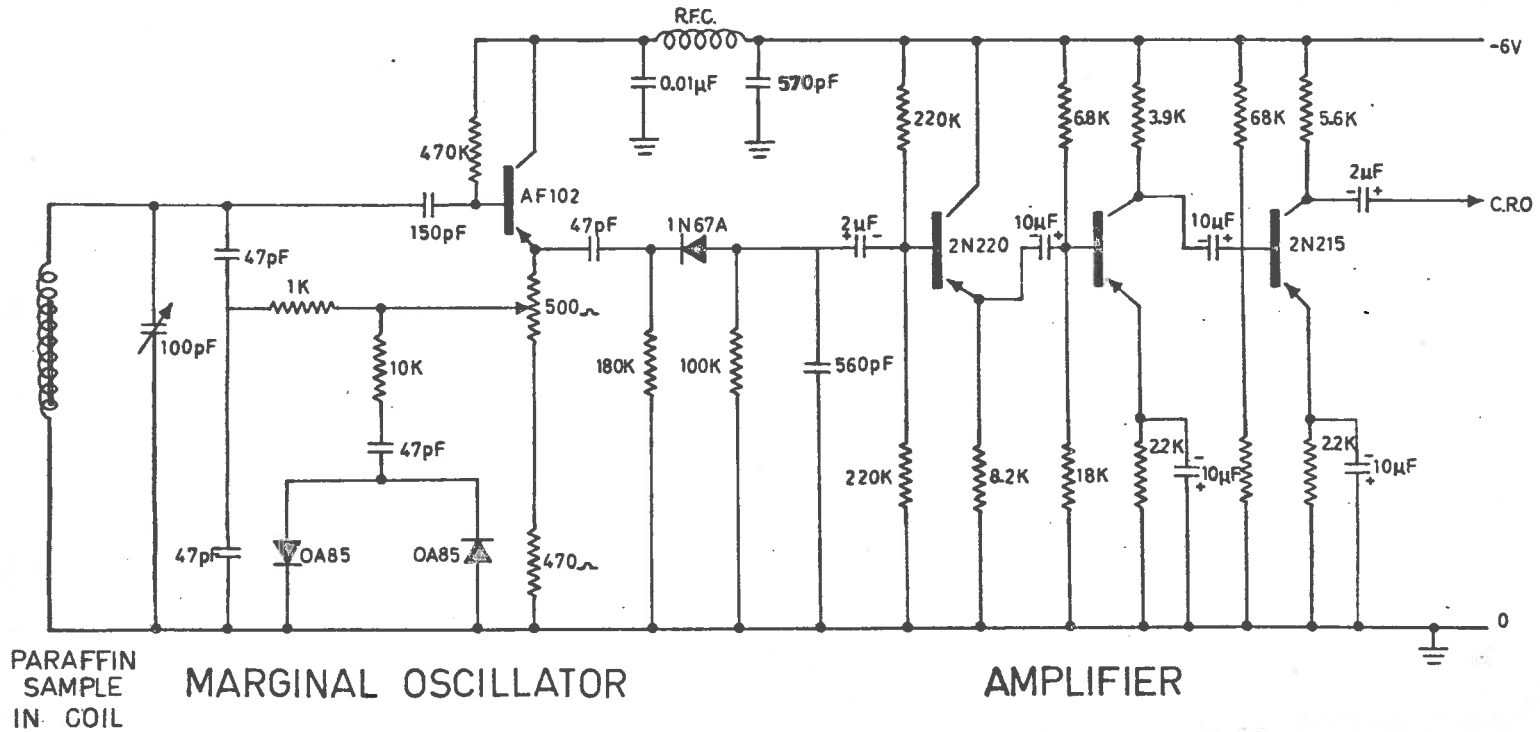

APPENDIX B

Fortran Statements of Programmes.

```
C       1009 S P BURLEY PHYSICS DEPT PHONE 293
C       EIGENVALUES OF BENITOITE HAMILTONIAN
C       INSERT CONSTANTS AND READ INPUT PARAMETERS
        DIMENSIONA(12,12)
        PI=3.1415926
        R8=SQRTF(8.)
        R5=SQRTF(5.)
    2   FORMAT(1H1,F9.0)
    3   FORMAT(3F8.3,F10.8,2F6.1)
    7   FORMAT(1H F10.4,I5,I5)
    8   FORMAT(21H1  ELEMENTS     I     J F10.0)
   11   FORMAT(1HOF10.4)
        READ,D,AF,AA,GF,U,V
        PRINT3,D,AF,AA,GF,U,V
        PUNCH3,D,AF,AA,GF,U,V
        X=(AA/3.)*SQRTF(20.0)
        Y=2.*D/3.
        Z=-AF/3.
        COSU=COSF(U*PI/180.)
        SINU=SINF(U*PI/180.)
        COSV=COSF(V*PI/180.)
        SINV=SINF(V*PI/180.)
    1   READ,H
        PUNCH8,H
        B=H*GF
        DO12I=1,12
        DO12J=1,12
   12   A(I,J)=0.0
C       ERECT BASIC ELEMENTS OF MATRIX
        A(1,1)=Z+5.*(Y-B*COSU)+800.
        A(1,2)=R5*B*SINU*COSV
        A(2,2)=-Y-3.*(Z+B*COSU)+800.
        A(2,3)=R8*B*SINU*COSV
        A(3,3)=-4.*Y+2.*Z-B*COSU+800.
        A(3,4)=3.*B*SINU*COSV
        A(4,4)=-4.*Y+2.*Z+B*COSU+800.
        A(4,5)=R8*B*SINU*COSV
        A(5,5)=-Y-3.*(Z-B*COSU)+800.
        A(5,6)=R5*B*SINU*COSV
        A(6,6)=Z+5.*(Y+B*COSU)+800.
        DO13I=1,6
   13   A(I+6,I+6)=A(I,I)
        A(1,8)=R5*B*SINU*SINV
        A(2,9)=R8*B*SINU*SINV
        A(3,10)=3.*B*SINU*SINV
        A(4,11)=R8*B*SINU*SINV
        A(5,12)=R5*B*SINU*SINV
        A(1,4)=-X
        A(3,6)=X
        A(7,10)=-X
        A(9,12)=X
        DO14I=1,5
        A(I+6,I+7)=A(I,I+1)
   14   A(I+1,I+6)=-A(I,I+7)
        DO16I=1,12
        DO16J=I,12
        IF(A(I,J))15,16,15
   15   PUNCH7,A(I,J),I,J
   16   CONTINUE
    9   FORMAT(12HOEIGENVALUES)
```

```
      PUNCH9
   27 FORMAT(4H H =F9.0)
      PRINT27,H
      PUNCH27,H
      N=12
      OFF=1.E-3
      DO4I=1,N
      DO4JP=I,N
    4 A(JP,I)=A(I,JP)
C     BEGIN JACOBI DIAGONALIZATION SUBROUTINE
      INDIC=0
      SUM=0.0
      KQ=N-1
      DO17I=1,KQ
      K=I+1
      DO17JP=K,N
   17 SUM=SUM+A(I,JP)*A(I,JP)
      VF=SQRTF(SUM*2.0)
   21 KQ=2
   22 JP=1
   23 IF(VF-ABSF(A(JP,KQ))) 24,56,56
   24 INDIC=1
      G=-A(JP,KQ)
      ZI=0.5*(A(JP,JP)-A(KQ,KQ))
      W=G/SQRTF(G*G+ZI*ZI)
      IF(ZI)29,30,30
   29 W=-W
   30 SN=W/(SQRTF(2.0*(1.0+SQRTF(1.0-W*W))))
      CS=SQRTF(1.0-SN*SN)
       HOLD1=A(JP,JP)*CS*CS+A(KQ,KQ)*SN*SN-2.0*A(JP,KQ)*SN*CS
       HOLD2=A(JP,JP)*SN*SN+A(KQ,KQ)*CS*CS+2.0*A(JP,KQ)*SN*CS
      DO 544 I=1,N
       D    =A(I,JP)*CS-A(I,KQ)*SN
       A(I,KQ)=A(I,JP)*SN+A(I,KQ)*CS
  544 A(I,JP)=D
      A(JP,JP)=HOLD1
      A(KQ,KQ)=HOLD2
      A(JP,KQ)=0.0
      DO 55 I=1,N
      A(JP,I)=A(I,JP)
   55 A(KQ,I)=A(I,KQ)
   56 IF(JP-KQ+1) 57,59,59
   57 JP=JP+1
      GO TO 23
   59 IF(KQ-N) 60,62,64
   60 KQ=KQ+1
      GO TO 22
   62 IF(INDIC)64,64,263
  263 INDIC=0
      GO TO 21
   64 IF(OFF-VF) 65,69,69
   65 VF=VF/10.0
      GO TO 21
   69 DO 1212 I=1,N
 1212 PUNCH11,A(I,I)
      GOTO1
      END
```

```
C       1009 S P BURLEY PHYSICS DEPT PHONE 293
C       MATRIX ELEMENTS OF BENITOITE HAMILTONIAN
C       INSERT CONSTANTS AND READ INPUT PARAMETERS
        DIMENSIONA(12,12)
        PI=3.1415926
        R8=SQRTF(8.)
        R5=SQRTF(5.)
    2   FORMAT(1H1,F9.0)
    3   FORMAT(3F8.3,F10.8,2F6.1)
    7   FORMAT(I5,I5,F10.5)
    8   FORMAT(21H1  ELEMENTS     I     J F10.0)
   11   FORMAT(1H0F10.4)
        READ,D,AF,AA,GF,U,V
        PRINT3,D,AF,AA,GF,U,V
        PUNCH3,D,AF,AA,GF,U,V
        X=(AA/3.)*SQRTF(20.0)
        Y=2.*D/3.
        Z=-AF/3.
        COSU=COSF(U*PI/180.)
        SINU=SINF(U*PI/180.)
        COSV=COSF(V*PI/180.)
        SINV=SINF(V*PI/180.)
    1   READ,H
        PUNCH8,H
        B=H*GF
        DO12I=1,12
        DO12J=1,12
   12   A(I,J)=0.0
C       ERECT BASIC ELEMENTS OF MATRIX
        A(1,1)=Z+5.*(Y-B*COSU)+800.
        A(1,2)=R5*B*SINU*COSV
        A(2,2)=-Y-3.*(Z+B*COSU)+800.
        A(2,3)=R8*B*SINU*COSV
        A(3,3)=-4.*Y+2.*Z-B*COSU+800.
        A(3,4)=3.*B*SINU*COSV
        A(4,4)=-4.*Y+2.*Z+B*COSU+800.
        A(4,5)=R8*B*SINU*COSV
        A(5,5)=-Y-3.*(Z-B*COSU)+800.
        A(5,6)=R5*B*SINU*COSV
        A(6,6)=Z+5.*(Y+B*COSU)+800.
        DO13I=1,6
   13   A(I+6,I+6)=A(I,I)
        A(1,8)=R5*B*SINU*SINV
        A(2,9)=R8*B*SINU*SINV
        A(3,10)=3.*B*SINU*SINV
        A(4,11)=R8*B*SINU*SINV
        A(5,12)=R5*B*SINU*SINV
        A(1,4)=-X
        A(3,6)=X
        A(7,10)=-X
        A(9,12)=X
        DO14I=1,5
        A(I+6,I+7)=A(I,I+1)
   14   A(I+1,I+6)=-A(I,I+7)
        DO16I=1,12
        DO16J=I,12
        IF(A(I,J))15,16,15
   15   PUNCH7,I,J,A(I,J)
   16   CONTINUE
        GOTO1
```

END

```
C       1009 S P BURLEY PHYSICS DEPT PHONE 293
C       EIGENVALUES-EIGENVECTORS OF BENITOITE HAMILTONIAN
        DIMENSIONA(12,12),S(12,12)
C       BEGIN JACOBI DIAGONALIZATION SUBROUTINE
    2 FORMAT(4E16.8)
   15 FORMAT(/E14.8)
        N=12
        OFF=1.E-4
    1 DO 3 I=1,12
        DO 3 J=1,12
    3 A(I,J)=0.0
        DO4K=1,26
        READ,I,J,A(I,J)
    4 A(J,I)=A(I,J)
        INDIC=0
        DO 1002 I=1,N
        DO 1002 J=1,N
 1002 S(I,J)=0.0
        DO 1004 I=1,N
 1004 S(I,I)=1.0
        SUM=0.0
        L=N-1
        DO17I=1,L
        K=I+1
        DO 17 J=K,N
   17 SUM=SUM+A(I,J)*A(I,J)
        VF=SQRTF(SUM*2.0)
        NB=1
   21 KQ=2
   22 JP=1
   23 IF(VF-ABSF(A(JP,KQ))) 24,56,56
   24 INDIC=1
        Y=-A(JP,KQ)
        ZI=0.5*(A(JP,JP)-A(KQ,KQ))
        W=Y/SQRTF(Y*Y+ZI*ZI)
        IF(ZI)29,30,30
   29 W=-W
   30 SN=W/(SQRTF(2.0*(1.0+SQRTF(1.0-W*W))))
        CS=SQRTF(1.0-SN*SN)
        IF(NB)43,43,34
   34 S(JP,JP)=CS
        S(KQ,JP)=-SN
        S(JP,KQ)=SN
        S(KQ,KQ)=CS
 43     HOLD1=A(JP,JP)*CS*CS+A(KQ,KQ)*SN*SN-2.0*A(JP,KQ)*SN*CS
        HOLD2=A(JP,JP)*SN*SN+A(KQ,KQ)*CS*CS+2.0*A(JP,KQ)*SN*CS
        DO 544 I=1,N
        D    =A(I,JP)*CS-A(I,KQ)*SN
        A(I,KQ)=A(I,JP)*SN+A(I,KQ)*CS
  544 A(I,JP)=D
        IF(NB)751,751,749
  749 NB=0
        GO TO 50
  751 DO 754 I=1,N
        D    =S(I,JP)*CS-S(I,KQ)*SN
        S(I,KQ)=S(I,JP)*SN+S(I,KQ)*CS
  754 S(I,JP)=D
   50 A(JP,JP)=HOLD1
        A(KQ,KQ)=HOLD2
        A(JP,KQ)=0.0
```

```
      DO 55 I=1,N
      A(JP,I)=A(I,JP)
   55 A(KQ,I)=A(I,KQ)
   56 IF(JP-KQ+1) 57,59,59
   57 JP=JP+1
      GO TO 23
   59 IF(KQ-N) 60,62,64
   60 KQ=KQ+1
      GO TO 22
   62 IF(INDIC)64,64,263
  263 INDIC=0
      GO TO 21
   64 IF(OFF-VF) 65,69,69
   65 VF=VF/10.0
      GO TO 21
C     END OF DIAGONALIZATION SUBROUTINE
C      PRINT SUBROUTINE FOR EIGENVALUES AND EIGENVECTORS
   69 DO 3008 J=1,N
      PRINT15,A(J,J)
      DO 3008 I=1,N,4
      IF (N-I-3) 3071,3070,3070
 3071 IF (N-I-2) 3073,3072,3072
 3073 IF (N-I-1) 3075,3074,3074
 3070 PRINT2, S(I,J),S(I+1,J),S(I+2,J),S(I+3,J)
      GO TO 3008
 3072 PRINT2 ,S(I,J),S(I+1,J),S(I+2,J)
      GO TO 3008
 3074 PRINT  2, S(I,J),S(I+1,J)
      GO TO 3008
 3075 PRINT2, S(I,J)
 3008 CONTINUE
C     END OF PRINT SUBROUTINE
      PAUSE
      GOTO1
      END
```

```
C     1009 S P BURLEY PHYSICS DEPT PHONE 293
C     TRANSITION AMPLITUDES FOR BENITOITE SPECTRUM
C     READ VECTORS COLUMNWISE IN REAL FORM
      DIMENSIONTA(6,6),TB(6,6),TC(6,6),V(6,6)
      DIMENSIONEY(6,6)
    1 READ,H
      DO2J=1,6
      DO2I=1,6
    2 READ,V(I,J)
      DO3J=1,6
      DO3I=1,6
      TD=SQRTF(5.)*(V(2,I)*V(1,J)+V(6,I)*V(5,J))
      TE=SQRTF(8.)*(V(3,I)*V(2,J)+V(5,I)*V(4,J))+3.*V(4,I)*V(3,J)
      TA(I,J)=TD+TE
      TF=-2.5*V(1,I)*V(1,J)-1.5*V(2,I)*V(2,J)-0.5*V(3,I)*V(3,J)
      TG=0.5*V(4,I)*V(4,J)+1.5*V(5,I)*V(5,J)+2.5*V(6,I)*V(6,J)
      TB(I,J)=TF+TG
      TR=SQRTF(5.)*(V(1,I)*V(2,J)+V(5,I)*V(6,J))
      TS=SQRTF(8.)*(V(2,I)*V(3,J)+V(4,I)*V(5,J))+3.*V(3,I)*V(4,J)
      TC(I,J)=TR+TS
    3 EY(I,J)=((TA(I,J)-TC(I,J))/2.)**2
   12 FORMAT(30H1            T+ MATRIX        H =F6.0)
   13 FORMAT(30H2            TO MATRIX        H =F6.0)
   14 FORMAT(30H2            T- MATRIX        H =F6.0)
   16 FORMAT(30H2            EY MATRIX        H =F6.0)
   15 FORMAT(1H 6F10.5)
      PUNCH12,H
      DO21J=1,6
   21 PUNCH15,TA(J,1),TA(J,2),TA(J,3),TA(J,4),TA(J,5),TA(J,6)
      PUNCH13,H
      DO22J=1,6
   22 PUNCH15,TB(J,1),TB(J,2),TB(J,3),TB(J,4),TB(J,5),TB(J,6)
      PUNCH14,H
      DO23J=1,6
   23 PUNCH15,TC(J,1),TC(J,2),TC(J,3),TC(J,4),TC(J,5),TC(J,6)
      PUNCH16,H
      DO24J=1,6
   24 PUNCH15,EY(J,1),EY(J,2),EY(J,3),EY(J,4),EY(J,5),EY(J,6)
      GOTO1
      END
```

T+ MATRIX H = 3187.

-2.47434	.99791	-.27714	-.06124	-.05540	-.00346
-.94139	-1.45891	-1.26721	-.22630	-.02954	-.04767
-.15924	1.36197	-.49545	1.52889	.22107	.00518
-.05369	-.33190	-1.50128	.47037	1.53464	.17905
-.00530	.05160	.25907	-1.48585	1.46982	1.20509
.00712	-.00885	-.08011	.10692	-1.23807	2.48849

TO MATRIX H = 3187.

.08242	1.26776	-.12587	-.00063	-.01623	-.00260
1.26776	-.20864	-1.48594	.07962	-.01476	-.02624
-.12587	-1.48594	.12836	1.45659	-.05854	.01318
-.00063	.07962	1.45659	.07119	1.30664	.06998
-.01623	-.01476	-.05854	1.30664	-.10547	1.01556
-.00260	-.02624	.01318	.06998	1.01556	.03210

T- MATRIX H = 3187.

-2.47434	-.94139	-.15924	-.05369	-.00530	.00712
.99791	-1.45891	1.36197	-.33190	.05160	-.00885
-.27714	-1.26721	-.49545	-1.50128	.25907	-.08011
-.06124	-.22630	1.52889	.47037	-1.48585	.10692
-.05540	-.02954	.22107	1.53464	1.46982	-1.23807
-.00346	-.04767	.00518	.17905	1.20509	2.48849

EY MATRIX H = 3187.

.00000	.94022	.00347	.00001	.00062	.00002
.94022	.00000	1.72815	.00278	.00164	.00037
.00347	1.72815	.00000	2.29550	.00036	.00181
.00001	.00278	2.29550	.00000	2.28086	.00130
.00062	.00164	.00036	2.28086	.00000	1.49226
.00002	.00037	.00181	.00130	1.49226	.00000

```
C      1009  S P BURLEY  PHYSICS DEPT  PHONE293                    B9
C      LINE POSITIONS FOR MN++ IN SMITHSONITE
       DIMENSIONH(5,6),HA(5,6),HB(5,6),HC(5,6).
     5 FORMAT(36H                    RESONANCE VALUES OF H)
     6 FORMAT(6F8.1)
     8 FORMAT(2HG=F9.4)
     9 FORMAT(2HD=F8.3)
    10 FORMAT(3HAF=F8.3)
    11 FORMAT(3HAA=F8.3)
    12 FORMAT(2HA=F8.3)
    13 FORMAT(2HX=F8.3)
     1 READ,G,D,AF,AA,A,X
       C=714.453*X/G
       E=20.*AA**2/(27.*C)
       DO3I=1,5
       DO3J=1,6
       P=I
       Q=J
       R=6-2*I
       S=-3.5+Q
       T=P**2-6.*P+35./4.
       HA(I,J)=C-R*D-A*S-A**2/(2.*C)*(35./4.-S**2+S*R)
       HB(I,J)=-A**3/(2.*C**2)*(2.*(8.75-S**2)*R-S*(8.75-3.*T-2.))
     3 HC(I,J)=A**2*D/C**2*((35./4.-S**2)*R-S*(35./4.-T-1.))
       DO4J=1,6
       H(1,J)=HA(1,J)+HB(1,J)+HC(1,J)+4./3.*AF-E
       H(2,J)=HA(2,J)+HB(2,J)+HC(2,J)-5./3.*AF+E
       H(3,J)=HA(3,J)+HB(3,J)+HC(3,J)-2.*E
       H(4,J)=HA(4,J)+HB(4,J)+HC(4,J)+5./3.*AF+E
     4 H(5,J)=HA(5,J)+HB(5,J)+HC(5,J)-4./3.*AF-E
       PRINT5
       DO7I=1,5
     7 PRINT6,H(I,1),H(I,2),H(I,3),H(I,4),H(I,5),H(I,6)
       PRINT8,G
       PRINT9,D
       PRINT10,AF
       PRINT11,AA
       PRINT12,A
       PRINT13,X
       IF(SENSE SWITCH1)1,14
    14 STOP
       END
```

```
*      IE5     9    UNIVERSITY OF ADELAIDE  S P BURLEY     D 98TX907     P
*      EXEC TIME 1 MIN
*      XEQ
*      CARDS COLUMN
CGD10          EIGENVALUES OF SPIN HAMILTONIAN OF GD+++ IN SCHEELITE
       DIMENSIONA(8),B(8)
       ALPHA1F(A)=-1.5*A(1)+A(2)+8.*A(3)-2.*A(4)
       ALPHA2F(A)=-0.5*A(1)-A(2)-8.*A(3)+2.*A(4)
       ALPHA3F(A)=+0.5*A(1)-A(2)-8.*A(3)+2.*A(4)
       ALPHA4F(A)=+1.5*A(1)+A(2)+8.*A(3)-2.*A(4)
       DISC1F(A)=SQRTF((-2.*A(1)+6.*A(2)-A(3)+3.*A(4))**2+1.4A(5)**2)
       DISC2F(A)=SQRTF((-2.*A(1)+2.*A(2)-5.*A(3)-7.*A(4))**2+3.*A(5)**2)
       DISC3F(A)=SQRTF(( 2.*A(1)+2.*A(2)-5.*A(3)-7.*A(4))**2+3.*A(5)**2)
       DISC4F(A)=SQRTF(( 2.*A(1)+6.*A(2)-A(3)+3.*A(4))**2+1.4A(5)**2)
     1 FORMAT(54H1EIGENVALUES OF SPIN HAMILTONIAN OF GD+++ IN SCHEELITE)
     2 FORMAT(6F10.4,F5.0,I5)
     3 FORMAT(1H0,6E15.5,F5.0,I5)
     4 FORMAT(1H0F10.0,8F12.4)
       READINPUTTAPE2,2,(A(I),I=1,6),STEP,NS
       WRITEOUTPUTTAPE3,3,(A(I),I=1,6),STEP,NS
       N=8
       A(7)=A(1)*A(6)
       DO5J=1,NS
       ANS=J-1
       A(1)=ANS*A(7)*STEP
       B(1)=ALPHA1F(A)+DISC1F(A)
       B(2)=ALPHA2F(A)+DISC2F(A)
       B(3)=ALPHA3F(A)+DISC3F(A)
       B(4)=ALPHA4F(A)+DISC4F(A)
       B(5)=(ALPHA1F(A))-(DISC1F(A))
       B(6)=(ALPHA2F(A))-(DISC2F(A))
       B(7)=(ALPHA3F(A))-(DISC3F(A))
       B(8)=(ALPHA4F(A))-(DISC4F(A))
       CALLRANK(N,B,)
     5 WRITEOUTPUTTAPE3,4ANS,(B(I),I=1,8)
       CALLEXIT
       END
*      CARDS COLUMN
       SUBROUTINERANK(N,X)
       DIMENSIONX(100)
       DO5J=1,N
       BIGX=X(J)
       DO4I=J,N
       IF(BIGX-X(I))3,3,4
     3 BIGX=X(I)
       K=I
     4 CONTINUE
       X(K)=X(J)
     5 X(J)=BIGX
       RETURN
       END
```

APPENDIX C

Theorems from Representation and Transformation Theory.

Representations of the Double Group C_3.

The characters of the irreducible representations of the double group C_3 are tabulated below, together with the characters of the representation of the group generated by the six substates of a term whose angular momentum is 5/2, (see e.g. Ballhausen (1962)).

	E	C_3	C_3^2	$\bar{E}$	$\bar{C}_3$	$\bar{C}_3^2$
$\Gamma 1$	1	1	1	1	1	1
$\Gamma 2$	1	ω^2	$-\omega$	1	ω^2	$-\omega$
$\Gamma 3$	1	$-\omega$	ω^2	1	$-\omega$	ω^2
$\Gamma 4$	1	ω	ω^2	-1	$-\omega$	$-\omega^2$
$\Gamma 5$	1	$-\omega^2$	$-\omega$	-1	ω^2	ω
$\Gamma 6$	1	-1	1	-2	1	-1
$\chi(\phi)_{5/2}$	6	0	0	-6	0	0

Here $E = 4\pi$, $\bar{E} = 2\pi$, $C_3 = \frac{2\pi}{3}$, $\bar{C}_3 = \frac{8\pi}{3}$ etc., and $\omega = \exp(i\pi/3)$.

Hence we can find which linear combinations we can make of the six substates of a term whose angular momentum is 5/2 such that they form bases for irreducible representations of C_3 by use of the group theory formula:

$$C_i = \frac{1}{g}\Sigma\chi(G)\chi_i^*(G)$$

where C_i = the number of times the ith. irreducible representation is contained in the original representation,

$x_i(G)$ = the character of the ith. irreducible representation,

$x(G)$ = the character of the representation generated by the original basis,

g = the order of the group (6 in this case).

(Weyl (1931)).

This implies that the irreducible representations of C_3 contained in functions transforming like those corresponding to an angular momentum of 5/2 are:

$$2\Gamma_4 + 2\Gamma_5 + 2\Gamma_6 .$$

These represent the symmetry types of the wavefunctions corresponding to the Kramers doublets in the absence of any applied magnetic field. We can allow for perturbations by an applied magnetic field by an operator $H_1 = \beta \underset{\sim}{H}.(\underset{\sim}{L} + 2\underset{\sim}{S})$ which gives a secular equation in terms of matrix elements of the form $\langle \Gamma_3^1 | H_1 | \Gamma_4^2 \rangle$ etc. (where we distinguish between the pairs of irreducible representations $\Gamma_{3,4,5}$ by upper indices 1 and 2).

We can simplify these matrix elements by decomposing H_1 into parts which transform irreducibly under the operations of the group and then making use of the orthogonality relations between the basic vectors of such representations. Thus for C_3 we note that :

$L_z + 2S_z$ transforms like $\Gamma 1$,

$(L_x + 2S_x) - i(L_y + 2S_y)$ transforms like Γ_2,

$-(L_x + 2S_x) - i(L_y + 2S_y)$ transforms like Γ_3.

Then we also note that $\langle \Gamma_a | H_1 | \Gamma_b \rangle = 0$ unless it is invariant under all symmetry operations of C_3, i.e. unless $\Gamma_a \times \Gamma_{H1} \times \Gamma_b$ contains the totally symmetric representation. This occurs only when $\Gamma_{H1}^* = \Gamma_a^* \times \Gamma_b$ where the asterisk represents a complex conjugate, (Ballhausen (1962)). We can check this condition by observation of the following table of the direct products of $\Gamma_a^* \times \Gamma_b$:

	Γ_4	Γ_5	Γ_6
Γ_4^*	Γ_1	Γ_3	Γ_2
Γ_5^*	Γ_2	Γ_1	Γ_3
Γ_6^*	Γ_3	Γ_2	Γ_1

One further way of reducing the number of independent matrix elements is to make use of the time inversion anti-symmetry (Wigner (1932)). This is particularly simple in this case where only one dimensional representations appear. We have an odd number of electroms so Wigner's arguments show us that :

1) When Γ is a real representation, it occurs in a paired form whose eigenfunctions have the same eigenvalues,
2) When Γ is a complex representation but $\Gamma \neq \Gamma^*$ then Γ and Γ^* each have the same eigenfunctions

and eigenvalues as some other irreducible representation,

3) When Γ is complex and $\Gamma = \Gamma^*$ there are no degeneracies.

Spherical Harmonics and Representations of the Rotation Group.

The spherical harmonic functions $r^{\ell}Y_{\ell}^{m}$ form the basic vectors of the irreducible representations $D_{\ell}(R)$ of the full rotation group R, (Wigner (1960)). Hence an orthogonal transformation of any one spherical harmonic polynomial produces another polynomial of the same degree which is a linear combination of all the spherical harmonics of that degree, i.e.

$$R(\alpha\beta\gamma)r^{\ell}Y_{\ell}^{m}(\theta,\phi) = \sum_{m'=-\ell}^{\ell} D_{\ell}(\alpha\beta\gamma)_{m'm}\, r^{\ell}Y_{\ell}^{m'}(\theta,\phi),$$

where $(\alpha\beta\gamma)$ are the Euler angles of the transformation and $D_{\ell}(\alpha\beta\gamma)_{m'm}$ are the elements of D_{ℓ}.

The first two single-valued irreducible representations of R are of considerable use in transformation theory. Thus $D_{o}(\alpha\beta\gamma) = 1$ and represents the transformation formula for a scalar, such as $S(S+1)$. We also have D_{1} given by :

$$\begin{bmatrix} e^{-i\alpha}e^{-i\gamma}(1+\cos\beta)/2, & -e^{-i\alpha}(\sin\beta)/\sqrt{2}, & e^{-i\alpha}e^{i\gamma}(1-\cos\beta)/2 \\ e^{-i\gamma}\sin\beta/\sqrt{2}, & \cos\beta, & -e^{i\gamma}\sin\beta/\sqrt{2} \\ e^{i\alpha}e^{-i\gamma}(1-\cos\beta)/2, & e^{i\alpha}(\sin\beta)/\sqrt{2}, & e^{i\alpha}e^{i\gamma}(1+\cos\beta)/2 \end{bmatrix}$$

which represents the transformation formula for a vector $\underline{r}$ when its components are written in the form :

$$T_{-1} = (x + iy)/\sqrt{2},$$
$$T_{o} = z,$$
$$T_{+1} = -(x - iy)/\sqrt{2},$$

In this project it was desired to transform analogous components of $\underline{S}$

viz $S_+ = S_x + iS_y$, S_z , $S_- = S_x - iS_y$,

by a transformation described by the Euler angles (0,90,0.). By substitution into the equation above we see that this corresponds to the transformation formulae :

$$S_- = \tfrac{1}{2}(-S'_+ + S'_-) + S'_z ,$$

$$S_z = \tfrac{1}{2}(S'_+ + S'_-),$$

$$S_+ = \tfrac{1}{2}(S'_+ - S'_-) + S'_z .$$

These formulae give a straightforward (although rather lengthy) method for transforming the Spin Hamiltonian polynomial (in the components of $\underline{S}$) from a system where the z axis is parallel to the c axis of a crystal to one where the z axis is parallel to the original x axis. Thus if we have the term describing the cubic component of a trigonal field expressed in a system where the z direction is parallel to the C_3 axis, and ϕ is chosen to be zero, viz :

$$\frac{\sqrt{2}a}{24}\left[S_z(S_+^3 + S_-^3) + (S_+^3 + S_-^3)S_z \right] ,$$

then we obtain the expression given on the next page :

$$\frac{a}{24}\Big[\; 2S'^{2}_{+}S'_{z}S'_{+} + 2S'^{2}_{-}S'_{z}S'_{-} + 2S'_{+}S'_{z}S'^{2}_{+} + 2S'_{-}S'_{z}S'^{2}_{-}$$

$$-2S'_{+}S'_{-}S'_{z}S'_{+} - 2S'_{-}S'_{+}S'_{z}S'_{-} - 2S'_{+}S'_{z}S'_{-}S'_{+} - 2S'_{-}S'_{z}S'_{+}S'_{-}$$

$$+S'_{z}S'^{3}_{+} + S'_{z}S'^{3}_{-} + S'^{3}_{+}S'_{z} + S'^{3}_{-}S'_{z}$$

$$-S'_{z}S'_{+}S'_{-}S'_{+} - S'_{z}S'_{-}S'_{+}S'_{-} - S'_{+}S'_{-}S'_{+}S'_{z} - S'_{-}S'_{+}S'_{-}S'_{z}$$

$$-S'_{z}S'_{-}S'^{2}_{+} - S'_{z}S'_{+}S'^{2}_{-} - S'^{2}_{+}S'_{-}S'_{z} - S'^{2}_{-}S'_{+}S'_{z}$$

$$+S'_{-}S'^{2}_{+}S'_{z} + S'_{+}S'^{2}_{-}S'_{z} + S'_{z}S'^{2}_{+}S'_{-} + S'_{z}S'^{2}_{-}S'_{+}$$

$$+4S'_{+}S'^{3}_{z} + 4S'_{-}S'^{3}_{z} + 4S'^{3}_{z}S'_{+} + 4S'^{3}_{z}S'_{-}\;\Big],$$

on applying the transformation given above.

Invariance Properties of a Hamiltonian Matrix Under a Unitary Transformation.

Following Parker and Brown (1959) we note that if a secular equation :

$$| H_{ij} - \delta_{ij} E | = 0$$

is expanded in the form :

$$E^n + C_1 E^{n-1} + C_2 E^{n-2} + \ldots + C_n = 0$$

then we have :

$$C_1 = -\sum_i E_i$$

$$C_2 = \sum_i \sum_j E_i E_j \,, \quad (i<j)$$

$$= -\tfrac{1}{2} \sum_i (E_i)^2 + \tfrac{1}{2} (\sum_i E_i)^2$$

where $E_{i,j}$ represent roots of the secular equation.

Under a unitary transformation, the $C_{1,2}$ are invariant and may also be written :

$C_1 = -\sum_i M_{ii}$ (where M_{ii} is the 1×1 determinant from row i and column j of H),

$C_2 = \sum_i \sum_j M_{ij}$ (i, j and M_{ij} is the 2×2 determinant formed by the intersection of rows i,j and columns i,j of H).

Hence we see that :

$$\sum_i E_i = \sum_i M_{ii}$$

$$= \sum_i M_{ii} \qquad (1)$$

and :

$$\sum_i (E_i)^2 = \left(\sum_i M_{ii}\right)^2 - 2\sum_i \sum_j M_{ij} ,$$

$$= \sum_i (H_{ii})^2 - 2 \sum_i \sum_j (H_{ii}H_{jj} - H_{ij}H_{ji}), \quad (i<j).$$

For a Hamiltonian matrix this becomes :

$$\sum_i (E_i)^2 = \sum_i (H_{ii})^2 + 2 \sum_i \sum_j (H_{ij})^2, \quad (i<j). \qquad (2)$$

Equations (1) and (2) are used as checks on the computed values of E_i. Using the form of the constants used to erect the 12x12 matrix in Appendix B1, equation (2) shows that the sum of the squares of the eigenvalues must be given by :

$$\sum_{i=1}^{12} (E_i)^2 = 168Y^2 + 56Z^2 - 8X^2 + 140B^2$$

Equation (1) shows that the sum of the eigenvalues must be the same as the trace of the original matrix.

BIBLIOGRAPHY

Aisenberg,S., Statz,H., and Koster,G.F. (1959) : Phys. Rev. 116, 811.

Ambler,E. et al. (1962) : J. Math. Phys. 3, 118.

Andrew,E.R. (1958) : Nuclear Magnetic Resonance. Cambr. Uni. Press, Cambr.

Ballhausen,C.J. (1962) : Introduction to Ligand Field Theory. McGraw-Hill, London, N.Y..

Bamford,C.R. (1962) : Physics and Chemistry of Glasses 3, 189.

Barrett,C. (1943) : Structure of Metals. McGraw-Hill, London.

Bil'Dyukevich, A.L. et al. (1960) : Reports to the Conference on Paramagnetic Resonance, Kazan, Izv., Kazansk gos. univ.

Bleaney,B. and Penrose,R.P. (1946) : Nature 157, 339.

Bleaney,B. et al. (1949) : Proc. Roy. Soc. (London), A198, 406.

Bleaney,B. and Ingram,D.J.E. (1951) : Proc. Roy. Soc. (London), A205, 336.

Bleaney,B. and Rubins,R.S. (1961) : Proc. Phys. Soc. (London), 77, 103.

Bleaney, B. and Stevens, K.W.H. (1953) : Repts. Prog. in Phys., 16, 108.

Bleaney, B. and Trenam, R.T. (1954) : Proc. Roy. Soc. (London), A223, 1.

Bogle, G.S. et al. (1961) : Proc. Phys. Soc., 77, 561.

Bowers, K.D. and Owen, J. (1955) : Repts. Prog. in Phys., 18, 304.

Cavenett, B.C. (1964) : Proc. Phys. Soc., (to be published).

Condon, E.U. and Shortley, G.H. (1959) : Theory of Atomic Spectra. Cambr. Uni. Press, Cambr.

Cummerow, R.L. and Halliday, D. (1946) : Phys. Rev., 70, 433.

Dana, E.S. (1932) : A Textbook of Mineralogy. 4th. ed., John Wiley and Sons, N.Y.

Deer, W.A., Howie, R.A. and Zussman, J. (1962) : Rock-Forming Minerals. Longmans, London.

Douglas, R.W. (1958) : Conference on non-crystaline solids, Alfred, N.Y.
Sept. 3-5 (ed Frechette, V.D.), John Wiley and Sons, N.Y.

Feher, G. (1957) : Bell System Tech. J., 36, 449.

Folen, V.J. (1962) : Phys Rev., 125, 1581.

Friedman, E. and Low, W. (1960) : Phys. Rev., 120, 408.

Gordon, J.P. (1961) : Rev. Sci. Inst., 32, 658.

Griffith, J.S. (1961) : The Theory of Transition Metal Ions. Cambr. Univ. Press.

Hamilton, D.R. et al. (1948) : Klystrons and Microwave Triodes. McGraw-Hill, N.Y.

Hartmann, H. and Schlafer, H.R. (1951) : Z. Naturf. 6a, 754.

Hempstead, C.F. and Bowers, K.D. (1960) : Phys. Rev. 118, 131.

Hirshon, J.M. and Fraenkel, G.E. (1955) : Rev. Sci. Insts., 26, 34.

Huggins, M.L. (1958) : Conference on non-crystalline Solids, Alfred, N.Y.
Sept. 3-5 (ed. V.D. Frechette) John Wiley and Sons, N.Y.

Ingram, D.J.E. (1955) : Spectroscopy at Radio and Mi Microwave Frequencies. Butterworth's Scientific Publications, London.

Ingram, D.J.E. (1958) : Free Radicals as Studied by Electron Spin Resonance. Butterworth's Publications, London.

Jackson, J.D. (1962) : Mathematics for Quantum Mechanics W.A. Benjamin, N.Y.

Judd,B.R. (1955) : Proc. Roy. Soc. (London), A227, 522.

Kasai,P.H. (1962) : J.Phys. Chem., 66, 674.

Kats,A. and Stevels,J.M. (1956) : Philips Research Repts., 11, 115.

Kneubuhl,F.K. (1960) : J. Chem. Phys., 33, 1074.

Kondo,J. (1960) : Prog. Theoret. Phys., 23, 106.

Kornienko, L.S. and Prokhorov,A.M. (1957) : J. Expl. Theoret. Phys., U.S.S.R. 33, 805.

Kornienko,L.S. and Prokhorov,A.M. (1961) : J.Expl. Theoret. Phys., U.S.S.R. 40, 1594.

Koster,G.F. and Statz,H. (1959) : Phys. Rev., 113, 445.

Krogh-Moe,J. (1962) : Physics and Chemistry of Glasses 3, 1.

Lacroix,R. (1957) : Helv. Phys. Acta 30, 374.

Lawson,J.L. and Uhlenbeck,G.H.E. (1948) : Threshold Signals. McGraw-Hill, N.Y.

Llewllyn,P.M. (1957) : J. Sci. Insts., 34, 236.

Low,W. (1960) : Solid State Physics. Supplement 2 Academic Press, N.Y.

Matarrese,L. (1961) : J. Chem. Phys., 34, 336.

McConnell,H.M. (1956) : J. Chem. Phys. 21, 1119.

Misra,M. (1958) : Rev.Sci. Insts. 29, 590.

Montgomery, C.G. et al. (1948) : Principles of Microwave Circuits. McGraw-Hill, N.Y.

Orgel, L.E. (1959) ; An Introduction to Transition Metal Chemistry : Ligand Field Theory. Methuen and Co. Ltd., London.

Pake, G.E. (1962) : Paramagnetic Resonance. W.A. Benejamin Inc., N.Y.

Palache, C. (1909) : Am. J. Sc., 27, 398.

Parker, P.M. and Brown, L.C. (1959) : Am. J. Phys. 27, 509.

Pohl, R.W. (1937) : Proc. Phys. Soc. (London), 49, 3

Polder, D. (1942) : Physica, 9, 709.

Powell, M.J.D. et al. (1960) : Phys. Rev. Letters, 5, 145.

Pryce, M.H.L. (1950) : Phys. Rev., 80, 1107.

Pryce, M.L.H. (1950) : Proc. Phys. Soc. (London), A63, 25.

Rei, D.K. (1962) Soviet Physics, Solid State, (U.S.A.) 3, 1838.

Rogers, G. (1909) : Science, 28, 616.

Sands, R.H. (1955) : Phys. Rev., 99, 1222.

Schiff, L.I. (1955) : Quantum Mechanics. McGraw-Hill N.Y.

Schneider,G.E. and England,T.S. (1951) : Physica, 17, 221.

Schneider,J. and Sircar,S.T. (1962) : Z. Naturforschg. 17a, 651.

Schulz-Du Bois (1959) : Bell System Tech. J., 38, 271.

Shamfarov, Ya.L (1960) : Instruments and Experimental Techniques (U.S.A.) 6, 916.

Slichter,C.P. (1963) : Principles of Magnetic Resonance. Harper and Row, N.Y.

Statz,H. and Koster,G.F. (1959) : Phys. Rev. 115, 1568.

Stevens,K.W.H. (1952) : Proc. Phys. Soc. A65, 209.

Teaney,M.P. et al. (1961) : Rev. Sci. Insts., 32, 721.

Tinkham,M. (1956) : Proc. Roy. Soc. (London), A236, 535.

Thewlis,J. et al. (1939) : Trans. Farad. Soc. 35, 358.

Turnbull, H.W. (1952) : Theory of Equations. Oliver and Boyd, London.

Van Vleck,J.H. and Penney, W.G. (1934) : Phil. Mag. 7, 961.

Van Vleck,J.H. (1948) : Phys. Rev. 74, 1168.

Van Vleck,J.H. (1940) : Phys. Rev. 57, 426.

Van Wieringen, J.S. (1955) : Disc. Faraday Soc. 19 118.

Van Wieringen, J.S. and Kats, A. (1957) : Philips Research Repts., 12, 432.

Watanabe, H. (1957) : Prog. Theoret. Phys., 18, 405.

Weyl, H. (1931) : The Theory of Groups and Quantum Mechanics. Dover, N.Y.

Weyl, W.A. (1959) : Coloured Glasses. Dawsons of Pall Mall, London.

Wigner, E.P. (1932) : Nachr. Akad. Wiss. Gottingen, Math-Physic. K1, 546.

Wigner, E.P. (1959) : Group Theory and its Application to the Quantum Mechanics of Atomic Spectra. Academic Press, N.Y.

Wilkinson, J.H. (1961) : The Computor Journal 4, 230.

Wilmshurst, T.H. et al (1962) : Journal of Electronics and Control. 13, 339.

Wolga, G.J. and Tseng, R. (1964) : Phys. Rev. 113, A1563.

Wyckoff, R.W.G. (1960) : Crystal Structures. Interscience Publishers, N.Y.

Yafaev, N.R. and Yablokov, Yu.V. (1962) : Soviet Physics, Solid State (U.S.A.) 4, 1123.

Yasaitis, E.L. and Smaller, B. (1953) : Phys. Rev. 92 1068.

Yokota, R. (1954) : Phys. Rev. 95, 1145.

Zachariasen, W.H. (1930) : Z. fur K. 74, 139.

Zacharaisen, W.H. (1932) : J. Am. Chem. Soc., 54, 3841.

Zavoisky, E.J. (1945) : J. Phys. (U.S.S.R.) 9, 211.